PB-245 344

INFLUENCE OF AERODYNAMIC PHENOMENA ON POLLUTANT FORMATION IN COMBUSTION. VOLUME I. EXPERIMENTAL RESULTS

Craig T. Bowman, et al

United Technologies Research Center

Prepared for:

National Environmental Research Center

July 1975

DISTRIBUTED BY:

NTIS

National Technical Information Service
U. S. DEPARTMENT OF COMMERCE

252153

PB 245 344

EPA-650/2-75-061-a

July 1975

Environmental Protection Technology Series

UNITED STATES ENVIRONMENTAL PROTECTION AGENCY

Reproduced by
NATIONAL TECHNICAL
INFORMATION SERVICE
U S Department of Commerce
Springfield VA 22151

TECHNICAL REPORT DATA

(Please read Instructions on the reverse before completing)

1. REPORT NO. **EPA-650/2-75-061-a**

2\.

3. RECIPIENT'S ACCESSION NO.

4. TITLE AND SUBTITLE
Influence of Aerodynamic Phenomena on Pollutant
Formation in Combustion
Volume I. Experimental Results

5. REPORT DATE
July 1975

6. PERFORMING ORGANIZATION CODE

7. AUTHOR(S)
Craig T. Bowman and Leonard S. Cohen

8. PERFORMING ORGANIZATION REPORT NO.

9. PERFORMING ORGANIZATION NAME AND ADDRESS
United Technologies Research Center
400 Main Street
East Hartford, CT 06108

10. PROGRAM ELEMENT NO.
1AB014; ROAP 21BCC-014

11. CONTRACT/GRANT NO.
68-02-1092

12. SPONSORING AGENCY NAME AND ADDRESS
EPA, Office of Research and Development
Industrial Environmental Research Laboratory
Research Triangle Park, NC 27711

13. TYPE OF REPORT AND PERIOD COVERED
Final; 7/73 - 12/74

14. SPONSORING AGENCY CODE

15. SUPPLEMENTARY NOTES

16. ABSTRACT

The report gives results of the measurement of average concentration levels of NO, NO2, CO, and unburned hydrocarbons (THC) at the exhaust of an axisymmetric combustor over a significant range of operating conditions. In addition, it gives detailed species concentration, temperature, and velocity maps throughout the combustor for seven representative operating conditions. In the combustor, natural gas, a synthesized CH4/CO/H2 fuel, or vaporized propane issued through a central duct to mix and burn with an annular air stream in a 1.8 m long cylindrical duct. In a few tests, liquid propane was the fuel. Major combustor input parameters varied over the following ranges: overall fuel/air equivalence ratio 0.5-1.3, air/fuel velocity ratio 0.1-40, inlet air swirl number zero-0.6, air flow rate 0.088-0.137 kg/sec, inlet air temperature 730-860K, and combustor pressure 1-7 atm. Water-cooled probes were used to remove samples from the flow for on-line concentration analysis and to measure temperature, velocity, and flow direction. Elevated pressure and introduction of swirl, to the extent considered in the present experiments, create 'unmixedness' in the combustor flow field which in turn results in enhanced NO formation and consumption of hydrocarbons. Aerodynamic flame stabilization produces strong stirring which results in relatively low NO formation and hydrocarbon consumption rates.

17. KEY WORDS AND DOCUMENT ANALYSIS

a. DESCRIPTORS		b. IDENTIFIERS/OPEN ENDED TERMS	c. COSATI Field/Group
Air Pollution	Propane	Air Pollution Control	13B
Combustion	Flow Distribution	Stationary Sources	21B
Aerodynamics		Chemical Heat Release	20D
Nitrogen Oxide (NO)		Flame Stabilization	07B
Nitrogen Dioxide		Flow Field Mapping	
Methane		Low-Btu Gas	07C

18. DISTRIBUTION STATEMENT
Unlimited

19. SECURITY CLASS *(This Report)*
Unclassified

20. SECURITY CLASS *(This page)*
Unclassified

21. NO. OF PAGES
159

22. PRICE
$6.25-2.25

EPA Form 2220-1 (9-73)

EPA-650/2-75-061-a

INFLUENCE OF AERODYNAMIC PHENOMENA ON POLLUTANT FORMATION IN COMBUSTION

VOLUME I. EXPERIMENTAL RESULTS

by

Craig T. Bowman and Leonard S. Cohen

United Technologies Research Center
400 Main Street
East Hartford, Connecticut 06108

Contract No. 68-02-1092
ROAP No. 21BCC-014
Program Element No. 1AB014

EPA Project Officer: W. Steven Lanier

Control Systems Laboratory
National Environmental Research Center
Research Triangle Park, North Carolina 27711

Prepared for

U. S. ENVIRONMENTAL PROTECTION AGENCY
OFFICE OF RESEARCH AND DEVELOPMENT
WASHINGTON, D. C. 20460

July 1975

EPA REVIEW NOTICE

This report has been reviewed by the National Environmental Research Center - Research Triangle Park, Office of Research and Development, EPA, and approved for publication. Approval does not signify that the contents necessarily reflect the views and policies of the Environmental Protection Agency, nor does mention of trade names or commercial products constitute endorsement or recommendation for use.

RESEARCH REPORTING SERIES

Research reports of the Office of Research and Development, U.S. Environmental Protection Agency, have been grouped into series. These broad categories were established to facilitate further development and application of environmental technology. Elimination of traditional grouping was consciously planned to foster technology transfer and maximum interface in related fields. These series are:

1. ENVIRONMENTAL HEALTH EFFECTS RESEARCH
2. ENVIRONMENTAL PROTECTION TECHNOLOGY
3. ECOLOGICAL RESEARCH
4. ENVIRONMENTAL MONITORING
5. SOCIOECONOMIC ENVIRONMENTAL STUDIES
6. SCIENTIFIC AND TECHNICAL ASSESSMENT REPORTS
9. MISCELLANEOUS

This report has been assigned to the ENVIRONMENTAL PROTECTION TECHNOLOGY series. This series describes research performed to develop and demonstrate instrumentation, equipment and methodology to repair or prevent environmental degradation from point and non-point sources of pollution. This work provides the new or improved technology required for the control and treatment of pollution sources to meet environmental quality standards.

This document is available to the public for sale through the National Technical Information Service, Springfield, Virginia 22161.

Publication No. EPA-650/2-75-061-a

TABLE OF CONTENTS

ABSTRACT iii

LIST OF FIGURES iv

LIST OF TABLES x

ACKNOWLEDGEMENTS xii

I. INTRODUCTION 1

II. EXPERIMENTAL INVESTIGATION 2

A. Experimental Configuration and Approach 2
B. Experimental Apparatus and Instrumentation 5

Combustor Facility 5
Probes 10
Sampling System 12

C. Experimental Results 15

Description of Experiments 15
Input-Output Experiments 17
Flow Field Mapping Experiments 36

III. CONCLUDING REMARKS 84

APPENDIX A - COMPUTATION OF THE SWIRL NUMBER

APPENDIX B - COMBUSTOR PROBE DESIGNS, CALIBRATION PROCEDURES AND REDUCTION OF PROBE DATA 87

APPENDIX C - GAS SAMPLING SYSTEM, CALIBRATION PROCEDURES AND DATA REDUCTION TECHNIQUES 97

APPENDIX D - EXHAUST CONCENTRATION DATA 104

APPENDIX E - SPECIES CONCENTRATION, TEMPERATURE AND VELOCITY DISTRIBUTIONS 115

APPENDIX F - FUEL COMPOSITION 138

NOMENCLATURE 140

REFERENCES 143

ABSTRACT

Average concentration levels of the pollutants NO, NO_2, CO and unburned hydrocarbons (THC) were measured at the exhaust of an axisymmetric combustor over a significant range of operating conditions. In addition, detailed species concentration, temperature and velocity maps were obtained throughout the combustor for seven representative operating conditions. Natural gas, a synthesized $CH_4/CO/H_2$ fuel or vaporized propane issued through a central duct to mix and burn with an annular air stream within the 1.8 m long cylindrical combustor. In a limited mumber of tests liquid propane was utilized as the fuel. Major combustor input parameters were varied over the following ranges: overall fuel/air equivalence ratio 0.5 - 1.3, air-fuel velocity ratio 0.1 -40, inlet air swirl number 0 - 0.6, air flow rate 0.09 - 0.14 kg/sec, inlet air temperature 730 - 860°K and combustor pressure 1-7 atm. Water-cooled probes were used to remove samples from the flow for on-line concentration analysis, and to measure temperature, velocity and flow direction.

Elevated pressure and introduction of swirl to the extent considered in the present experiments, creates "unmixedness" in the combustor flow field, producing high local temperatures, which in turn results in enhanced NO formation and consumption of hydrocarbons. Aerodynamic flame stabilization, achieved without benefit of swirl or physical flameholders in systems having large air-fuel momentum flux ratios, produces strong stirring which results in reduced temperatures and in relatively low NO formation and hydrocarbon consumption rates.

LIST OF FIGURES

Figure No.		Page
1	Recirculation Zone in Initial Region Downstream of Coaxial Streams.	3
2	Schematic Diagram of Axisymmetric, Water-Cooled Combustion System.	6
3	Injector and Swirl Vane Geometries.	8
4	Combustor Facility.	9
5	Exhaust Sampling Rake.	11
6	Combustor Probing Device.	12
7	On-line Gas Analysis System.	14
8	Average Species Concentrations in Combustor Exhaust Gas. Combustion of Natural Gas with 0.132 kg/sec of 740°Air, S=0, V_a/V_f=22, at 1 atm. Species Concentrations Reported As Measured.	18
9	Exhaust Temperature Profiles for Non-Swirling (S=0) Flow. Combustion of Natural Gas with 0.132 kg/sec of 740°K Air, V_a/V_f=22, at 1 atm.	19
10	Influence of Inlet Air Swirl and Combustor Pressure on Average Exhaust NO Concentration for Combustion of Natural Gas with 0.132 kg/sec of 740°K Air, V_a/V_f=22.	20
11	Exhaust Temperature Profile for a Swirling (S=0.6) Flow. Combustion of Natural Gas with 0.132 kg/sec of 740°K Air, V_a/V_f=22, at 3.5 atm.	22
12	Influence of Inlet Air Swirl on Average Exhaust CO and THC Concentrations for Combustion of Natural Gas with 0.132 kg/sec of 740°K Air, V_a/V_f=22, at 1 atm.	23
13	Influence of Combustor Pressure on Average Exhaust CO and THC Concentration for Combustion of Natural Gas with 0.132 kg/sec of 740°K Air, V_a/V_f=22, S=0.	25

LIST OF FIGURES (CONT.)

Figure No.		Page
14	Influence of Air-Fuel Velocity Ratio on Average Exhaust NO Concentration in a Swirling (S=0.6) Flow. Combustion of Natural Gas with 0.132 kg/sec of $740^{\circ}K$ Air at 1 atm.	26
15	Influence of Air-Fuel Velocity Ratio on Average Exhaust CO and THC Concentrations in a Swirling (S=0.6) Flow. Combustion of Natural Gas with 0.132 kg/sec of 740 K°Air at 1 atm.	27
16	Influence of Air Flow Rate and Inlet Temperature on Average Exhaust NO Concentrations for Combustion of Natural Gas with Air, V_a/V_f =22, S=0, at 1 atm.	28
17	Influence of Air Flow Rate on Average Exhaust CO and THC Concentrations for Combustion of Natural Gas with $740^{\circ}K$ Air, V_a/V_f=22, S=0, at 1 atm.	29
18	Influence of Inlet Air Temperature on Average Exhaust CO and THC Concentrations for Combustion of Natural Gas with 0.132 kg/sec of Air, V_a/V_f=22, S=0, at 1 atm.	30
19	Average Exhaust NO Concentrations for Combustion of Natural Gas, Synthesized Fuel and Vaporized Propane. Combustion with 0.132 kg/sec of $740^{\circ}K$ Air at 1 atm. V_a/V_f=22, for Natural Gas, V_a/V_f=15 for the Synthesized Fuel, V_a/V_f=35 for Vaporized Propane.	32
20	Average Exhaust NO Concentrations for Combustion of Vaporized and Liquid Propane with 0.136 kg/sec of $740^{\circ}K$ Air.	33
21	Average Exhaust THC Concentrations for Combustion of Vaporized and Liquid Propane with 0.136 kg/sec of $740^{\circ}K$ Air.	34
22	Average Exhaust CO Concentrations for Combustion of Vaporized and Liquid Propane wiht 0.136 kg/sec of $740^{\circ}K$ Air.	35
23	Velocity Profiles for Baseline Case. Combustion of Natural Gas (T_f=$303^{\circ}K$) with 0.132 kg/sec of $752^{\circ}K$ Air, V_a/V_f=22.9, S=0 at 1 atm.	40

LIST OF FIGURES (CONT.)

Figure No.		Page
24	Temperature Profiles for Baseline Case.	41
25	Oxygen Concentration Map for Baseline Case. Average Exhaust Concentration = 0.02.	42
26	THC Concentration Map for Baseline Case. Average Exhaust Concentration = 1300 ppm.	43
27	CO Concentration Map for Baseline Case. Average Exhaust Concentration = 0.016.	45
28	CO_2 Concentration Map for Baseline Case. Average Exhaust Concentration = 0.0881.	46
29	NO and NO_2 Concentration Maps for Baseline Case. Average Exhaust Concentration: NO=156 ppm and NO_2=30 ppm.	47
30	Comparison of the O_2 Concentration Distributions at the Baseline Condition ($\Phi = 0.9$) with Those at $\Phi = 0.7$. At the Lower Equivalence Ratio, Natural Gas (307°K) is Burned with 0.136kg/sec of 754°K Air, V_a/V_f=29.2, $\Phi = 0.68$, S=0 at 1 atm.	49
31	Effect of Overall Equivalence Ratio on THC Concentration Map. Operating Conditions Identical to Fig. 30.	50
32	Effect of Overall Equivalence Ratio on CO Concentration Map. Operating Conditions Identical to Fig. 30.	51
33	Effect of Overall Equivalence Ratio on CO_2 Concentration Map. Operating Conditions Identical to Fig. 30.	52
34	Velocity Profiles for Combustion of Synthesized Fuel (T_f=309°K) with 0.132 kg/sec of 730°K Air, V_a/V_f=14.6, S=0, Φ=0.87, at 1 atm.	54
35	Temperature Profiles for Synthesized Fuel Combustion Test.	55
36	CO_2 Concentration Maps for Synthesized Fuel and Baseline (Natural Gas) Combustion Tests.	56

LIST OF FIGURES (CONT.)

Figure No.		Page
37	NO Concentration Maps for Synthesized Fuel and Baseline (Natural Gas) Combustion Tests.	57
38	Temperature Profiles in Swirling Flow Combustion Test. Combustion of Natural Gas (T_f=360°K) with 0.134 kg/sec of 750°K Air Having a Swirl Number of 0.3, V_a/V_f=23, Φ=0.885, 1 atm.	59
39	Oxygen Concentration Maps for Swirling (S=0.3) and Baseline (S=0) Combustion Tests.	61
40	Total Hydrocarbon Concentration Maps for Swirling (S=0.3) and Baseline (S=0) Combustion Tests.	62
41	CO Concentration Maps for Swirling (S=0.3) and Baseline (S=0) Combustion Tests.	63
42	CO_2 Concentration Maps for Swirling (S=0.3) and Baseline (S=0) Combustion Tests.	64
43	NO Concentration Maps for Swirling (S=0.3) and Baseline (S=0) Combustion Tests.	65
44	Velocity Profiles in Swirling Combustor Flow (S=0.3).	66
45	Direction of Flow in Combustor with S=0.3.	68
46	Temperature Profiles for Baseline (P=1 atm) Combustion Test and for High Pressure (P=3.6 atm) Combustion of Natural Gas (T_f=305°K) with 0.137 kg/sec of 750°K Air, V_a/V_f=22.9, Φ=0.87, S=0.	69
47	Oxygen Concentration Maps for High Pressure (P=3.6 atm) and Baseline (P=1 atm) Combustion Tests.	70
48	Total Hydrocarbon Concentration Maps for High Pressure (P=3.6 atm) and Baseline (P=1 atm) Combustor Tests.	71
49	CO Concentration Maps for High Pressure (P=3.6 atm) and Baseline (P=1 atm) Combustion Tests.	72

LIST OF FIGURES (CONT.)

Figure No.		Page
50	CO_2 Concentration Maps for High Pressure (P=3.6 atm) and Baseline (P=1 atm) Combustion Tests.	73
51	NO Concentration Maps for High Pressure (P=3.6 atm) and Baseline (P=1 atm) Combustion Tests.	74
52	Temperature Profiles for Combustion of Liquid Propane with 0.137 kg/sec of 739°K Air, S=0.3, at 1 atm. Data Obtained Using Calibrated Thermocouple Probe.	76
53	Temperature Profiles for Combustion of Liquid Propane with 0.137 kg/sec of 739°K Air, S=0.3, at 1 atm. Data Obtained Using Calibrated Thermocouple Probe.	77
54	Oxygen Concentration Maps for Liquid Propane Combustion Tests.	78
55	Total Hydrocarbon Maps for Liquid Propane Combustion Tests.	79
56	CO Concentration Maps for Liquid Propane Combustion Tests.	80
57	CO_2 Concentration Maps for Liquid Propane Combustion Tests.	81
58	NO Concentration Maps for Liquid Propane Combustion Tests.	83
59	Exhaust Gas Sampling Probe.	88
60	Calibration Set-Up for Impact-Static Probe.	91
61	Impact-Static Probe Pitch Plane-Angle Calibration Data.	92
62	Impact-Static Probe Yaw Plane-Angle Calibration Data.	93
63	Correlation of Total Flow Angle.	95
64	Double Sonic Orifice (DSO) Calibration.	96

LIST OF FIGURES (CONT.)

Figure No.		Page
65	Exhaust Gas Analytical System.	99
66	Typical Mass Spectrum of Exhaust Gas Sample.	101
67	MBTH Formaldehyde Analysis Apparatus.	102

LIST OF TABLES

Table		Page
I	Matrix of Nominal Test Conditions: Input-Output Experiments	16
II	Matrix of Nominal Test Conditions: Mapping Experiments	37
III	Legend for Mapping Data: Axial Probe Location	39
D-1	Exhaust Concentration Data - Natural Gas Fuel, S=0.	104
D-2	Exhaust Concentration Data - Natural Gas Fuel, S=0.3.	105
D-3	Exhaust Concentration Data - Natural Gas Fuel, S=0.6.	106
D-4	Exhaust Concentration Data - Synthesized Fuel, S=0.	107
D-5	Exhaust Concentration Data - Synthesized Fuel, S=0.6.	108
D-6	Exhaust Concentration Data - Gaseous Propane.	109
D-7	Exhaust Concentration Data - Liquid Propane.	110
D-8	Exhaust Temperature Profiles for Natural Gas Combustion at Various Φ.	111
D-9	Exhaust Temperature Profiles for Natural Gas Combustion at Various Inlet Air Conditions.	112
D-10	Exhaust Temperature Profiles for Natural Gas Combustion - S=0.6.	113
D-11	Exhaust Temperature Profiles for Synthesized Gas Combustion at Various Φ .	114

LIST OF TABLES (CONT.)

Table		Page
E-1	Baseline Case Concentration Distributions.	115
E-2	Species Concentration Distributions for Low Equivalence Ratio Case.	118
E-3	Species Concentration Distributions for Synthesized Gas Case.	121
E-4	Species Concentration Distributions for Swirling Flow Case.	124
E-5	Species Concentration Distributions for High Pressure Case.	127
E-6	Species Concentration Distributions for Liquid Propane.	129
E-7	Baseline Case Velocity Profiles.	131
E-8	Baseline Case Temperature Profiles.	131
E-9	Velocity Profiles for Low Equivalence Ratio Case.	132
E-10	Temperature Profiles for Low Equivalence Ratio Case.	132
E-11	Synthesized Gas Case Velocity Profiles.	133
E-12	Synthesized Gas Case Temperature Profiles.	133
E-13	Velocity Profiles for Swirling Flow Case.	134
E-14	Flow Direction Data for Swirling Flow Case.	134
E-15	Temperature Profiles for Swirling Flow Case.	135
E-16	Temperature Profiles for High Pressure Case.	136
E-17	Temperature Profiles for Liquid Propane Combustion.	137
F-1	Natural Gas Composition.	138
F-2	Synthesized Fuel Composition.	138
F-3	Propane Fuel Composition.	139

ACKNOWLEDGMENTS

A number of individuals at UTRC made significant contributions to the experimental investigation. Dr. M. F. Zabielski and Mr. G. L. Dodge designed the sampling system used in the investigation and developed the calibration and data reduction procedures employed in the gas sampling portion of the experiments. Mr. R. Smus was responsible for fabrication of the sampling system and maintenance of the gas analysis equipment. Mr. T. A. Murrin assisted throughout the experimental program, and was responsible for operation of the combustor and for reduction of much of the experimental data. Mr. R. Lehrach and Dr. M. N. Director contributed to the design and calibration of the probes. Mrs. P. A. Rose, Mrs. P. Jankot and Mrs. J. Andrew assisted in reduction and compilation of the experimental data and in the preparation of the final report.

This research program was carried out under the sponsorship of the Environmental Protection Agency, EPA Contract 68-02-1092, Durham, North Carolina, under the direction of Mr. G. Blair Martin and Mr. W. S. Lanier, Project Officers.

I. INTRODUCTION

Recent experimental investigations of factors affecting pollutant emissions from various continuous combustion devices have shown that changes in operating conditions, which alter the flow pattern in the combustion chamber, can have a substantial effect on pollutant emissions. Heap and his co-workers (Ref. 1) have shown that in gas- and pulverized coal-fired furnaces, changes in the velocity and swirl of the air stream and in the fuel injection configuration produce significant changes in nitrogen oxide emissions. Shoffstall and Larson (Ref. 2) observed substantial variations in NO emissions from gas-fired industrial burners with changes in the gas injection method. Furthermore, the work of Mellor, et al.(Ref. 3) and Jones and Grobman (Ref. 4) provide evidence that changes in the air flow distribution in the combustion chamber can significantly affect the emissions of carbon monoxide and unburned hydrocarbons from gas turbines. All of these observations suggest that coupling between fluid dynamic and chemical processes inside the combustion chamber is a major factor in governing pollutant emissions from many combustion devices. Analytical studies of reacting flow fields (Refs. 5-8) have indicated in a qualitative manner how mixing and turbulence can influence pollutant formation. However, at the present time our understanding of the nature of the coupling between fluid dynamic and chemical processes is insufficient to permit extrapolation of results obtained from one combustion device to other devices or to allow a priori determination of the effects of changes in operating conditions on pollutant emissions.

The present report documents the results of an experimental and analytical investigation, sponsored by EPA Contract 68-02-1092, of the interaction between fluid dynamics and chemistry in a combustor and the subsequent effects on pollutant formation and destruction. The overall objectives of this investigation are:

(i) To examine experimentally the interaction between fluid dynamic and chemical processes inside a model combustor as operating conditions are varied, and to correlate changes in pollutant emissions with these variations.

(ii) To further develop an existing elliptic flow computational procedure for predicting fluid dynamic and chemical processes occurring in combustors.

(iii) To compare the experimental results with results from the combustor flow analysis in order to evaluate and calibrate the theoretical model and to assist in interpretation of the experimental results.

The report consists of two parts. Part 1 documents results from the experimental investigation. Part 2 presents details of the combustor flow analysis together with a preliminary comparison of analytical and experimental results for gaseous fuel combustion.

II. EXPERIMENTAL INVESTIGATION

A. Experimental Configuration and Approach

The selection of the experimental configuration and approach utilized in the present investigation was predicated on a number of requirements. For example, an experimental geometry was desired which models the essential features of practical continuous flow combustion devices. Furthermore, a versatile combustor design was sought to permit independent variation of the various inlet parameters, e.g., air-fuel velocity ratio, inlet air swirl, overall equivalence ratio, inlet air flow rate and temperature and pressure. The combustor design also must allow the accurate determination of inlet conditions to facilitate meaningful comparisons between experimental and analytical results. Finally, extensive combustor instrumentation was provided to permit measurement of pollutant emissions and determination of the radial and axial variations of temperature, velocity and species concentrations throughout the flow field.

The experimental configuration selected for the present study is an axisymmetric combustor in which a central fuel stream, gaseous or liquid, mixes with a coaxial annular air stream. In this configuration, which resembles the primary combustion zone in many practical combustion devices, the resulting flame will not be stabilized in general, and blow-off (extinguishment) will occur. In order to stabilize a flame in such a system, it is necessary to provide a continuous ignition source either by means of a pilot flame or through creation of zones of hot recirculating combustion gases. These stabilizing recirculation zones may be created by the introduction of physical flameholders into the flow or by imparting a swirl component to the flow (c.f. Ref. 9). Swirl stabilization techniques have been used extensively in continuous flow combustion devices such as furnaces and gas turbines. Hence, a significant portion of the current effort focuses on swirl-stabilized flames.

At the outset of the program, it appeared that detailed characterization of inlet conditions (a major program objective) using probe techniques would be difficult in swirling flows because of the relatively large tangential velocity components necessary to stabilize the flame. Hence, alternative methods of flame stabilization were examined. The use of physical flameholders (e. g., v-gutter and cylindrical-shaped bodies or rearward-facing steps) was considered undesirable since the processes which occur in the flame zone are influenced by the specific flameholder geometry (Ref. 10), thereby complicating specification of the inlet conditions. Flame stabilization by means of pilot flames was considered undesirable because of the primary interest in flames stabilized on recirculation zones. A review of the recent literature on mixing of coaxial non-reacting jets indicated that flame stabilization might be achieved in gaseous-fueled systems by judicious selection of the momentum flux ratio of the fuel and air streams. This flameholding approach relies neither on a physical flameholder nor on swirl. Rather, as shown in Fig. 1, it makes use of the observation that a recirculation zone is formed in the initial region of coaxial

Recirculation Zone in Initial Region Downstream of Coaxial Streams.

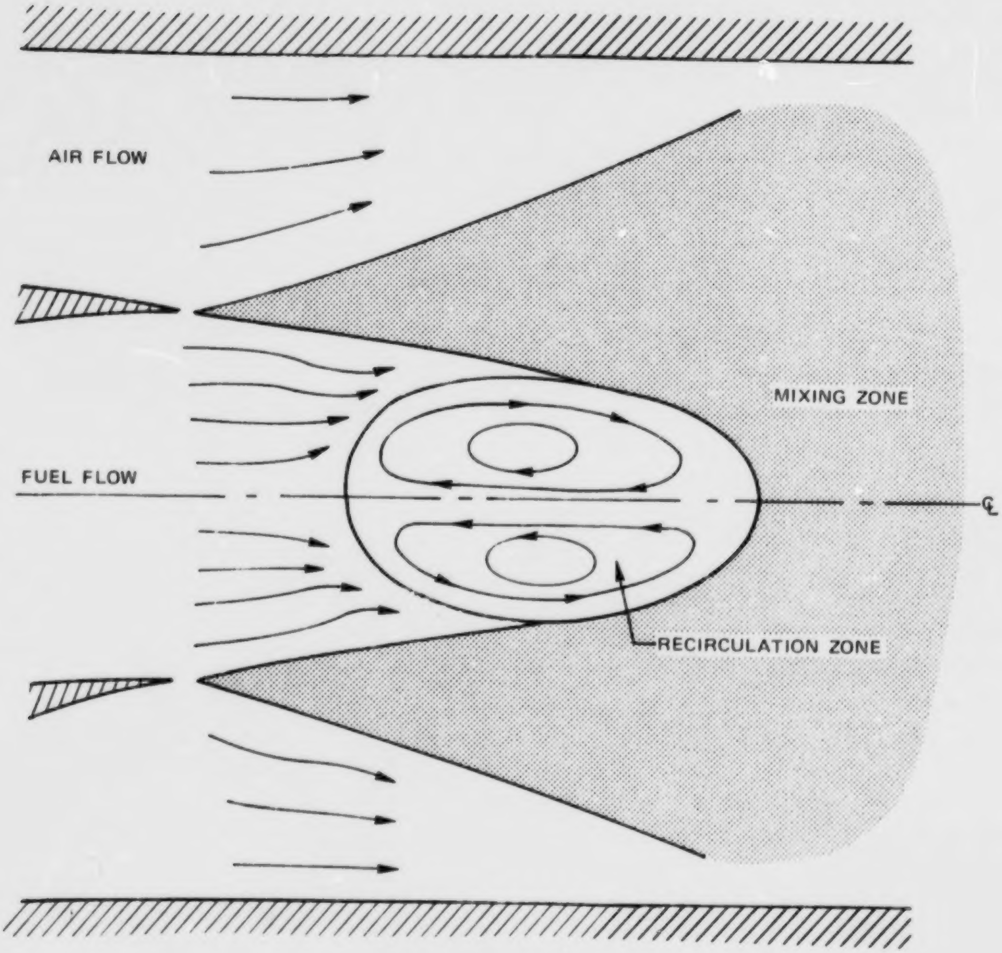
AIR FLOW
MIXING ZONE
FUEL FLOW
℄
RECIRCULATION ZONE

streams when the outer, annular stream, i.e., the air stream, is moving very rapidly relative to the central (fuel) jet. It was shown in Ref. 11 that recirculation zones exist in a constant density, coaxial jet flow when the outer stream to inner stream velocity ratio is 13 or larger. For higher velocity ratios, a circulating vortex is established at the central jet centerline which enhances mixing between the streams. This "aerodynamic" phenomenon can be utilized to effect flameholding. In a practical demonstration of aerodynamic flameholding as part of the present study, a fuel injector was designed to produce an air-to-fuel velocity ratio of approximately 20:1 at stoichiometric operation using natural gas. The lip of the injector was made as small as practicable, i.e., ~0.018 cm, to prevent flameholding on back-step-associated recirculation zones. The particular injector design was based on the requirement that the momentum flux ratio of the air stream relative to the fuel stream exceeds 169, which evolves from a minimum air-to-fuel velocity ratio (V_a/V_f) of 13 for constant density flow. That is,

$$\rho_a V_a^2 / \rho_f V_f^2 > 169 \qquad (1)$$

Since the density ratio, ρ_a/ρ_f, for air at 800°K and nautral gas at 300°K is about 0.75, the design velocity ratio must exceed 15:1 to satisfy the criterion given by Eq. (1). A margin of uncertainty was applied to arrive at the 20:1 injector actually selected. In the course of the demonstration experiments, a natural gas-air flame was stabilized over a wide range of inlet air temperatures and flow velocities and overall fuel-air ratios. These data, presented later, constitute the foundation for aerodynamic flame stabilization, an approach which relies on the formation of a recirculation zone from a momentum flux imbalance between concentric jets.

The aerodynamic flameholding technique, in principle, should result in a simplified determination of inlet conditions. In addition, this approach provides a unique opportunity to contrast swirling and non-swirling flow fields without the disruptive presence of a physical flameholder. Swirl vanes have been installed in the annular air passage for certain tests and omitted in others to provide swirl numbers, S, of 0, 0.3 and 0.6. The swirl number, defined as the ratio of the angular momentum flux to the product of the axial momentum flux and an effective nozzle diameter, may be expressed in terms of swirl vane angle and injector section geometry (see Appendix A).

The nature of the mixing-combusting flow field and, hence, pollutant formation rates are known to be dependent on the fluid residence times within the recirculation zone and the combustor and also on the temperature and pressure levels. Variations in mean combustor residence times can be effected simply through changes in the initial velocity of the air stream. In the present experimental study, the air flow rate was varied from 0.088 to 0.137 kg/sec for a fixed injector configuration, i.e., a fixed air/fuel area ratio, to produce significant changes in mean throughput velocity. Fluid residence times within the recirculation zone are dependent on the mixing rates, which are influenced by the air-fuel velocity ratio. In the present study, installation of injectors with different air/fuel area ratios provided air-fuel velocity ratios in the range 0.1 to 40. Variation in combustor pressure was obtained by the placement of a choke downstream from the combustor with allowed operation at pressure levels of approximately 4 and 7 atm, and correspondingly reduced flow velocities. Operation at different temperature levels, for a fixed overall fuel-air equivalence ratio, was accomplished by varying the temperature of the inlet air stream from 730-860°K.

Recent analytical studies (e.g., Ref. 12) have shown that fuel composition can significantly influence NO emissions from gas turbines operating on gaseous fuels. This effect, which is believed to be due primarily to the variation in heating value with fuel composition, was examined in the present program. Most of the experiments were conducted using natural gas, with a nominal higher heating value of 55 kJ/g. However, a number of tests were conducted using a synthesized fuel (natural gas/hydrogen/carbon monoxide in approximate molar proportions of 1.0/0.39/0.34), with a nominal heating value of 42 kJ/g, and vaporized propane, with a nominal heating value of 50 kJ/g.

Since many practical combustion devices operate on liquid fuels, a limited number of experiments was carried out using liquid propane to provide a comparison with results from the vaporized propane tests.

None of the fuels used in the present investigation contained organic-nitrogen compounds, so that the only source of combustion-generated NO is atmospheric (molecular) nitrogen.

B. Experimental Apparatus and Instrumentation

Combustor Facility

Tests were conducted in an instrumented, water-cooled combustion system (Fig. 2). The facility design was based on the considerations outlined in the previous section, with particular emphasis placed on acquisition of species concentration, temperature and velocity distributions throughout the reacting flow field for comparison with results obtained in the analytical study.

Air from a 30-atm supply, at flow rates up to 0.65 kg/sec, may be heated in an electrical heater section to provide inlet air temperatures up to 1000°K. Within the heater, the air flows through and around four, 6 m long stainless steel tubes which may be supplied with as much as 720 kw of electrical power. The heated air enters the circular annulus of a replaceable injector which is installed in the 12.23 cm diameter entry section. Fuel, introduced through three (air foil shaped) struts into the center delivery duct, is brought into contact with the annular air stream at the exit of the injector. Thereafter, mixing and chemical reaction

Schematic Diagram of Axisymmetric, Water-Cooled Combustion System.

ALL DIMENSIONS IN CM

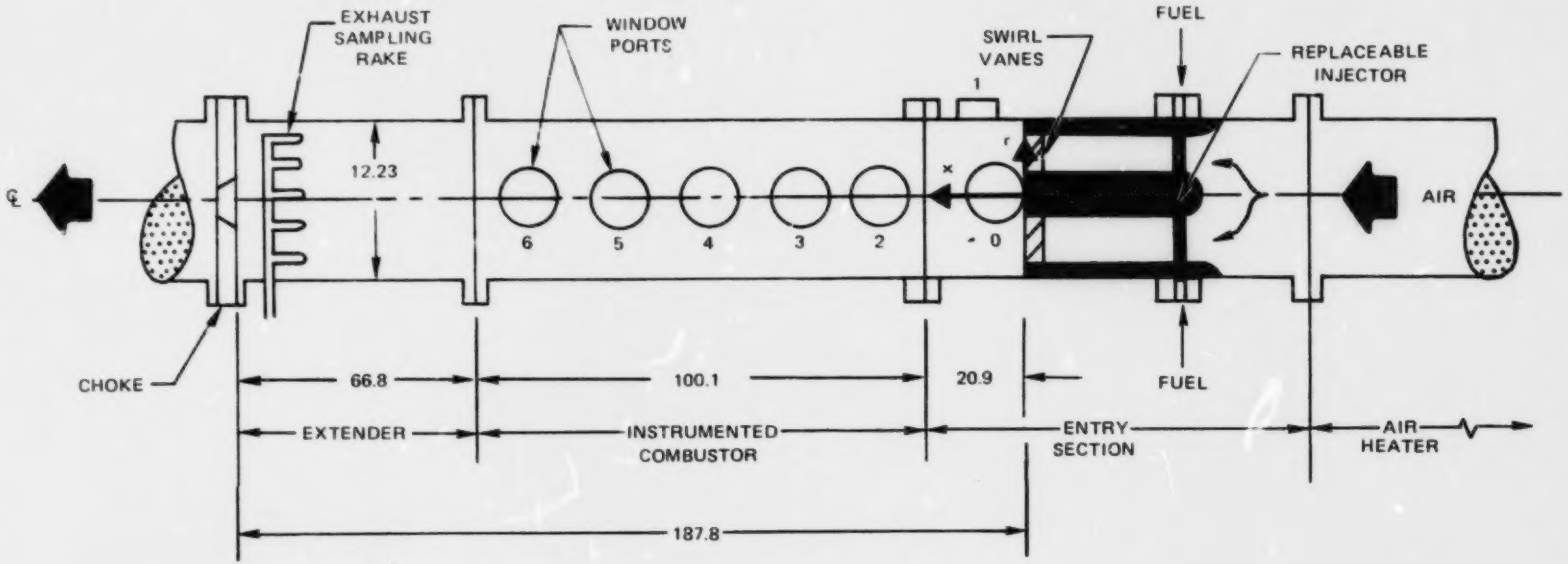
EXHAUST SAMPLING RAKE
WINDOW PORTS
SWIRL VANES
FUEL
REPLACEABLE INJECTOR
1
r
x
12.23
6
5
4
3
2
0
AIR
℄
CHOKE
66.8
100.1
20.9
FUEL
EXTENDER
INSTRUMENTED COMBUSTOR
ENTRY SECTION
AIR HEATER
187.8

WINDOW PORT LOCATIONS

PORT NO.	x_{c_i} (CM)	x_{c_i}/r_o
0	3.18	0.52
1	7.62	1.25
2	37.29	6.10
3	54.28	8.88
4	71.27	11.66
5	88.27	14.43
6	105.26	17.21

EXHAUST SAMPLING RAKE LOCATION AT 182.45 CM

FIG. 2

N12–171

proceed at constant area in the remainder of the injection section and into the instrumented combustor and extender sections. In order to impart swirl to the air flow, straight swirl vanes are inserted into the annular passage of the injector. The trailing edges of the swirl vanes are flush with the injector exit plane. The three injectors utilized in the study are described in Fig. 3 in terms of the ratio of the inner and outer diameters of the air annulus, $Z = d_h/d$, and the nominal air-to-fuel velocity ratio, $m = V_a/V_f$, associated with air and natural gas coaxial jets having an equivalence ratio, Φ, of 0.92. Swirl vane designs also are shown in Fig. 3, where the swirl number, S, has been computed from the injector geometry, Z, and the angle of the swirl vanes, η, according to the following expression (derived in Appendix A):

$$S = \frac{1}{3} \frac{(1 - Z^3)}{(1 - Z^2)^{1.5}} \tan \eta \qquad (2)$$

A swirl number of 0.3 connotes moderate swirl, while $S = 0.6$ results in a relatively high swirl situation. A practical upper limit of $S = 0.8$ exists for straight blades from the standpoint of packaging the vanes.

Observation of the combusting flow may be made through the 6.4-cm diameter window ports in the entry and combustor sections (Fig. 2). A pair of window ports 180 deg apart are present at each location, with the exception of station no. 1. The location of a port directly downstream of the injector exit plane allows an unhindered view of the flame in the vicinity of the fuel delivery duct. A second port in the entry section (no. 1) was located to permit acquisition of probe measurements very close to the injector exit. These measurements should provide the inlet or initial conditions needed in the analytical modeling effort. The combustor probing device used to make these measurements is compatible with all ports and may replace a glass window or water-cooled plug in any given port. Port locations are listed on Fig. 2.

The 12.23 cm diameter, 100.1 cm long instrumented combustor is divided into three water-cooling zones of approximately equal length. Water flow can be set independently in each zone, as needed, to keep wall temperature roughly constant along the entire length of the combustor. Temperatures are set and monitored using thermocouples installed on the combustor surface, and at various depths in the combustor wall and cooling passages. Two static pressure tap locations also are available at opposite ends of the combustor. Flow exhausts from the combustor and extender sections to the facility exhaust stack. Combustor extender (spool) pieces, 33.4 cm in length, are inserted when appropriate to fully contain the flame; the extender consisted of two spool pieces for the entirety of the current experimental effort. Chokes can be installed downstream of the extender to raise the pressure in the combustor. To date, high pressure operation has been limited to about 7 atm. A photograph of the combustion facility is given in Fig. 4.

FIG. 3

Injector and Swirl Vane Geometries

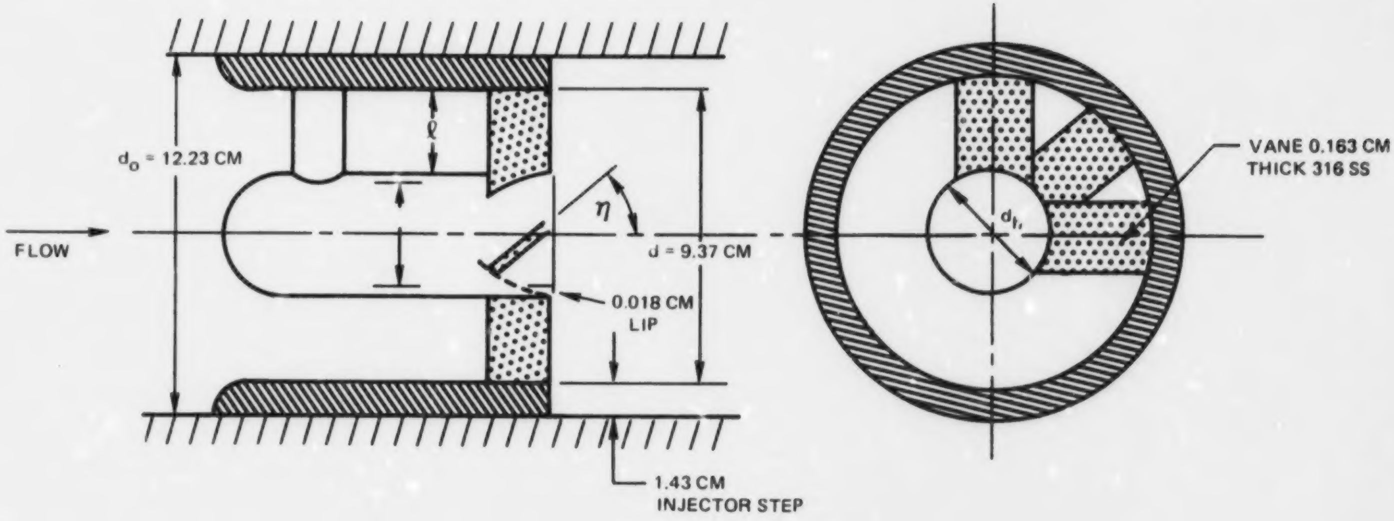
d_o = 12.23 CM
FLOW
ℓ
η
d = 9.37 CM
0.018 CM LIP
1.43 CM INJECTOR STEP
d_h
VANE 0.163 CM THICK 316 SS

INJECTOR DESIGNATION	m, VELOCITY RATIO*	d_f (CM)	$Z = d_h/d$	ℓ (CM)	S	η (DEG)	NO. OF VANES
I	20:1	6.314	0.677	1.499	0.3 0.6	28 47	18 12
II	8:1	4.727	0.508	2.306	0.6	53	12
III	0.3:1	0.757	0.084	4.290	0.6	60	8

*BASED ON NATURAL GAS AND Φ = 0.92

R05–5F

Combustor Facility

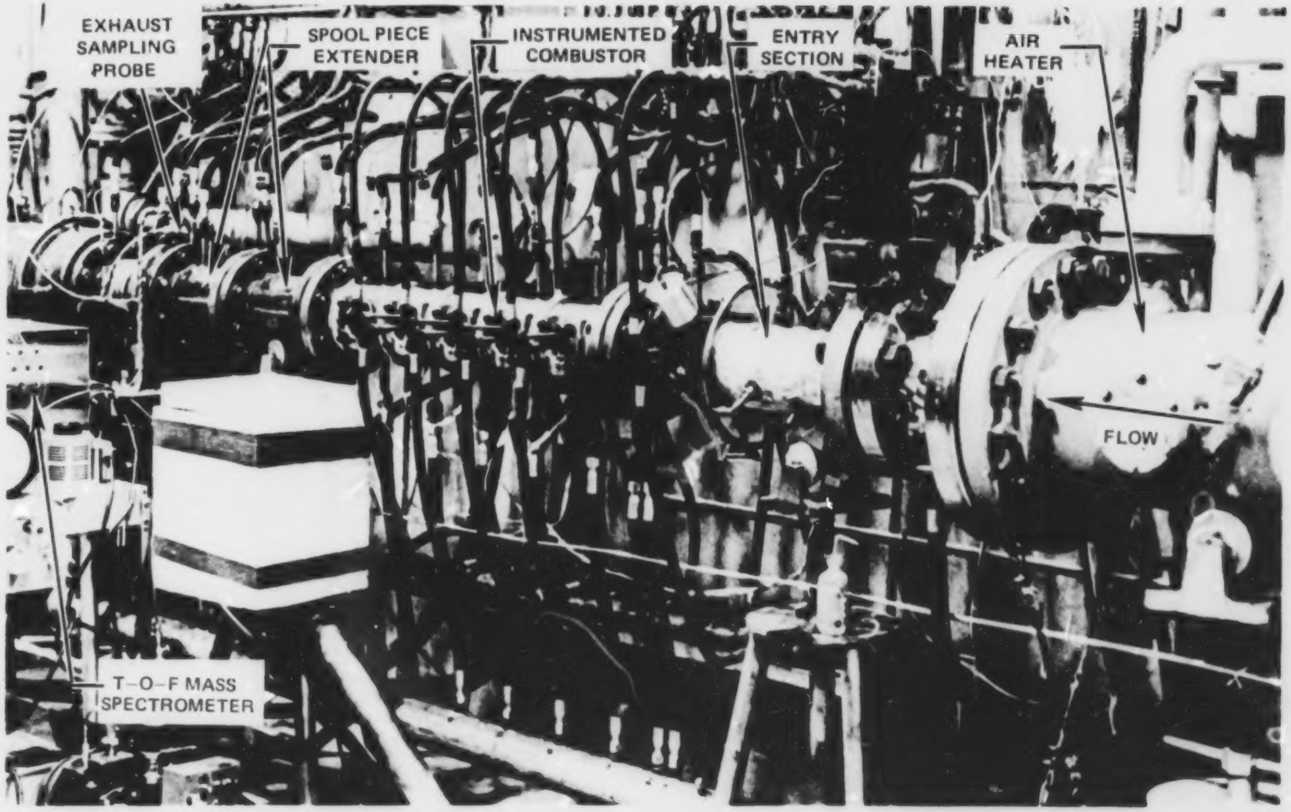
EXHAUST SAMPLING PROBE
SPOOL PIECE EXTENDER
INSTRUMENTED COMBUSTOR
ENTRY SECTION
AIR HEATER
FLOW
T–O–F MASS SPECTROMETER

FIG. 4

Probes

An exhaust probe rake is placed at the exit of the extender in certain tests to sample flow which has had the entire test section length to mix and react. Composition information is determined on-line by aspirating flow through a five-probe rake and analyzing the combined gas sample in a time-of-flight (TOF) mass spectrometer and a Scott Model 119 Exhaust Analyzer. The identical, choked probes constituting the rake (Fig. 5) are centered on equal areas to insure the acquisition of a flow sample which is truly representative at the exhaust plane. Pressurized hot water at 400°K was used as the coolant for the probes to minimize wall-catalyzed reactions and to prevent water condensation within the sample lines. Other details of the rake design are discussed in Appendix B, which contains descriptions of all the probes used in the investigation.

Temperature profiles at the exhaust plane and within the combustor were measured by traversing a calibrated-heat-loss thermocouple probe across a combustor diameter. Ordinarily, thermocouple materials limit application of these sensors to temperatures below about 2000°K. It is recognized, however, that radiation and conduction heat losses may reduce thermocouple temperature significantly below stream temperature. If proper calibration information is acquired simultaneously with the required temperature measurement, then the heat loss situation may be exploited to extend the range of thermocouple utilization up to 2500°K (Appendix B). A thermocouple probe of this type was applied without difficulty in the present combustion environment.

Temperature distributions in the combustor also were obtained with the double-sonic-orifice (DSO) probe portion of a two-probe rake (Fig. 6) inserted through the window ports. In the operation of this probe, ingested flow passes through two choked orifices in series, resulting in an interrelationship between orifice stagnation conditions:

$$\left(\frac{P_T A^* C_D F}{\sqrt{T_T}}\right)_1 = \left(\frac{P_T A^* C_D F}{\sqrt{T_T}}\right)_2 \qquad (3)$$

If orifice no. 1 is integrated with the probe tip, then P_{T_1} is the impact pressure and T_{T_1} is the total temperature to be determined. The parameter, F, which depends on the ratio of specific heats and molecular weight, is essentially the same at both orifices (i.e., $F_1 \approx F_2$). Also, A_1^* and A_2^* are readily established and P_{T_2} and T_{T_2} are available from measurements at orifice no. 2. Thus, T_{T_1} may be calculated from Eq. (3) if the ratio of flow coefficients, C_{D_1}/C_{D_2}, is known. Such information must be generated in calibrations over a range of orifice Reynolds numbers at various values of the ratio of wall temperature to stream temperature (see Appendix B). Calibrations of DSO probes are laborious and often frustrating since the presence of any foreign matter in the flow to deposit in or to scratch or pit throat regions,

Exhaust Sampling Rake

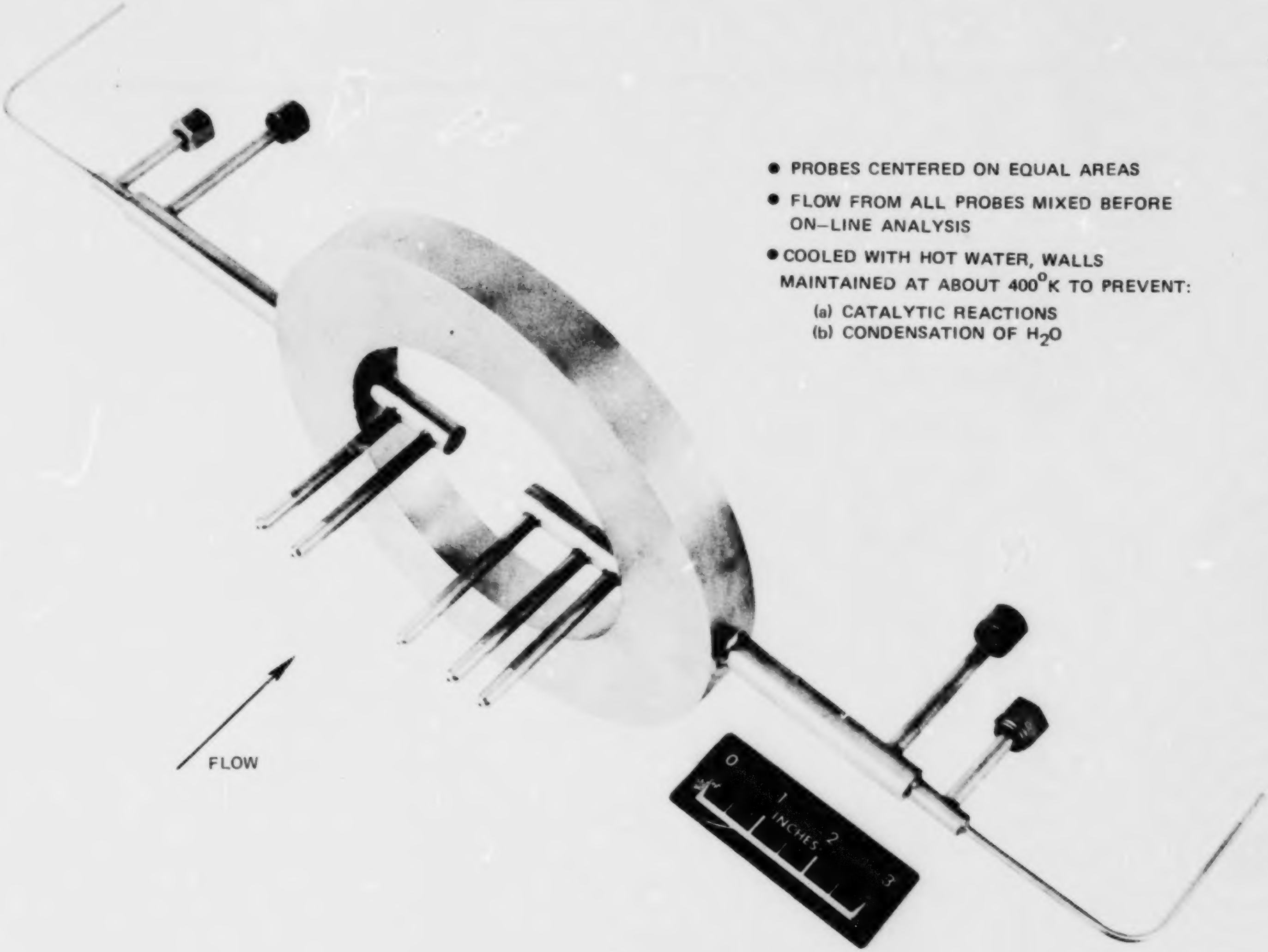

- PROBES CENTERED ON EQUAL AREAS
- FLOW FROM ALL PROBES MIXED BEFORE ON–LINE ANALYSIS
- COOLED WITH HOT WATER, WALLS MAINTAINED AT ABOUT $400^{o}K$ TO PREVENT:
  - (a) CATALYTIC REACTIONS
  - (b) CONDENSATION OF H_2O

FIG. 5

FIG. 6

Combustor Probing Device.

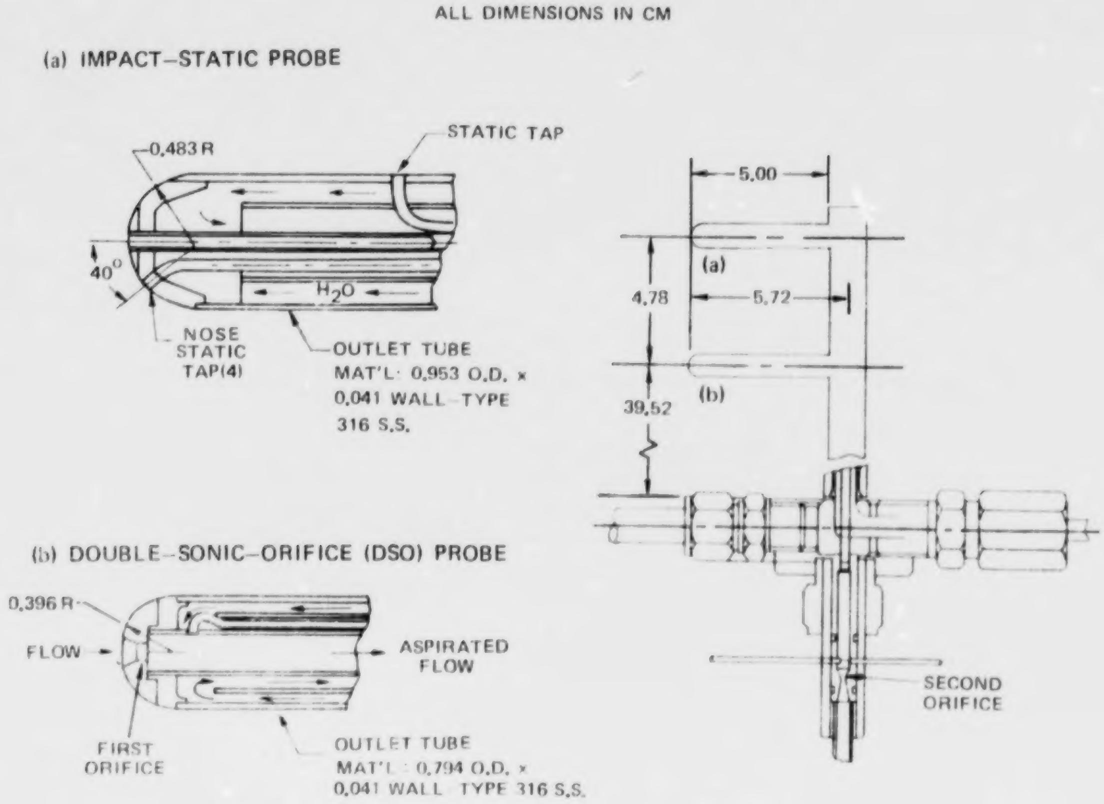
ALL DIMENSIONS IN CM
(a) IMPACT–STATIC PROBE
STATIC TAP
0.483 R
40°
H_2O
NOSE STATIC TAP(4)
OUTLET TUBE MAT'L: 0.953 O.D. × 0.041 WALL–TYPE 316 S.S.
5.00
(a)
4.78
5.72
(b)
39.52
(b) DOUBLE–SONIC–ORIFICE (DSO) PROBE
0.396 R
FLOW
ASPIRATED FLOW
FIRST ORIFICE
OUTLET TUBE MAT'L: 0.794 O.D. × 0.041 WALL TYPE 316 S.S.
SECOND ORIFICE

can affect the accuracy of the calibration. This limitation generally precludes application of the DSO technique to flows containing significant concentrations of particulates (soot, liquid droplets or coal particles). In the current effort, however, a probe was designed which minimizes flow coefficient corrections and which performed satisfactorily in all of the gaseous fuel tests. In addition, measurements obtained at identical test conditions with both the DSO probe and the thermocouple probe generally were in agreement (see Appendix B), thereby establishing a high confidence level in the temperature measurements.

The gas stream leaving the DSO probe is channeled to the sampling system (described below) where species concentration levels are identified.

The companion probe on the combustor rake is an impact-static probe. Flow velocity and direction can be determined from an interpretation of pressure differences between various static pressure locations on the probe and the impact pressure. Four static pressures are sensed at taps located on a centerline circle 40 deg from the probe tip (Fig. 6). Additional taps located along the probe at 2.11 cm and 4.02 cm from the tip provide useful local axial pressure information. Calibration of the probe in pitch and yaw and the use of this information to determine total flow angle is discussed in Appendix B. The impact-static probe performed satisfactorily in all regions of the combustor, except those regions with reverse flow. In these reverse flow (recirculation) zones, meaningful measurements of gas velocity were not obtained. Since the size, location and behavior of these recirculation zones significantly influence the combustor flow field (see Section II-C), the lack of velocity data in these zones is a major short-coming of the present experimental program.

Sampling System

The gas samples withdrawn via the exhaust probe or combustor DSO probe are analyzed on-line for the time-average concentration (mole fraction) of a number of species using a time-of-flight mass spectrometer and a Scott Exhaust Analyzer. In the schematic diagram of the sampling system, Fig. 7, the gas samples pass into a heated ($\sim 400^{\circ}K$), teflon-coated manifold. A portion of the gas sample is directed through a heated, teflon-coated line to the TOF mass spectrometer, located close to the probe assembly. In all experiments, the distance from the sample probe inlet to the mass spectrometer inlet was less than 60 cm. The mass spectrometer was used to measure the concentration of CO_2, O_2 and NO in the gas sample. The remainder of the gas sample passed successively through a condensate trap ($\sim 277^{\circ}K$) to remove water vapor, and an unheated teflon-coated line to the Scott Analyzer. The Analyzer, located in the combustion facility control room approximately 10 m from the combustor, was used to measure the concentration of CO, CO_2, O_2, NO, NO_2, and unburned hydrocarbons (THC) in the gas sample. The redundant sampling instrumentation provided a measure of the influence of the long line (and condensate trap) connecting the sampling probe to the Analyzer on the gas sample received by the Analyzer. Output signals from the TOF mass spectrometer and Analyzer were sent through a multiplexer

FIG. 7

On-Line Gas Analysis System.

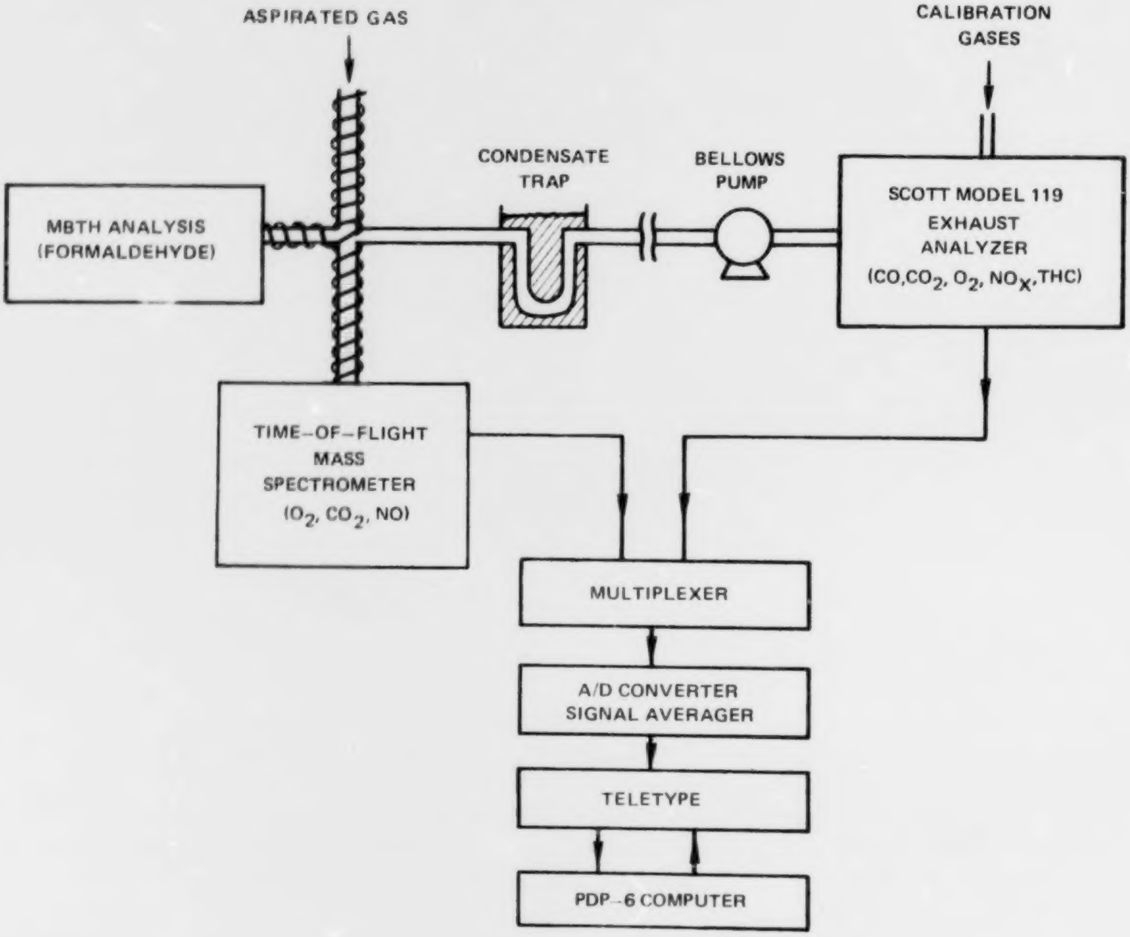

ASPIRATED GAS
CALIBRATION GASES
CONDENSATE TRAP
BELLOWS PUMP
MBTH ANALYSIS (FORMALDEHYDE)
SCOTT MODEL 119 EXHAUST ANALYZER (CO, CO_2, O_2, NO_x, THC)
TIME-OF-FLIGHT MASS SPECTROMETER (O_2, CO_2, NO)
MULTIPLEXER
A/D CONVERTER SIGNAL AVERAGER
TELETYPE
PDP-6 COMPUTER

N12-1

and an analog-digital converter to be processed and stored in a signal averager. Typically, at each test condition, sampling data were acquired for a period of 2-3 minutes. Upon completion of the tests, the stored data were processed immediately using a direct link to a PDP-6 computer. Processed data received via teletype were verified prior to initiation of subsequent tests. In a limited number of tests, the formaldehyde concentration in the exhaust was measured using the MBTH wet chemical method. Gas samples for these measurements were withdrawn from the heated manifold and passed through the sampling device. Formaldehyde data were reduced manually.

A detailed description of the TOF mass spectrometer, the Scott Exhaust Analyzer and the MBTH wet chemical method is presented in Appendix C, together with a discussion of calibration procedures, data reduction techniques and evaluation of experimental errors.

C. Experimental Results

Description of the Experiments

The experimental program was comprised of two different types of tests: (1) input-output tests, and (2) flow-field mapping tests. In the input-output tests, approximately fifty experiments were conducted with the objective of determining the influence of various combustor input parameters on species concentration levels in the exhaust flow. Generally, for a particular injector model and swirl vane insert, fuel-air equivalence ratio was varied from fuel lean to rich conditions at two or more levels of inlet air temperature, air flow rate and combustor pressure. Exhaust flow temperature profiles also were acquired for selected input-output test conditions. A matrix of test conditions for natural gas, synthesized fuel and vaporized propane is given in Table I. The ranges of parameters investigated encompass those found in practical combustion devices.

Results from the input-output tests were used to determine which combustor input parameters had the greatest influence on pollutant emissions. From this information, a matrix of test conditions was established for the flow field mapping experiments. In each of these mapping experiments, the mole fractions of NO, NO_2, CO, CO_2, O_2 and total hydrocarbons, the total temperature and the axial flow velocity and flow direction were measured throughout the combustor. Detailed combustor maps developed from these data were studied to provide an understanding of the changes in flow field characteristics and, ultimately, pollutant formation which accompany variations in key input parameters. During each of the combustor mapping tests, the two-probe rake was inserted and traversed along a diameter at every window port location. Occasionally, both window ports at a particular port location were entered in order to acquire data for assessing the symmetry of the flow with respect to the combustor centerline. In addition, high-speed color motion pictures (500 frames per sec) were taken at port location "0" for most test conditions to provide visual records of the combusting flow in the vicinity of the injection plane.

TABLE I. MATRIX OF NOMINAL TEST CONDITIONS: INPUT-OUTPUT EXPERIMENTS

Fuel*	S	V_a/V_f	P (atm)	Φ	T_a (°K)	$\dot{w}_a$ (kg/sec)
NG	0	22	1	0.7-1.2	740	0.132
NG	0	22	3.6	0.8-1.1	740	0.132
NG	0	22	1	0.8-1.1	860	0.132
NG	0	22	1	0.8-1.1	740	0.088
NG	0.3	22	1	0.8-1.1	740	0.132
NG	0.6	22	1	0.8-1.1	740	0.132
NG	0.6	22	3.6	0.8-1.1	740	0.132
NG	0.6	9.4	1.0	0.8-1.1	740	0.132
NG	0.6	0.2	1.0	0.5-1.3	740	0.132
SYN	0	15	1.0	0.8-1.1	740	0.132
SYN	0.6	15	1.0	0.8-1.0	740	0.132
SYN	0.6	15	3.6	0.8-1.0	740	0.132
PG	0	35	1.0	0.8-1.1	740	0.132
PG	0.3	35	1.0	0.8-1.0	740	0.132
PL	0.3	--	1.0	0.8-1.0	740	0.132
PL	0.3	--	6.6	0.8-1.0	740	0.132

* NG = natural gas
SYN = synthesized fuel ($CH_4/H_2/CO$)
PG = gaseous propane
PL = liquid propane

Input-Output Experiments

Significant trends in the exhaust concentration and temperature data obtained in the input-output experiments are illustrated by a series of graphs showing variations in the exhaust emissions and temperature with changes in combustor input parameters. A complete compilation of the data is given in tabular form in Appendix D.

Average exhaust gas concentrations (dry basis) of CO, CO_2, O_2, NO, NO_2 and THC for a 1 atm, non-swirling natural gas-air flame in Fig. 8 typify the input-output measurements. The natural gas used in the experiments is principally CH_4 (>97%) with small amounts of other gaseous hydrocarbons, CO_2 and N_2. Detailed analyses of the gaseous fuels are given in Appendix F. During acquisition of the data, the inlet air flow rate was held constant, and a range of overall equivalence ratios was obtained by varying the fuel flow rate. The concentration data shown in Fig. 8 are reported as measured and were obtained using the 22:1 injector; however, the air-fuel velocity ratio varied between 16.6 and 27.4 in these tests as the fuel flow was varied. As the overall equivalence ratio is increased, the exhaust O_2 concentration decreases significantly while the CO and THC concentrations substantially increase. Concentrations of CO , NO and NO_2 in the exhaust gas are only moderately dependent on overall equivalence ratio, Φ. Measured levels of O_2 and CO_2 are approximately equal to the calculated equilibrium concentrations in the exhaust gas over the entire range of equivalence ratios investigated. Equilibrium calculations assumed adiabatic combustion of the fuel-air mixture for the measured inlet conditions. For $\Phi < 1$, measured CO levels are somewhat larger than the equilibrium values; however, as the equivalence ratio increases, measured CO levels approach the equilibrium values. Measured THC concentrations are very large compared with calculated equilibrium values over the entire range of equivalence ratios investigated. Measured NO concentrations are substantially less than equilibrium values. Similar trends of CO, THC and NO emissions with overall equivalence ratio have been reported for furnaces (Ref. 2) and gas turbines (Ref. 3). The observed NO_2 concentrations are larger than equilibrium levels in the exhaust gas. However, as noted in Appendix C, it is likely that some NO_2 is produced by oxidation of NO and some NO_2 is lost during transfer of gas samples to the Exhaust Analyzer, so that reported NO_2 levels must be considered as uncertain.

Exhaust plane temperature profiles for several non-swirling flows are compared to calculated adiabatic combustion temperatures in Fig. 9. Predictably, the exhaust plane temperature is highest on the combustor centerline, and decreases as the cooled combustor walls are approached. Exhaust plane temperature profiles are similar for this combustor configuration for overall equivalence ratios between 0.8 and 1.2, with small differences most notable near the combustor centerline. Measured centerline temperatures are 10-15 percent lower than the calculated adiabatic combustion temperatures.

The influence of inlet air swirl and pressure on the average NO concentration in the exhaust of the combustor operating on natural gas-air is shown in Fig. 10. For

FIG. 8

Average Species Concentration in Combustor Exhaust Gas. Combustion of Natural Gas with 0.132 kg/sec of 740°K Air, S=0, V_a/V_f=22, at 1 atm. Species concentrations reported as measured.

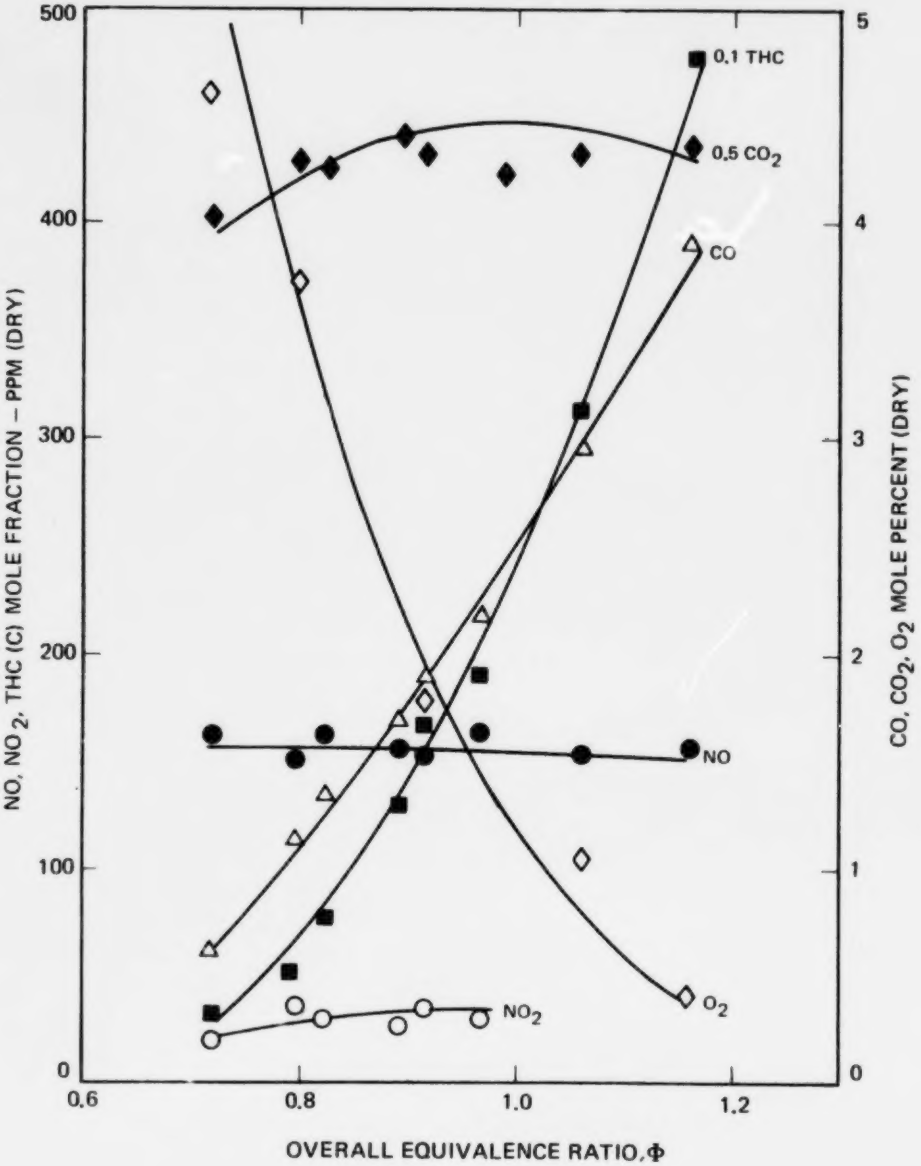

N12–133

FIG. 9

Exhaust Temperature Profiles for Non-Swirling ($S=0$) Flow. Combustion of Natural Gas with 0.132 kg/sec of 740°K Air, $V_a/V_f=22$, at 1 atm.

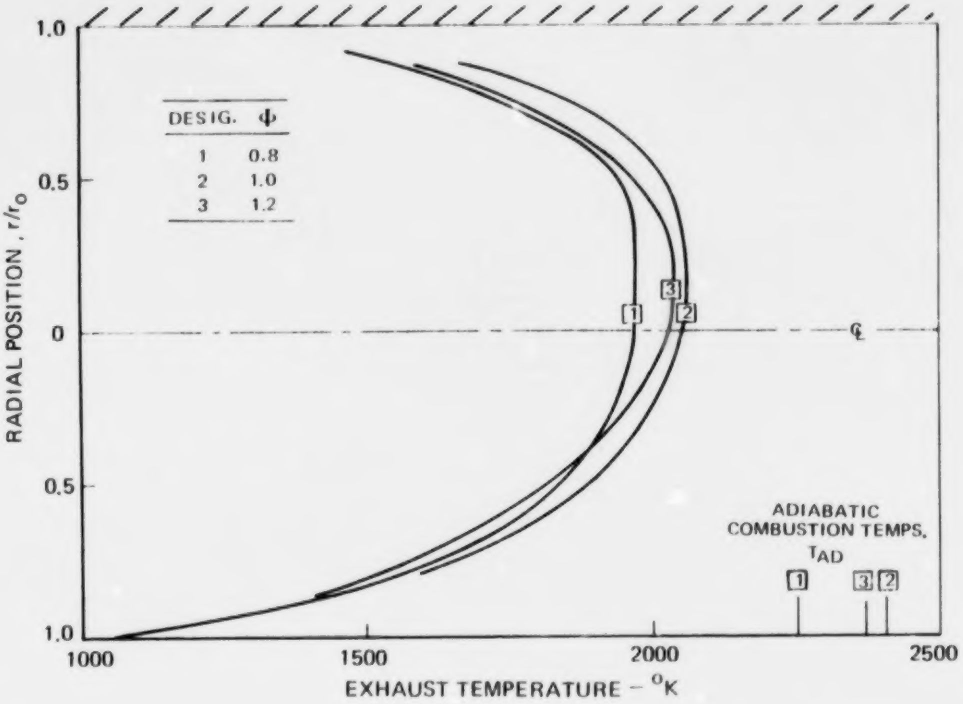

FIG. 10

Influence of Inlet Air Swirl and Combustor Pressure on Average Exhaust NO Concentration for Combustion of Natural Gas with 0.132 kg/sec of 740°K Air, V_a/V_f=22.

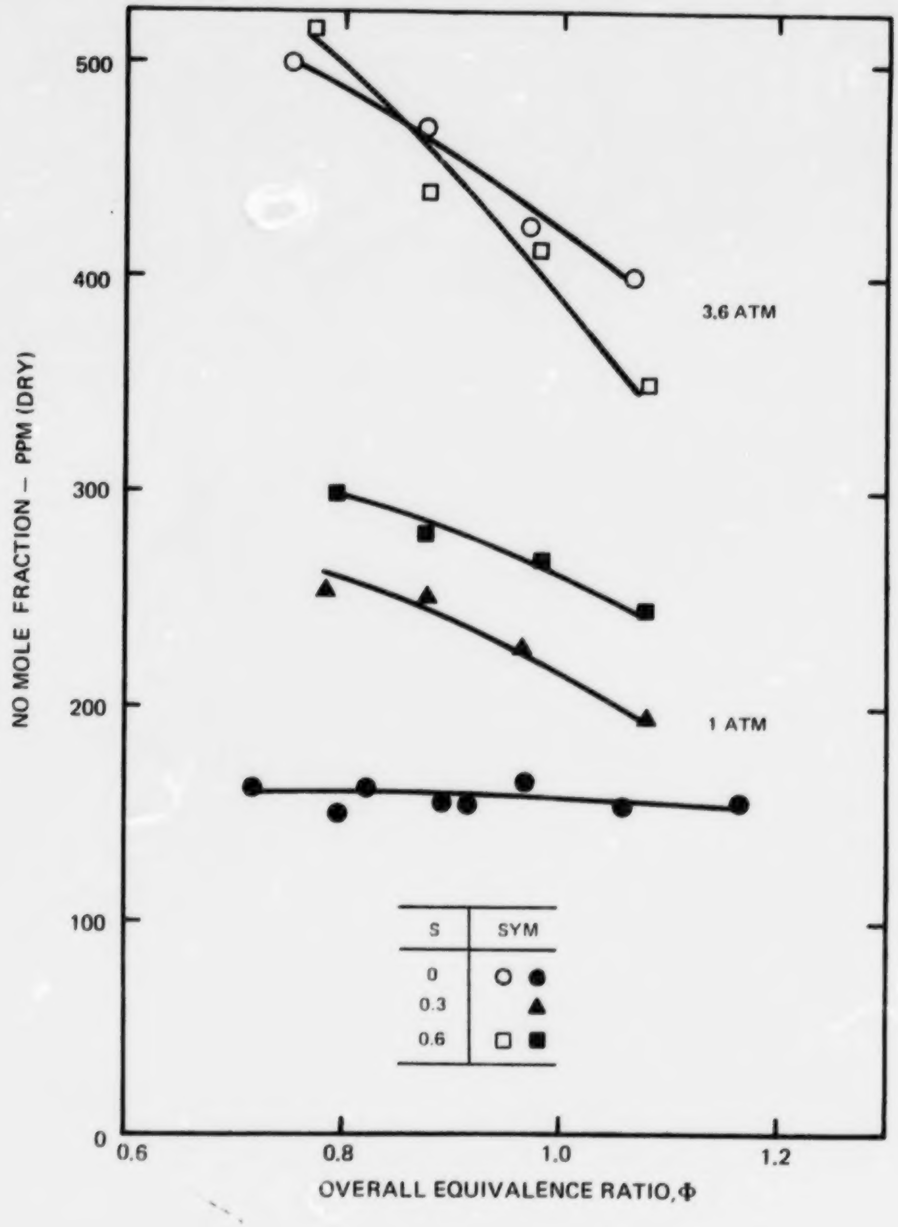

N12-133-

the range of overall equivalence ratios investigated, the air-fuel velocity ratio varied between 19.4 and 26.0. The data for no inlet air swirl (S=0) were taken from Fig. 8. For a combustor pressure of 1 atm, increasing inlet air swirl raises the NO concentration in the exhaust gas. This effect is more pronounced for the lower overall equivalence ratios. Heap and his co-workers (Ref. 1) have reported similar behavior for NO emissions from nautral-gas-fired furnaces using axial fuel injection. It should be noted, however, that other fuel injection geometries (e.g., radial) can give variations in NO emissions with swirl which are significantly different from that observed with the present experimental configuration (See, for example, Ref. 1).

The double-lobed appearance of the exhaust plane temperature profile for a swirling flow (Fig. 11) provides a partial explanation for the enhanced NO production. In swirling flows, peak temperatures at the exhaust are significantly larger than in the non-swirling flows and, in fact, are in excess of the adiabatic combustion temperature calculated for the overall fuel-air equivalence ratio. Thus, since the NO formation rate is known to be strongly dependent on temperature, the higher temperatures found in swirling flows result in higher NO levels than in comparable non-swirling flows. For fixed inlet air swirl, increasing the combustor pressure generally results in a significant increase in the exhaust NO concentration. A similar trend of NO emissions with pressure has been reported by Mellor and his co-workers (Ref. 3) for a gas turbine. Some portion of the increase in exhaust NO with increasing combustor pressure may be attributed to increased gas residence time in the combustor. For a pressure of 3.6 atm, residence time is roughly 0.075 sec versus about 0.02 sec at 1 atm operation. At elevated combustor pressures, swirl has only a slight effect on the exhaust NO concentration. Reasons for this behavior are explored in a later section of this report.

Average CO and THC concentrations in the exhaust gas for the three swirl numbers investigated are given in Fig. 12 for a combustor operating at 1 atm. Imparting swirl to the inlet air stream reduces levels of THC in the exhaust gas. A similar variation in THC emissions with inlet air swirl was observed at a combustor pressure of 3.6 atm. Increasing the inlet air swirl also results in a reduction in exhaust CO concentrations for overall equivalence ratios less than one. However, for equivalence ratios greater than one, inlet air swirl has little or no effect on exhaust CO concentrations. The dashed line on Fig. 12 is the calculated equilibrium CO concentration, assuming adiabatic combustion. For the two swirling flows investigated, the measured exhaust CO concentrations are approximately equal to the equilibrium values over the entire range of overall equivalence ratios. For the non-swirling flow, the measured exhaust CO concentrations approach the equilibrium values for $\Phi > 1$. A similar effect of inlet air swirl on CO emissions was observed at a combustor pressure of 3.6 atm. Enhanced burnout of THC and CO with swirl can be explained in terms of associated changes which occur in temperature, velocity and O_2 distributions within the combustor (See results presented in the following section). The influence of an increase in pressure from 1 to 3.6 atm on average CO and THC exhaust concentrations is not large at any of the swirl numbers investigated. Data for

FIG. 11

Exhaust Temperature Profile for a Swirling (S=0.6) Flow. Combustion of Natural Gas with 0.132 kg/sec of 740°K Air, V_a/V_f=22, at 3.6 atm.

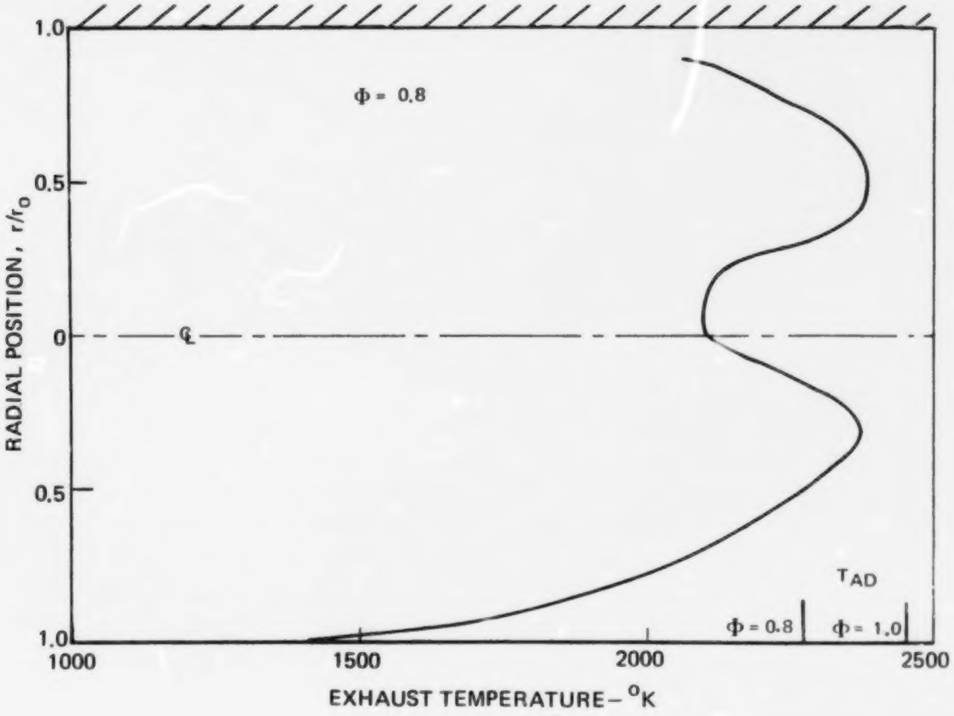

N12--13

FIG. 12

Influence of Inlet Air Swirl on Average Exhaust CO and THC Concentrations for Combustion of Natural Gas with 0.132 kg/sec of 740°K Air, V_a/V_f=22, at 1 atm.

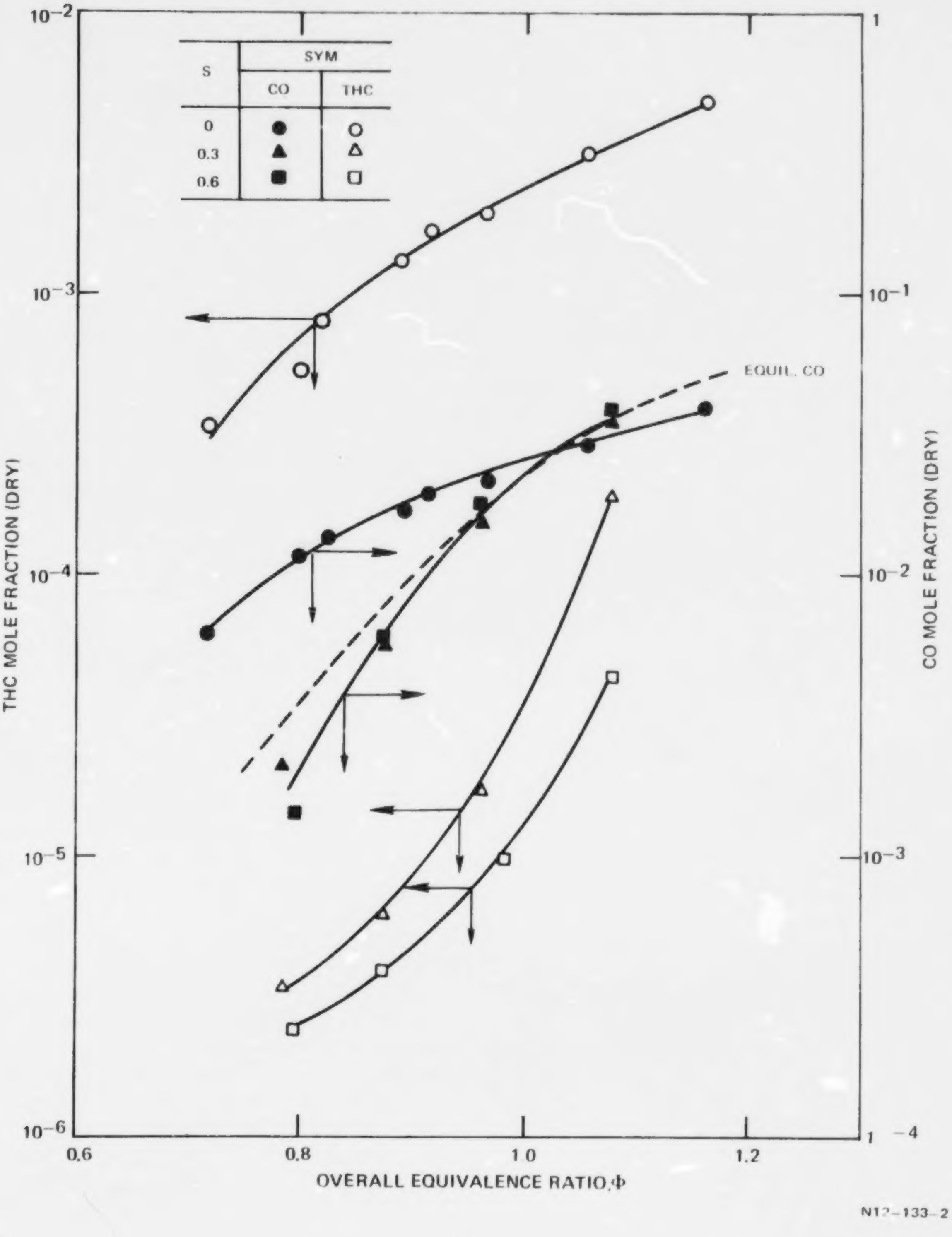

N12-133-2

non-swirling flow in Fig. 13 illustrate the extent of the pressure effect, i.e. a modest decrease in THC and virtually no change in CO as pressure is increased.

As indicated earlier, the interaction between fluid dynamic and chemical processes must be understood before it is possible to devise a model for pollutant formation in combustors. One parameter which has been identified as key to the establishment of the flow field within the combustor, the air-fuel velocity ratio, m, was varied during a series of input-output tests. Results from these tests are summarized in Figs. 14 and 15. The swirl number was approximately 0.6 for these tests. For data designated by nominal air-fuel velocity ratios of 22 and 9, the actual velocity ratios varied between 19.4 and 25.6 and between 7.6 and 10.3, respectively, as the fuel flow rate was reduced at constant air flow rate. Data at a nominal velocity ratio of 0.2 covered the range 0.13-0.26 as the fuel flow rate was decreased at constant air flow rate. A striking difference exists between NO exhaust concentrations levels in swirl-stabilized flames for air-fuel velocities much greater than unity and those for air-fuel velocities much less than unity. It is likely that this differen is due, in part, to a reduction in the volume of the hot zone in the vicinity of the injection plane, resulting from the relatively small diameter fuel injector, Fig. 3, used for the $V_a/V_f = 0.2$ experiments.

Average exhaust CO and THC concentration measurements for high air-fuel velocity ratios, i.e., 9-22, and low air-fuel velocity ratios of approximately 0.2 are shown in Fig. 15. Equilibrium CO values are plotted as the dashed line. These data are consistent with input-output data already presented, in that the set of initial conditions which yields lowest levels of NO in the exhaust, generally also displays the highest THC levels. Further, as observed for the exhaust NO concentration in Fig. 14, CO and THC concentrations in the exhaust gas are independent of air-fuel velocity ratios in the range 9-22. Measured exhaust CO concentrations closely correspond to the calculated equilibrium values for these ratios. In fact, measured and calculated CO concentrations agree for all velocity ratios, m, investigated for overall equivalence ratios exceeding 0.9. Leaner mixtures ($\Phi<0.9$) yield CO levels for $m \approx 0.2$ which are somewhat larger than those predicted on the basis of equilibrium considerations.

Variations in exhaust pollutant concentrations with inlet air velocity and pre-heat level are shown in Figs. 16-18. For a fixed inlet air temperature, a reduction in air flow rate (and hence velocity at constant ρA) of 50% resulted in an increase of about 30% in NO in the exhaust (Fig. 16). This behavior, which can be attributed primarily to changes in recirculation zone and combustor residence times, has been noted by Heap, et al. (Ref. 1) for gas-fired furnaces. The increased time for burnout also brought about reduced THC exhaust concentrations for all Φ investigated, Fig. 17. However, no significant change in exhaust CO with air flow rate was observed. At a fixed air flow rate, an increase in inlet air temperature from 742°K to 860°K resulted in an approximately doubling of the exhaust NO concentration. Other authors (Refs. 2 and 3) have noted similar trends of NO emissions with inlet air temperature in natural gas-fired furnaces and gas turbine combustors. Exhaust CO concentrations were unchanged for air inlet temperatures of 742°K and 860°K (Fig. 18), while exhaust THC levels were generally lower at 860°K. By comparison, Mellor, et al. (Ref. 3)

FIG. 13

Influence of Combustor Pressure on Average Exhaust CO and THC Concentration for Combustion of Natural Gas with 0.132 kg/sec of 740°K Air, V_a/V_f=22, S=0.

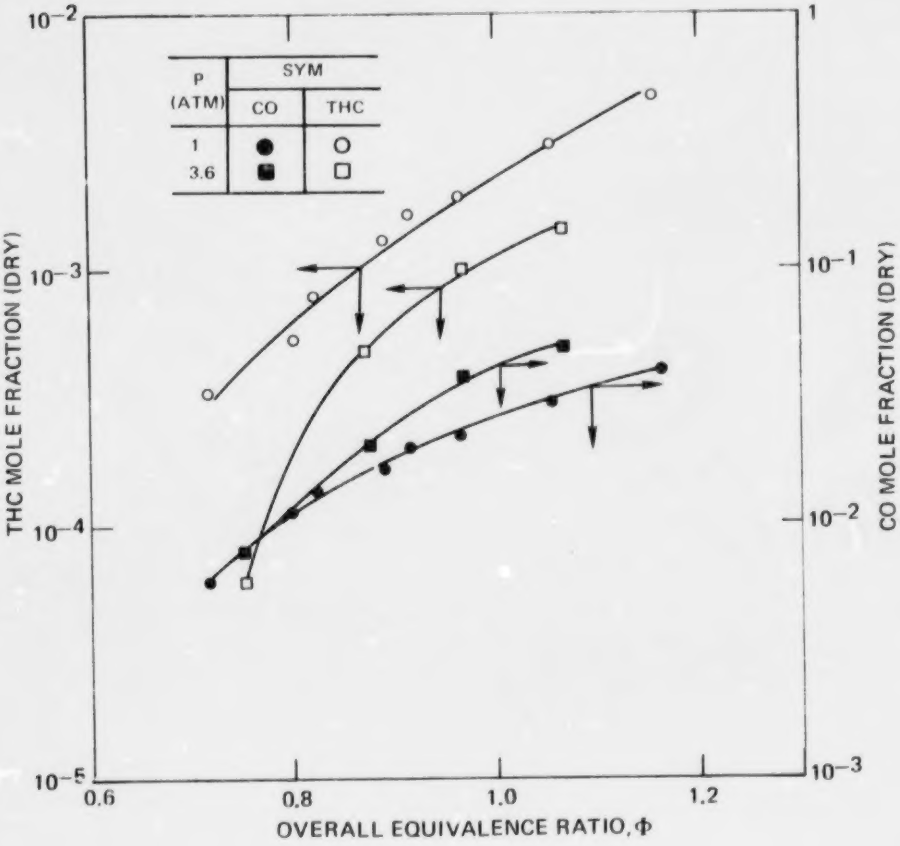

N12-133-9

FIG. 14

Influence of Air-Fuel Velocity Ratio on Average Exhaust NO Concentration in a Swirling (S=0.6) Flow. Combustion of Natural Gas with 0.132 kg/sec of 740°K Air at 1 atm.

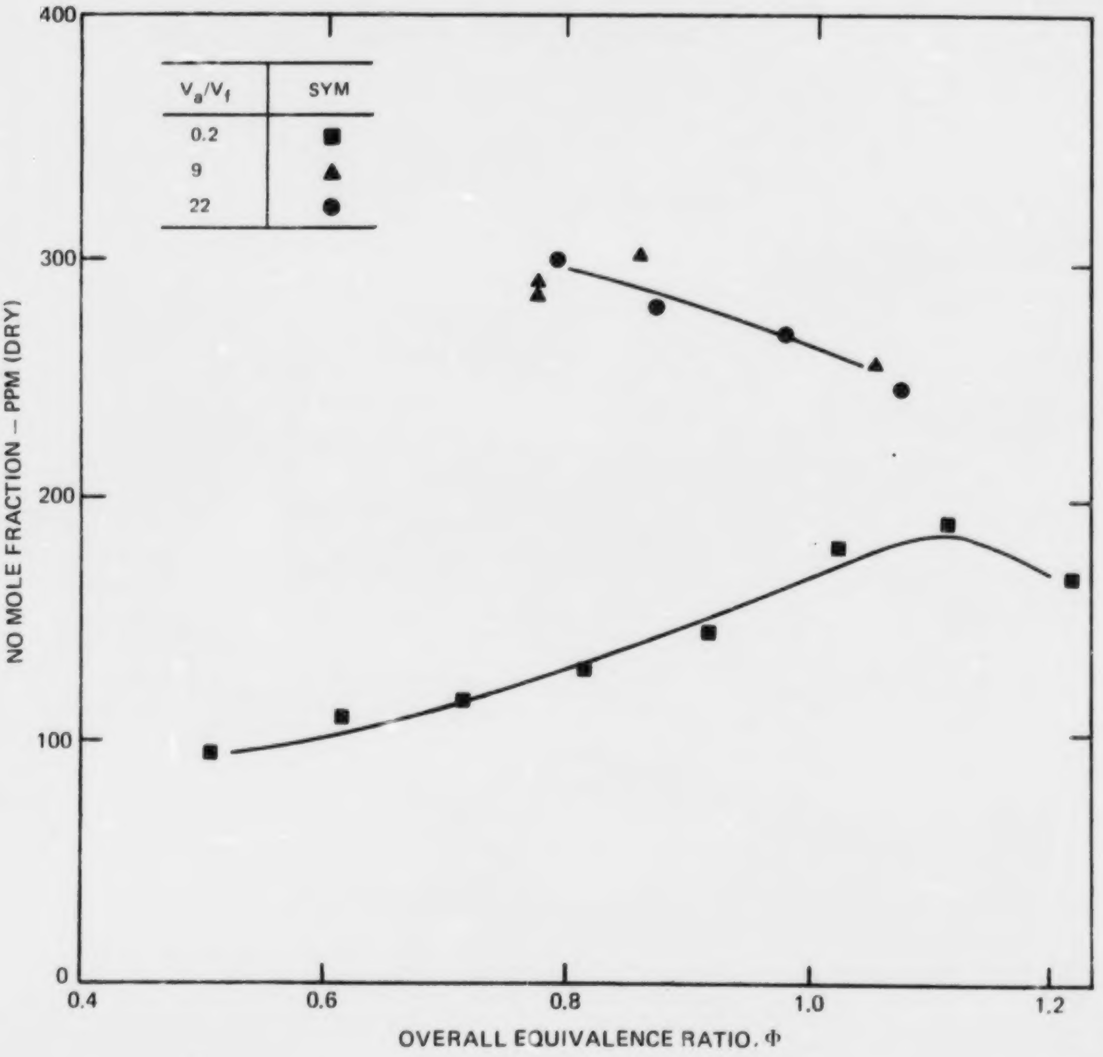

N12-13'

FIG. 15

Influence of Air-Fuel Velocity Ratio on Average Exhaust CO and THC Concentrations in a Swirling (S=0.6) Flow. Combustion of Natural Gas with 0.132 kg/sec of 740°K Air at 1 atm.

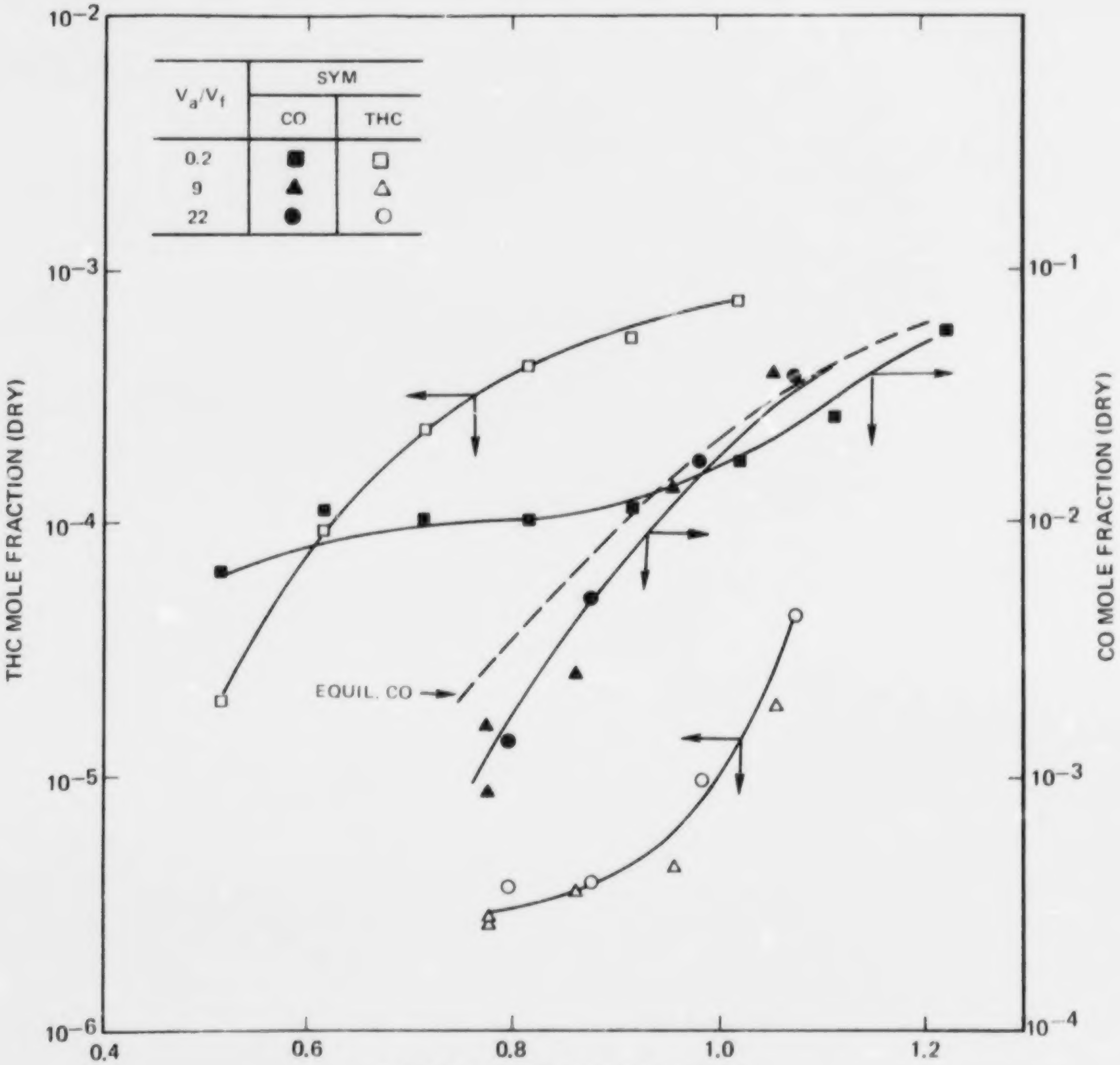

N12-133-12

FIG. 16

Influence of Air Flow Rate and Inlet Temperature on Average Exhaust NO Concentrations for Combustion of Natural Gas with Air, $V_a/V_f=22$, S=0, at 1 atm.

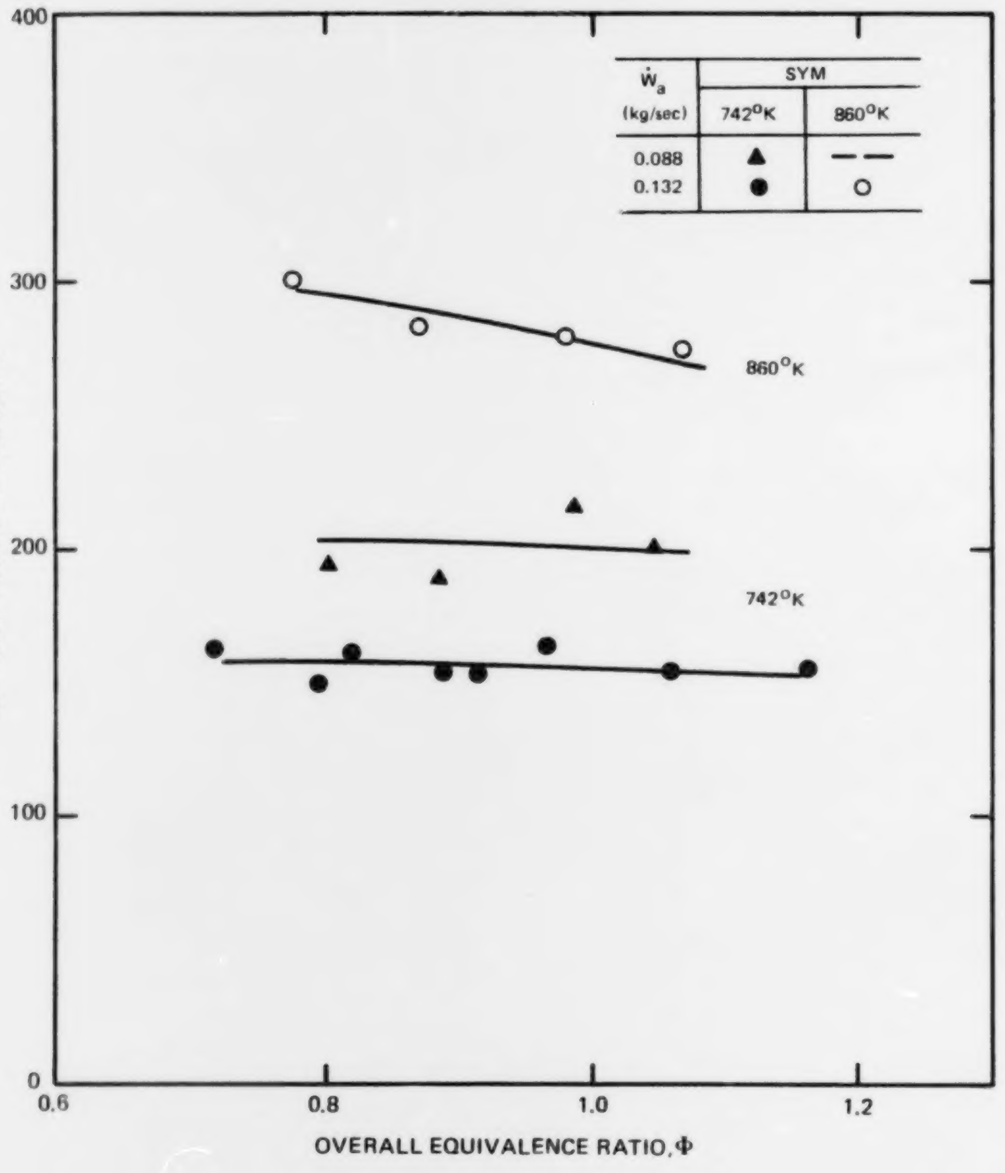

N12–133–1

FIG. 17

Influence of Air Flow Rate on Average Exhaust CO and THC Concentrations for Combustion of Natural Gas with 740°K Air, $V_a/V_f=22$, S=0, at 1 atm.

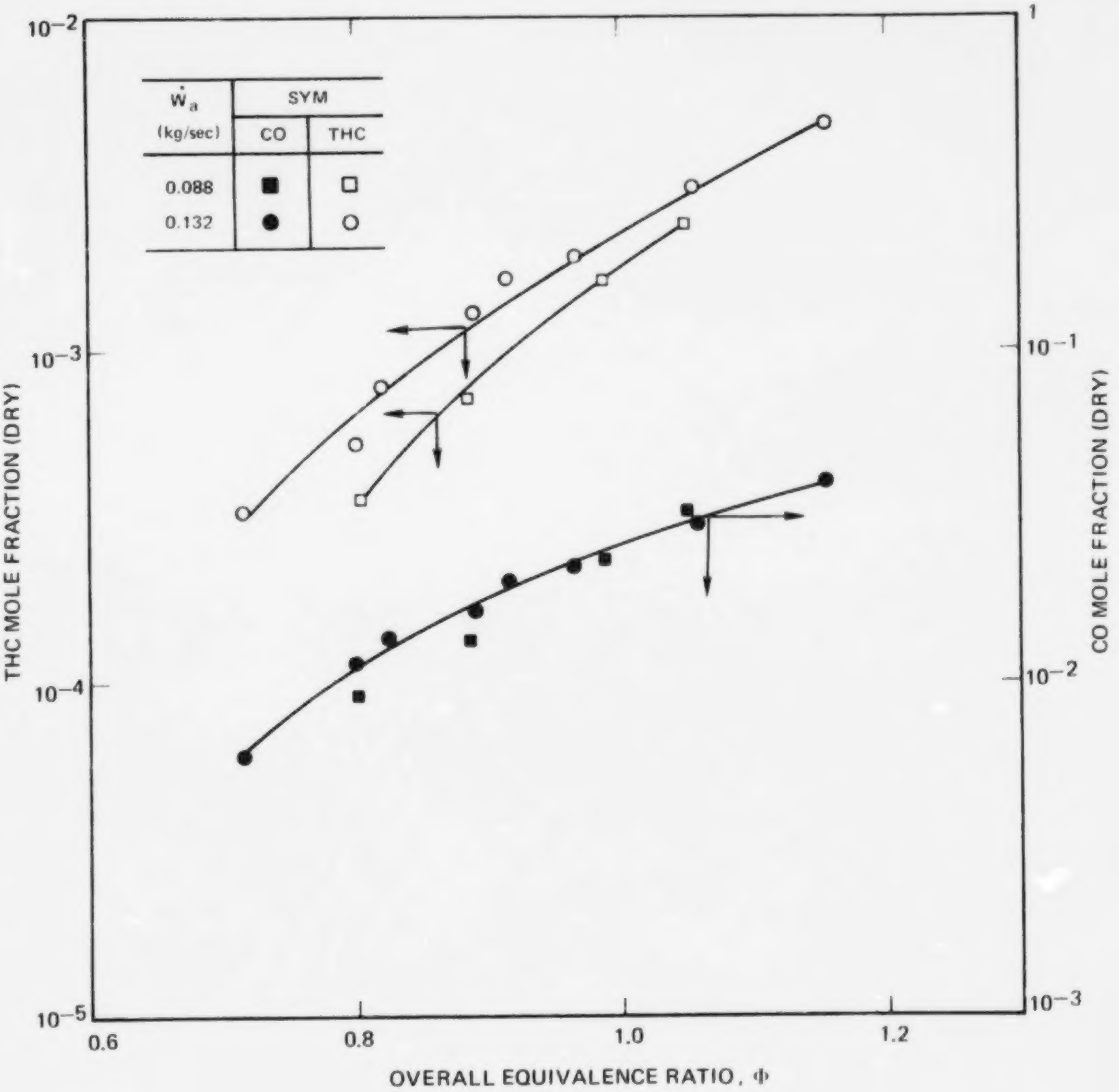

N12-133-1

FIG. 18

Influence of Inlet Air Temperature on Average Exhaust CO and THC Concentrations for Combustion of Natural Gas with 0.132 kg/sec of Air, V_a/V_f=22, S-0, at 1 atm.

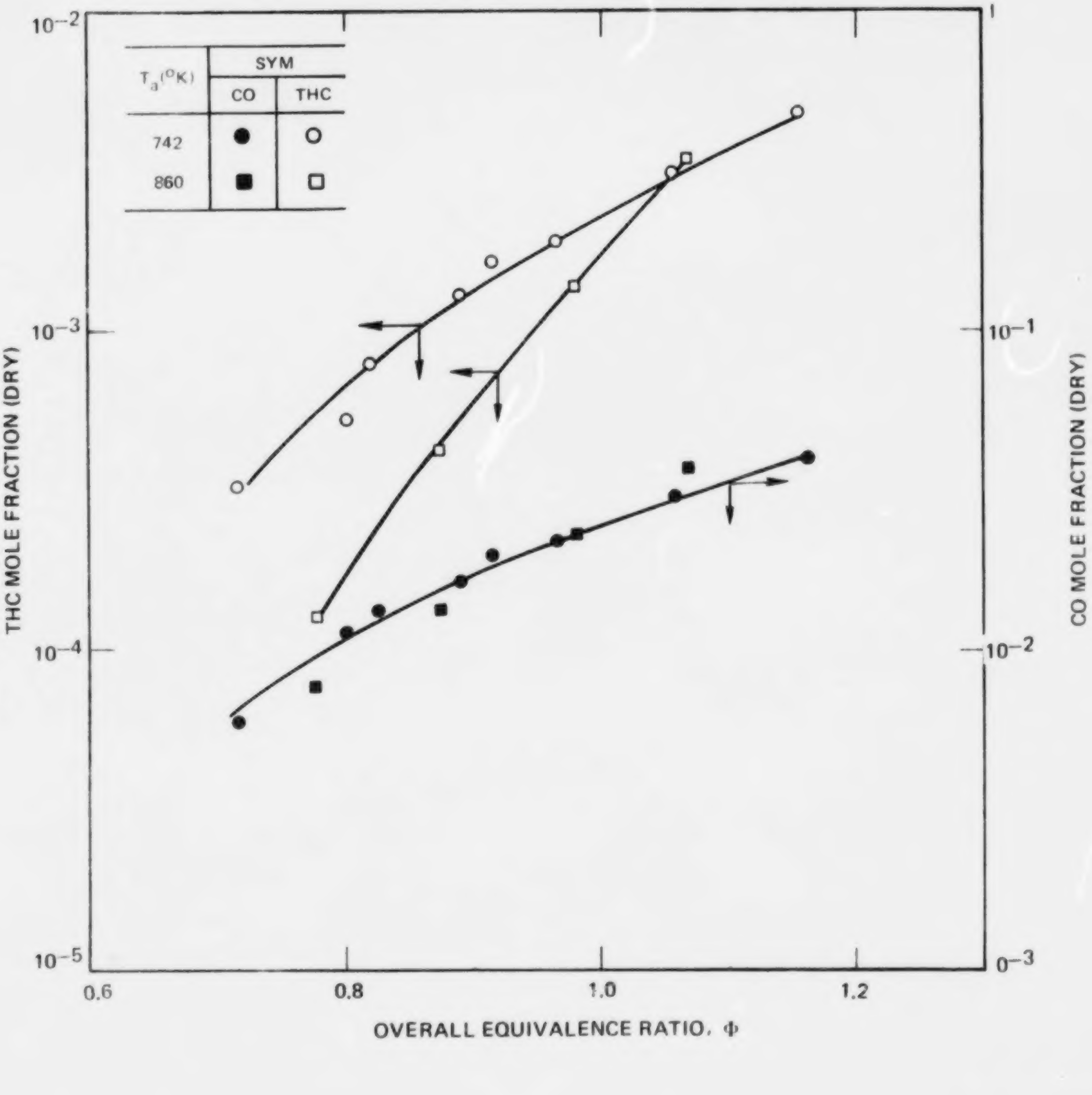

observed reductions in both CO and THC emissions from a gas turbine as the air inlet temperature was increased from 456°K to 536°K.

A number of input-output tests were conducted to determine the effect of fuel composition (heating value) on exhaust NO concentrations. Two gaseous fuels with heating values different from natural gas were employed in these tests -- a synthesized fuel ($CH_4/H_2/CO$), with a higher heating value of approximately 42 kJ/g* and vaporized propane, with a higher heating value of approximately 50 kJ/g. Measured exhaust NO concentrations for these two fuels are compared with NO concentration data for natural gas in Fig. 19. At zero swirl, exhaust NO levels for natural gas and the synthesized fuel are essentially the same, while the NO levels for propane are somewhat larger. Introduction of swirl increases exhaust NO concentrations for the synthesized fuel, but to a lesser degree than observed with natural gas. For a given overall fuel-air equivalence ratio, the firing rates (i.e., heat input per unit time) for the three gaseous fueld are ordered as follows: synthesized gas > vaporized propage > natural gas. From thermochemical considerations, one would expect the trend in NO exhaust concentrations to follow that of the firing rates. The observation that this is not the case, Fig. 19, suggests that there are significant differences in the flow fields for the three gaseous fuels and that these differences are influencing NO formation in the combustor. This point is examined in more detail in the following section.

The final series of input-output tests was conducted using liquid propane as the fuel. In these tests, the injector modification required for liquid fuel operation is the only notable change in the combustor. The injector module for liquid propane fuel resembled Injector I in that the air gap height, ℓ, is 1.499 cm. However, the 6.372 cm O.D. circular fuel delivery duct is capped off, in contrast to the configuration used with gaseous fuels. A Delevan nozzle was installed at the center of the cap, on the combustor centerline, to deliver a nominal 60 deg, solid cone liquid spray. Thus, in the liquid fuel tests, a large base region was present. Water cooling passages within the fuel delivery duct provided cooling of the base region.

Significant trends in the exhaust sampling data are illustrated in Figs. 20-22. Figure 20 shows the variation of the average NO concentration in the exhaust gas with inlet air swirl, pressure and overall equivalence ratio for the combustor operating on liquid propane and air. For purposes of comparison, exhaust NO concentrations for

---

*The fuel composition, and hence the heating value, was selected so as to provide air-fuel velocity ratios which matched those employed in the natural gas tests. For the composition selected, nominal air-fuel velocity ratios obtained using Injector I approximate those obtained with natural gas using Injector II.

FIG. 19

Average Exhaust NO Concentrations for Combustion of Natural Gas, Synthesized Fuel and Vaporized Propane. Combustion with 0.132 kg/sec of 740°K Air at 1 atm. $V_a/V_f=22$, for Natural Gas, $V_a/V_f=15$ for the Synthesized Fuel, $V_a/V_f=35$ for Vaporized Propane.

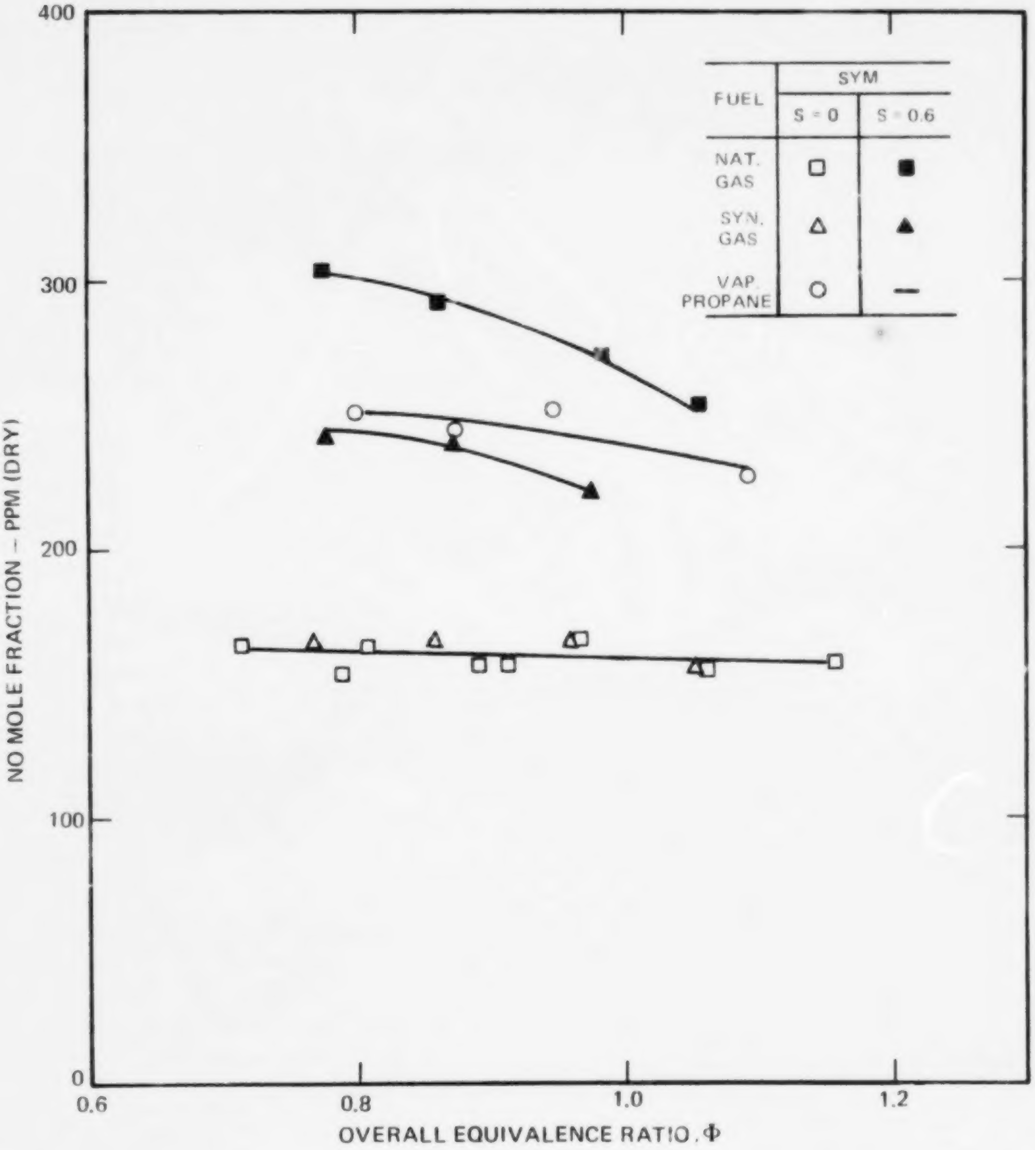

FIG. 20

Average Exhaust NO Concentrations for Combustion of Vaporized and Liquid Propane with 0.136 kg/sec of 740°K Air.

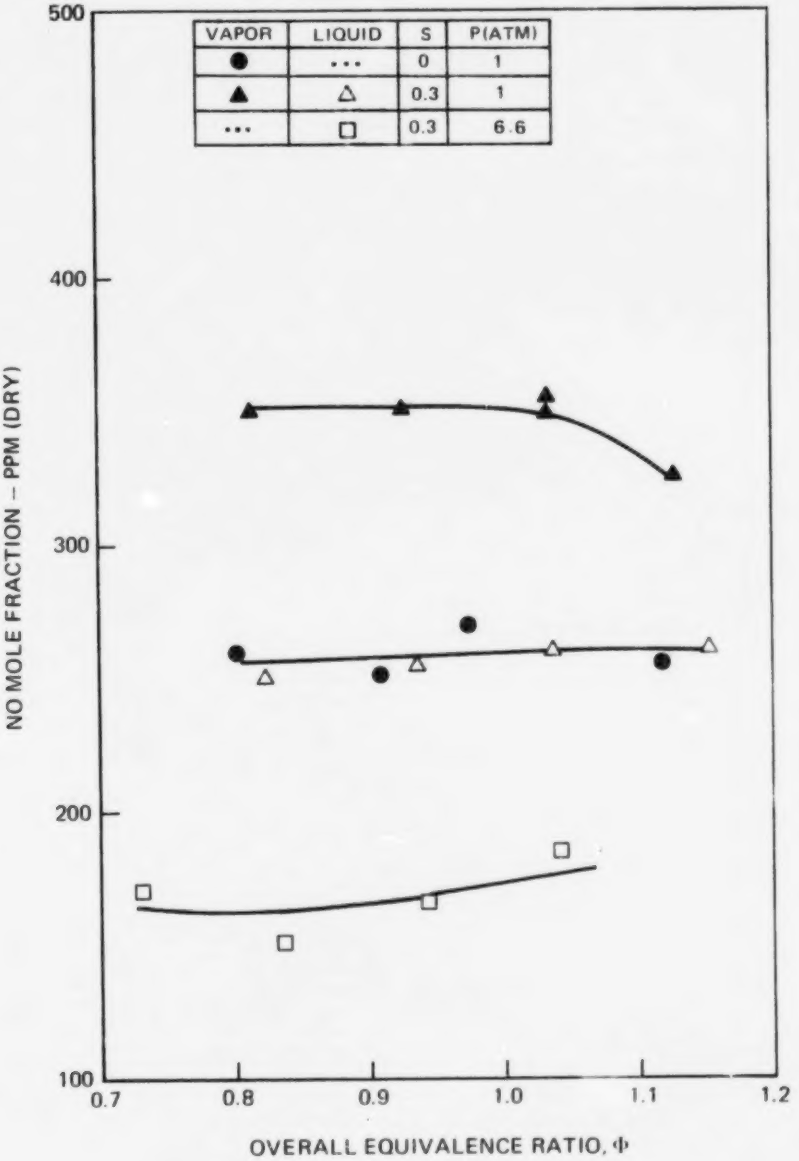

R02-29-8

FIG. 21

Average Exhaust THC Concentrations for Combustion of Vaporized and Liquid Propane with 0.136 kg/sec of 740°K Air.

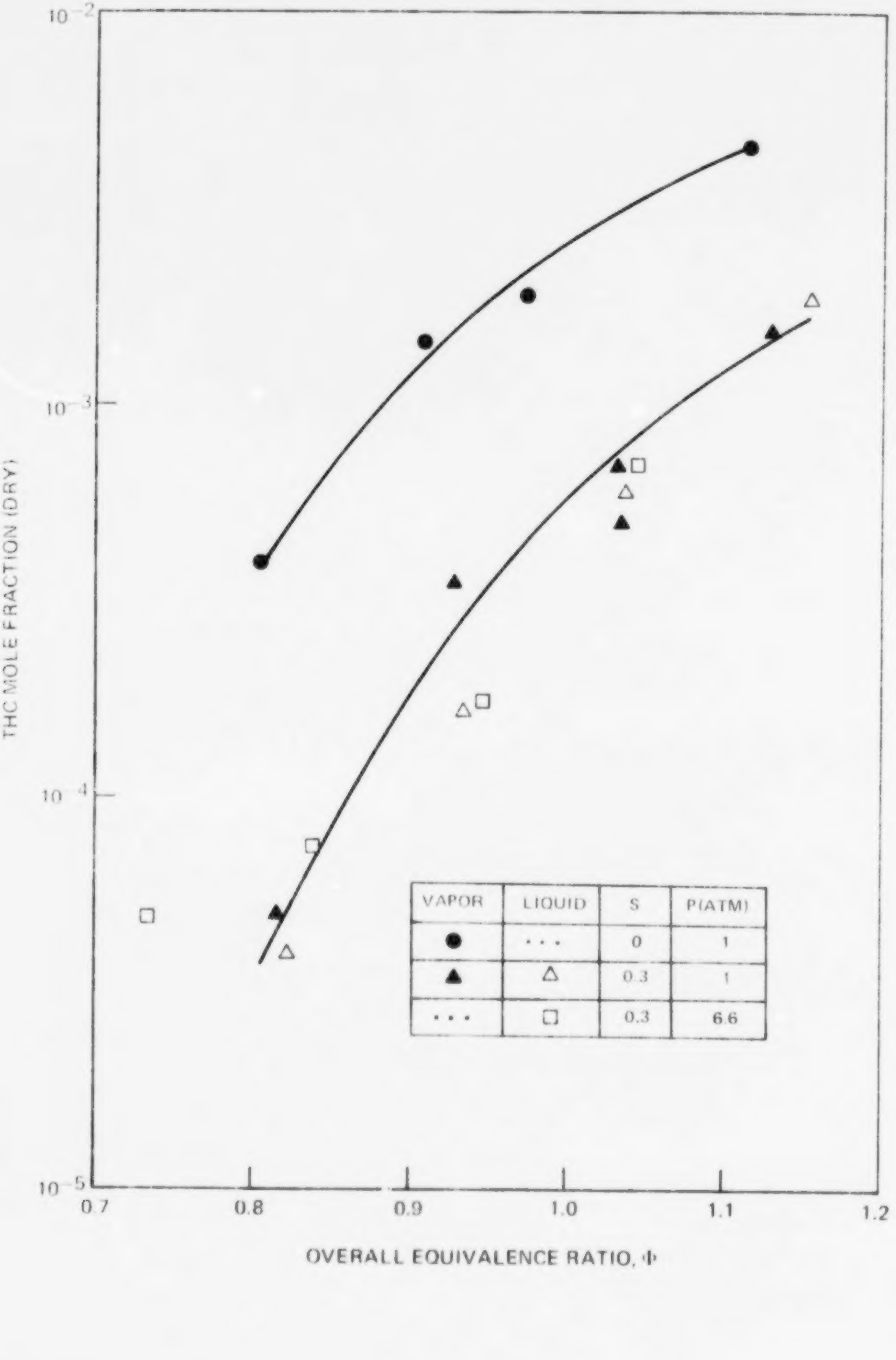

R02-29

FIG. 22

Average Exhaust CO Concentrations for Combustion of Vaporized and Liquid Propane with 0.136 kg/sec of 740°K Air.

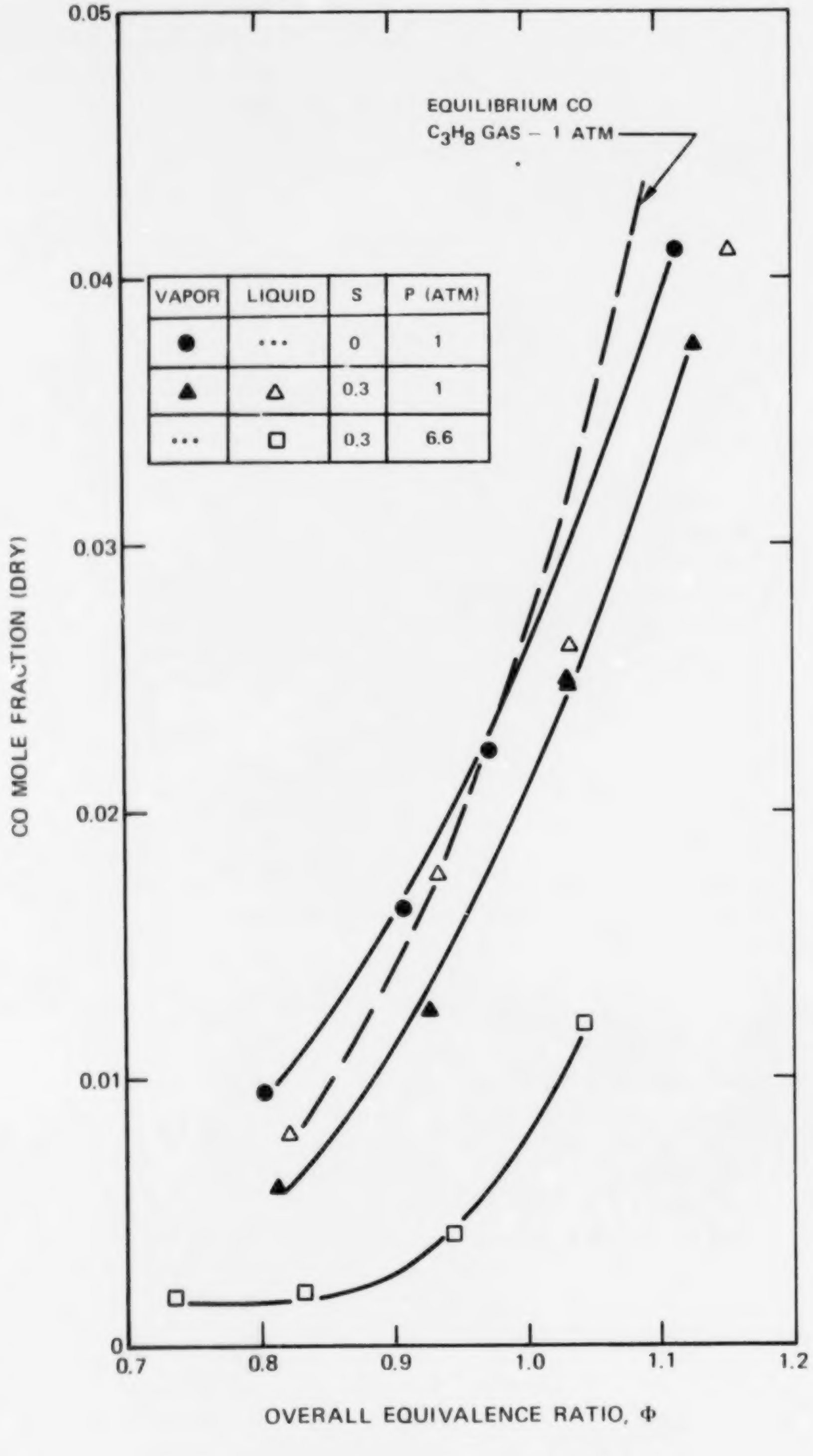

RO2-29-3

vaporized propane also are plotted on Fig. 20. In all of the tests, the NO levels in the exhaust are nearly independent of the overall fuel-air equivalence ratio. For the swirling flow with liquid propane, a decrease in NO emissions was observed when the combustor pressure was increased from one atmosphere to approximately 6.6 atm. This trend is opposite to that observed using gaseous fuels and likely is due to changes in the spray characteristics with increasing pressure (Ref. 13). For the swirling flow and a combustor pressure of one atmosphere, changing from prevaporized to liquid propane produced a decrease in exhaust NO emissions.

Figure 21 shows the variation of the average THC concentration in the exhaust gas with inlet air swirl, pressure and overall equivalence ratio for the combustor operating on vaporized and liquid propane. In all of the tests, the THC levels in the exhaust increased with increasing equivalence ratio. For a combustor pressure of 1 atm, the THC levels in the exhaust for vaporized propane decrease with increasing inlet air swirl. For swirling flow and a combustor pressure of 1 atm, changing from prevaporized to liquid propane produced very little change in the exhaust THC emissions. For liquid propane, only a slight change in exhaust THC emissions was observed when the combustor pressure was increased from one atmosphere to 6.6 atm.

Figure 22 shows the variation of the average CO concentration in the exhaust gas with inlet air swirl, pressure and overall equivalence ratio for the combustor operating on vaporized and liquid propane. For a combustor pressure of 1 atm, the CO levels decrease slightly with increasing inlet air swirl. The measured exhaust CO levels are very nearly equal to the calculated equilibrium CO levels over the entire range of equivalence ratios investigated. For swirling flow and a combustor pressure of one atmosphere, changing from vaporized to liquid propane produced very little change in the exhaust CO emissions. For the swirling flow, with liquid propane, an increase in combustor pressure from 1 atm to 6.6 atm produced a significant reduction in the measured exhaust CO levels. At the elevated pressure, the measured exhaust CO levels were less than calculated equilibrium values.

Flow Field Mapping Experiments

Examination of the results of the input-output tests, presented above, indicates that pollutant emission levels are particularly sensitive to certain combustor input parameters. NO and THC emissions are strongly dependent on swirl and pressure and also are dependent on air-fuel velocity ratio. Changing fuel composition produces some experimental trends which cannot be predicted on the basis of thermochemistry alone, suggesting significant coupling between the fluid dynamic and chemical processes in the combustor. Over most of the ranges of combustor input parameters investigated, exhaust CO concentrations are the equilibrium levels; however, for non-swirling flows and for swirling flows with low air-fuel velocity ratios, exhaust CO levels significantly exceed equilibrium levels as the overall equivalence ratio is decreased. Operation on liquid fuels produces some variations in emissions with input parameters which are different from those observed using gaseous fuels. To investigate how changes in these significant input parameters influence the combustor flow field and subsequent pollutant formation, detailed maps of the flow field properties were obtained for the seven test conditions listed in Table II.

TABLE II. MATRIX OF NOMINAL TEST CONDITIONS: MAPPING EXPERIMENTS

Fuel*	S	V_a/V_f	P(atm)	ϕ	T_a(°K)	$\dot{w}_a$(kg/sec)
NG	0	22	1	0.9	740	0.132
NG	0	22	1	0.7	740	0.132
NG	0.3	22	1	0.9	740	0.132
NG	0	22	3.6	0.9	740	0.132
SYN	0	15	1	0.9	740	0.132
PL	0.3	--	1	0.9	740	0.132
PL	0.3	--	1	1.0	740	0.132

* NG = natural gas
SYN - synthesized fuel ($CH_4/H_2/CO$)
PL = liquid propane

In these mapping experiments, the radial distributions of axial flow velocity, flow direction, temperature and species concentrations were acquired at all six combustor port locations. Variations in swirl number, pressure, overall equivalence ratio and fuel heating values are represented by the test conditions selected. During this effort, the two-probe rake was traversed in a "stop-go" mode at each axial location, i.e., the probe was moved to a desired radial position, data were taken and the probe was moved to a new radial position, and so on. A typical radial traverse consisted of 8-12 measurements. Approximately 4-5 minutes were required at each radial position to conduct on-line species concentration determinations.

Dynamic pressure, $0.5\,\rho V^2$, and flow direction were computed from impact pressures and differential static pressures (i.e., impact pressure minus static pressure) following the method given in Appendix B. DSO impact pressure and second orifice total temperature and pressure provided the necessary input for the determination of stream temperature. Ultimately, velocity was extracted from the temperature and dynamic pressure information.

An examination of the data generated during the mapping experiments reveals that there are several common features for all five of the gaseous fuel test conditions. It is worthwhile, therefore, to consider the data for one of the test conditions in some detail and to point out similarities and differences with respect to the remaining four test conditions. The test condition chosen for illustrating the significant characteristics of the confined, mixing/reacting flow, designated the baseline condition, involves the combustor operating on natural gas-air at an overall equivalence ratio of about 0.9, a pressure of 1 atm, with no swirl on the inlet air.

A preliminary description of the flow field was obtained from high-speed (500 frame/sec motion pictures of the flow in the vicinity of the injector. The motion pictures for "baseline" operation disclosed a light blue flame whose initial ignition location varied with time from axial positions downstream of port location "0" to positions inside the fuel delivery duct. The frequency of movement of the ignition location was estimated to be 40-100 Hz. On the basis of these observations, it can be concluded that the aerodynamically-induced recirculation zone is very mobile and, therefore, that its influence is extended over a larger portion of the flow than would be surmised on the basis of its size. At any given moment it might be far downstream of the injector exit so that the central fuel and annular air streams are unaffected by its presence, or it might be partially swallowed by the fuel delivery duct in which case hot air is recirculated to mix and burn with fuel upstream of the injector exit plane. Therefore, actual flow conditions at the injector exit will reflect recirculation behavior to some degree, thereby complicating the specification of initial conditions. The observed instability is primarily a fluid dynamic instability and is not the result of a coupling of the combustion process with the acoustic properties of the combustor or mechanical properties of the injector.* Similar recirculation zone instabilities have been observed in nonreacting flow fields for geometries nearly identical to the present combustor geometry (Ref. 14).

Baseline case velocity and temperature distributions at several axial locations are given in Figs. 23 and 24, respectively. In these figures and in all others to follow, the symbols in Table III will be used to identify the axial location of the probe tip. In addition, the extent of the fuel delivery port and air annulus will be indicated on the figures by vertical dashed lines normal to the abscissa.

---

* It should also be mentioned, for completeness, that a pressure instability was noted for combustor operation at 1 atm. Visicorder records of the signals from a pressure transducer located at the downstream end of the combustor section revealed that the magnitude of the fluctuations increased with overall equivalence ratio while the frequency of the temporal component remained unchanged at 130 Hz for both swirling and non-swirling flows. Amplitudes of 0.092 atm, 0.136 atm and 0.143 atm were recorded for Φ = 0.8, 1.0 and 1.2, respectively, during tests at zero swirl.

TABLE III. LEGEND FOR MAPPING DATA

Port No.	Axial Probe Tip Location* x(cm)	x/ro	Symbol**
1	1.93	0.32	▽
2	31.60	5.17	△
3	48.59	7.95	◇
4	65.58	10.73	□
5	82.58	13.50	D
6	99.57	16.28	○

* Injector exhaust plane is at x=0

** Solid symbols indicate either:
(1) entry through opposing port or
(2) non-basline data in comparative plots.

Generally, when data from ports on both sides of the combustor are presented, the ordinate label will be placed to read horizontally in the upper right hand corner of the plot.

The velocity profile in the vicinity of the injector exit plane for the baseline aerodynamically-stabilized flame, Fig. 23, is highly distorted relative to the theoretical, inviscid situation of a step profile with a 22.9:1 velocity ratio, as the result of the recirculation zone being imbedded in the fuel injection port and boundary layer effects. In addition, the chaotic movements of the recirculation zone, discussed above, effectively stir the fuel and air streams to reduce gradients (except those associated with the wall boundary layer) prior to the x=31.6 cm axial location. Downstream temperature distributions, Fig. 24, also are relatively flat and unchanging with longitudinal distance, suggesting that only a small portion of the total available chemical heat release occurs beyond the initial stirred zone and that such heat production is approximately matched by heat loss to the cold combustor wall. The behavior exemplified by the data in Figs. 23 and 24 is that of a stirred reactor, of length less than 31.6 cm, followed by a plug flow region in which the (inviscid) velocity is 82 ± 8 m/sec and the temperature is approximately 1900°K. Such a system appears to be chemistry-limited in that mixing is rapid relative to characteristic chemical reaction times.

By virtue of the rapid transport associated with the fluid mechanics in the baseline case, relatively high oxygen concentrations are available throughout the fuel stream (See Figs. 25 and 26). Depletion of oxygen is rapid upstream of the x=31.6-cm

FIG. 23

Velocity Profiles for Baseline Case. Combustion of Natural Gas (T_f=303°K) with 0.132 kg/sec of 752°K Air, V_a/V_f =22.9, S=0, at 1 atm.

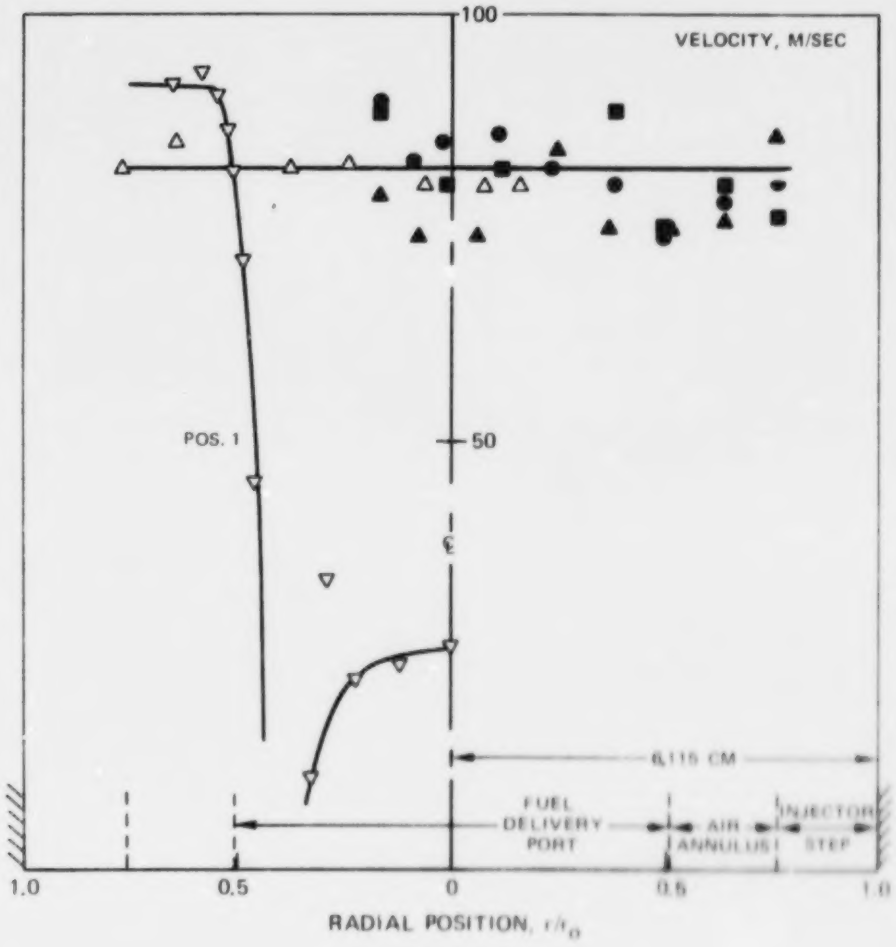

FIG. 24

Temperature Profiles for Baseline Case.

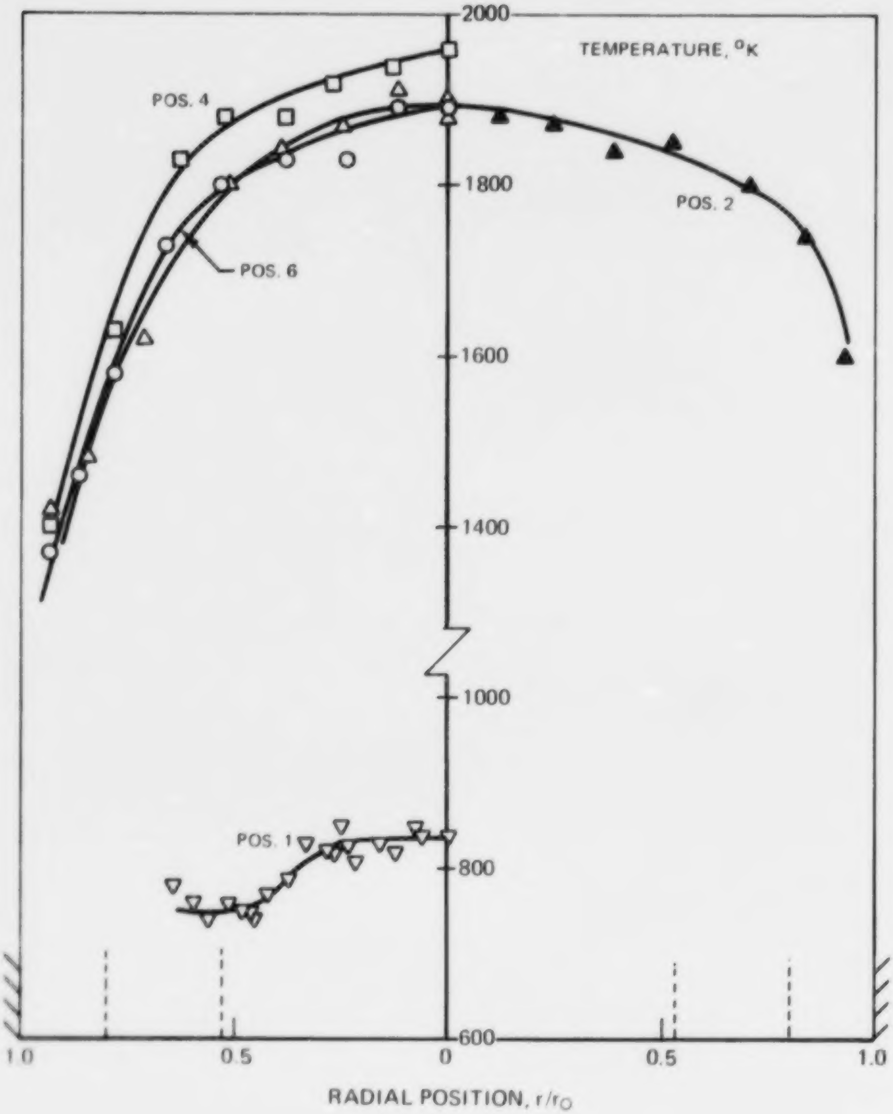

Oxygen Concentration Map for Baseline Case. Average Exhaust Concentration = 0.02.

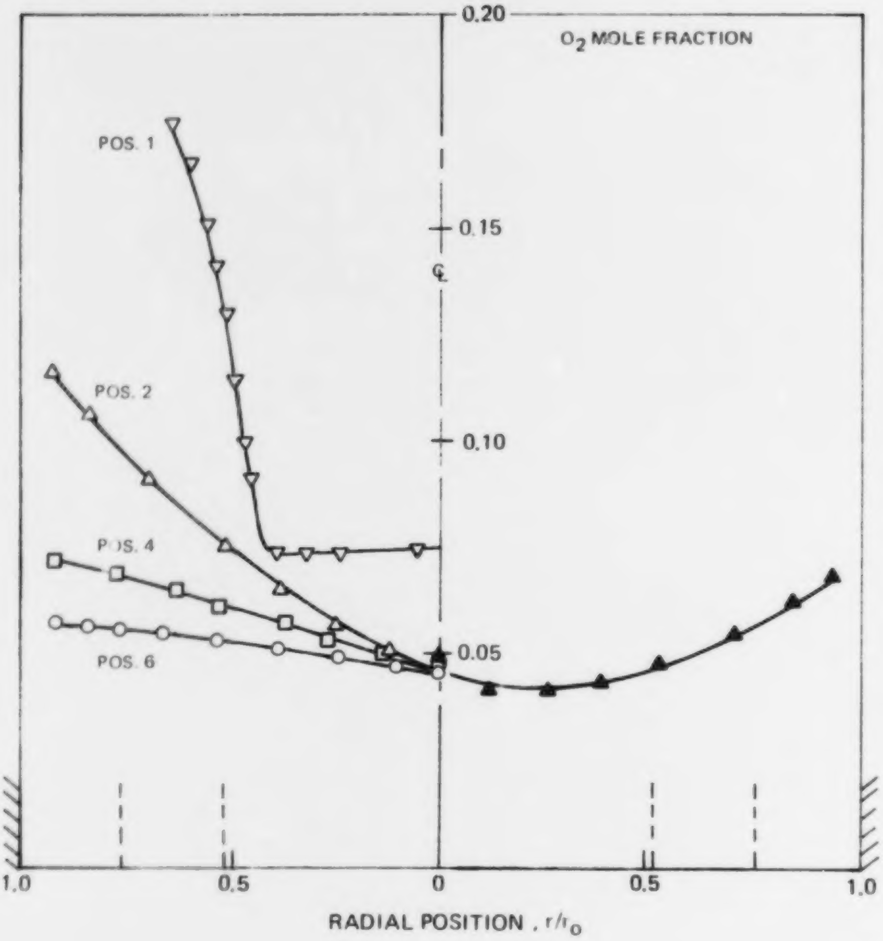

FIG. 26

THC Concentration Map for Baseline Case. Average Exhaust Concentration = 1300 ppm.

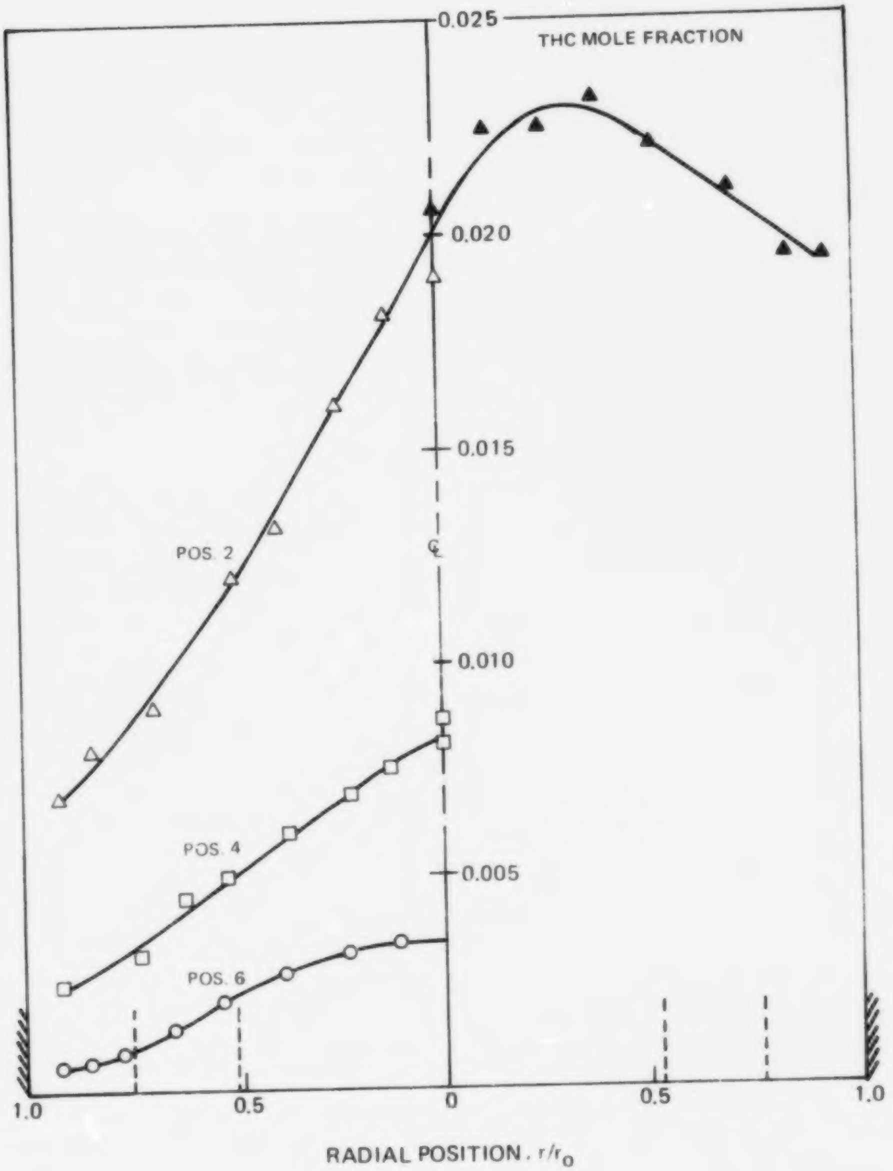

N12–139–5

location, i.e. in the highly stirred region of the combustor. In this region there is significant oxidation of the hydrocarbon fuel to form CO, Fig. 27, which in turn reacts forming CO_2, Fig. 28, and there is significant nitrogen oxide formation, Fig. 29. Downstream from the x=31.6 cm location, oxygen is consumed at a slower rate as the hydrocarbons continue to burn out. Concurrent with the hydrocarbon burnout, the CO increases and then burns out and CO_2 and nitrogen oxides form.

Referring to Fig. 25, oxygen concentration at the most upstream measurement location is seen to decrease rapidly from the air annulus position, as through a shear layer, and achieve a constant concentration level from $r/r_o \approx 0.4$ to the centerline ($r/r_o=0$). Examination of the CO and CO_2 concentration profiles, Figs. 27 and 28, at the same location also shows relatively constant concentration levels in the vicinity of the centerline. This central well- mixed portion of the flow, covering about 65% of the area of the fuel delivery duct, reflects the time-average extent of the recirculation region.

The regions of NO and NO_2 formation in the combustor are indicated in Fig. 29. At the axial location nearest the injection plane, the NO concentrations are very small; however, in the vicinity of the fuel injector lip, NO_2 concentrations in excess of the NO concentrations were measured. In several recent investigations of nitrogen oxide formation in gaseous turbulent diffusion flames (Refs. 2, 16 and 17), relatively large $(NO_2)/(NO)$ ratios were measured near the combustion zone. It should be noted, however, that there is considerable difficulty in making quantitative measurements of NO_2 in the combustor (See Appendix C). It was not possible to measure NO_2 concentrations in fuel-rich regions in the combustor because of problems with the stainless-steel thermal converter in the chemiluminescent analyzer. Similar limitations of stainless-steel converters have been reported by other investigators (Ref. 15). Furthermore, in regions where NO_2 measurements were obtained there is considerable uncertainty in the observed levels because of potential sources and sinks for NO_2 during transfer of the gas sample to the Exhaust Analyzer. Significant levels of NO and NO_2 are achieved within 5 combustor radii downstream of the injector exit. Thereafter, NO_2 concentration remains relatively constant with axial distance, while NO continues to form at an approximately steady rate; the centerline value of NO increases at about 1.36 ppm/cm.

The temperature and concentration distributions typically are not symmetric about the combustor centerline. The apparatus itself was eliminated as the source of this asymmetry following extensive inspections and careful alignment of all components at the test site and recalibrations of traversing gear and analytical instrumentation. Thus, the asymmetry must be related to the erratic motion of the recirculation zone, and it may be anticipated that profile three-dimensionaltiy will be aggrevated (or improved) with changes in air-fuel velocity ratio and swirl number. This preliminary observation is explored in more detail later in the report.

The general flow field characteristics discussed above are typical of all of the experimental conditions investigated in the flow field mapping experiments. However, as combustor operating conditions are varied from the "baseline" conditions,

FIG. 27

CO Concentration Map for Baseline Case. Average Exhaust Concentration = 0.016.

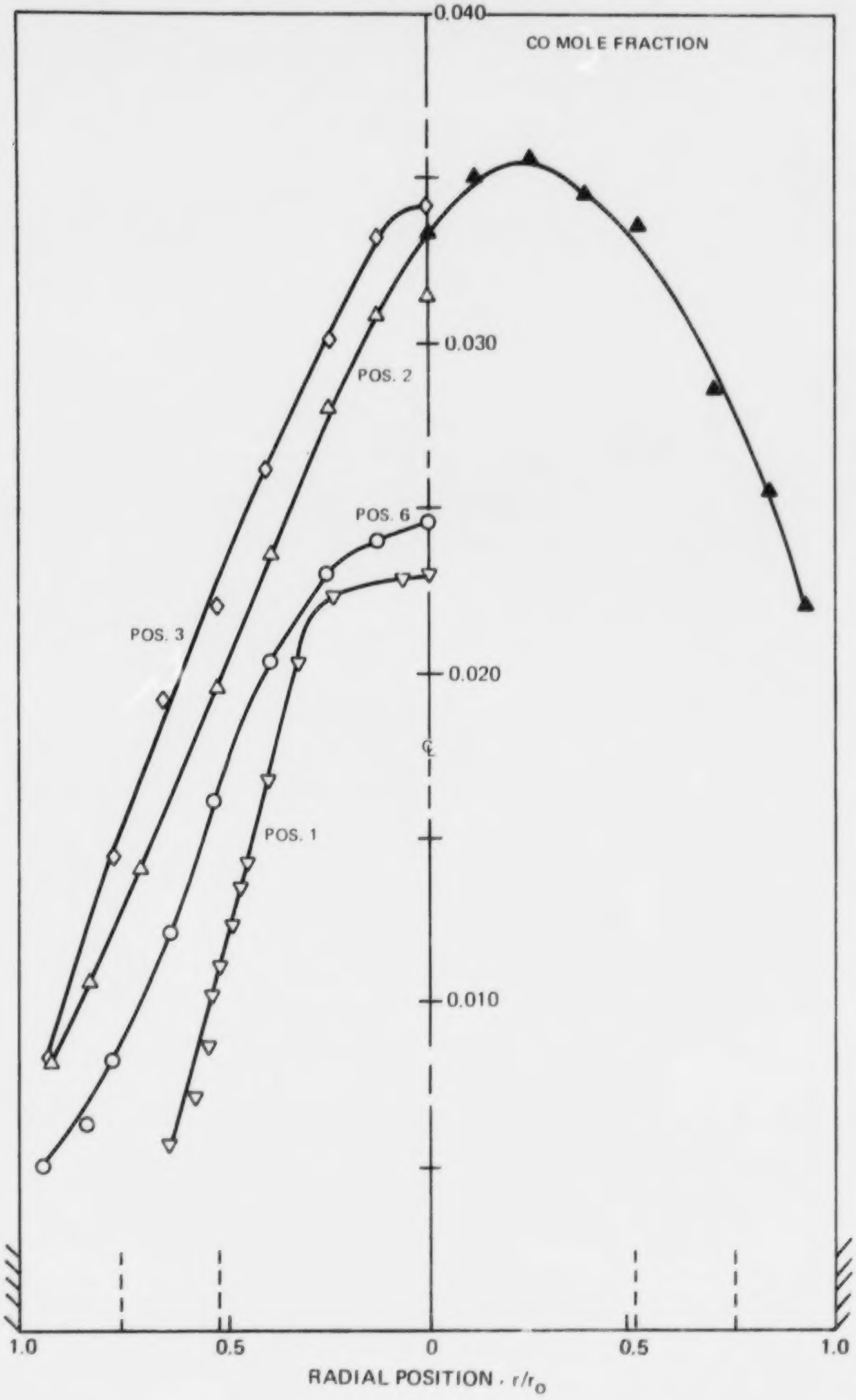

N12–139–2

CO_2 Concentration Map for Baseline Case. Average Exhaust Concentration = 0.0881.

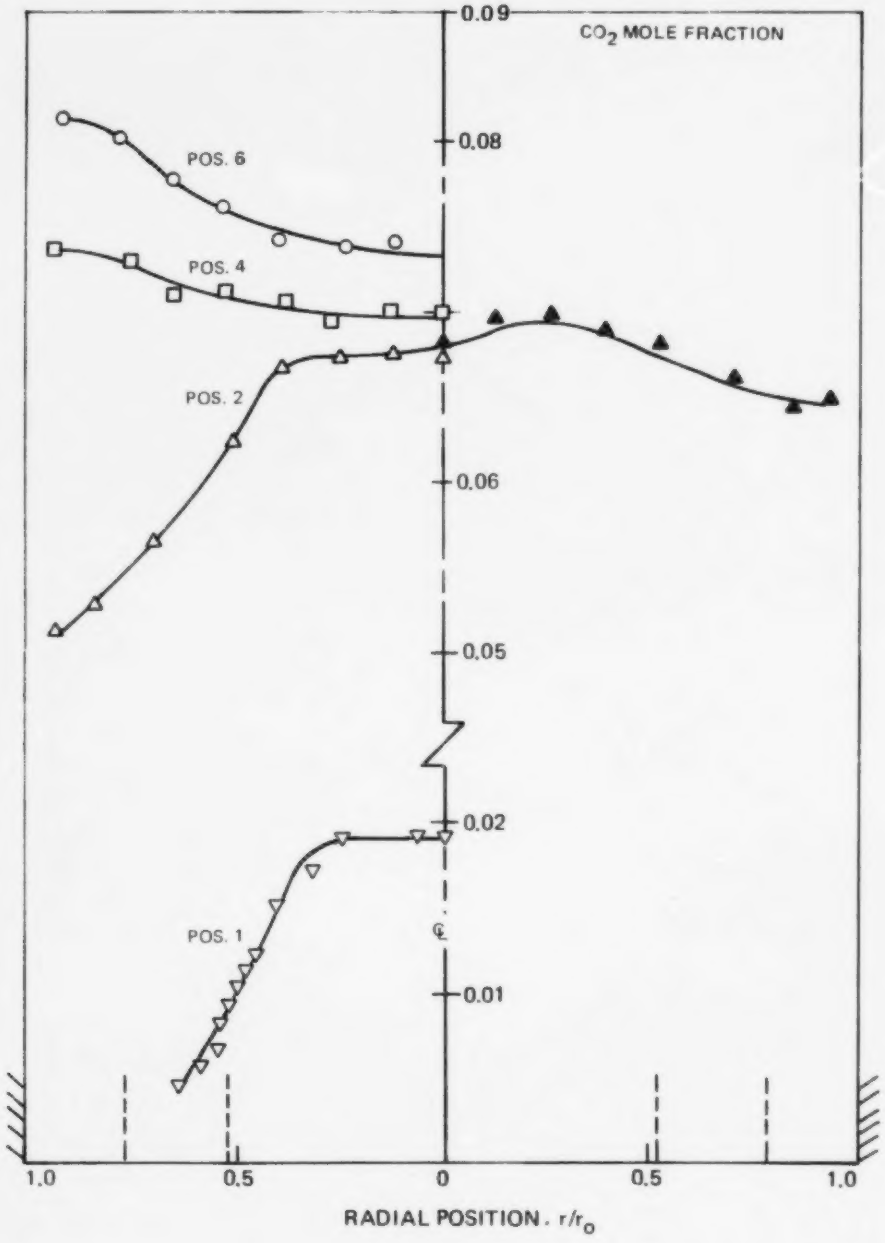

FIG. 29

NO and NO_2 Concentration Maps for Baseline Case. Average Exhaust Concentration: NO=156 ppm and NO_2=30 ppm.

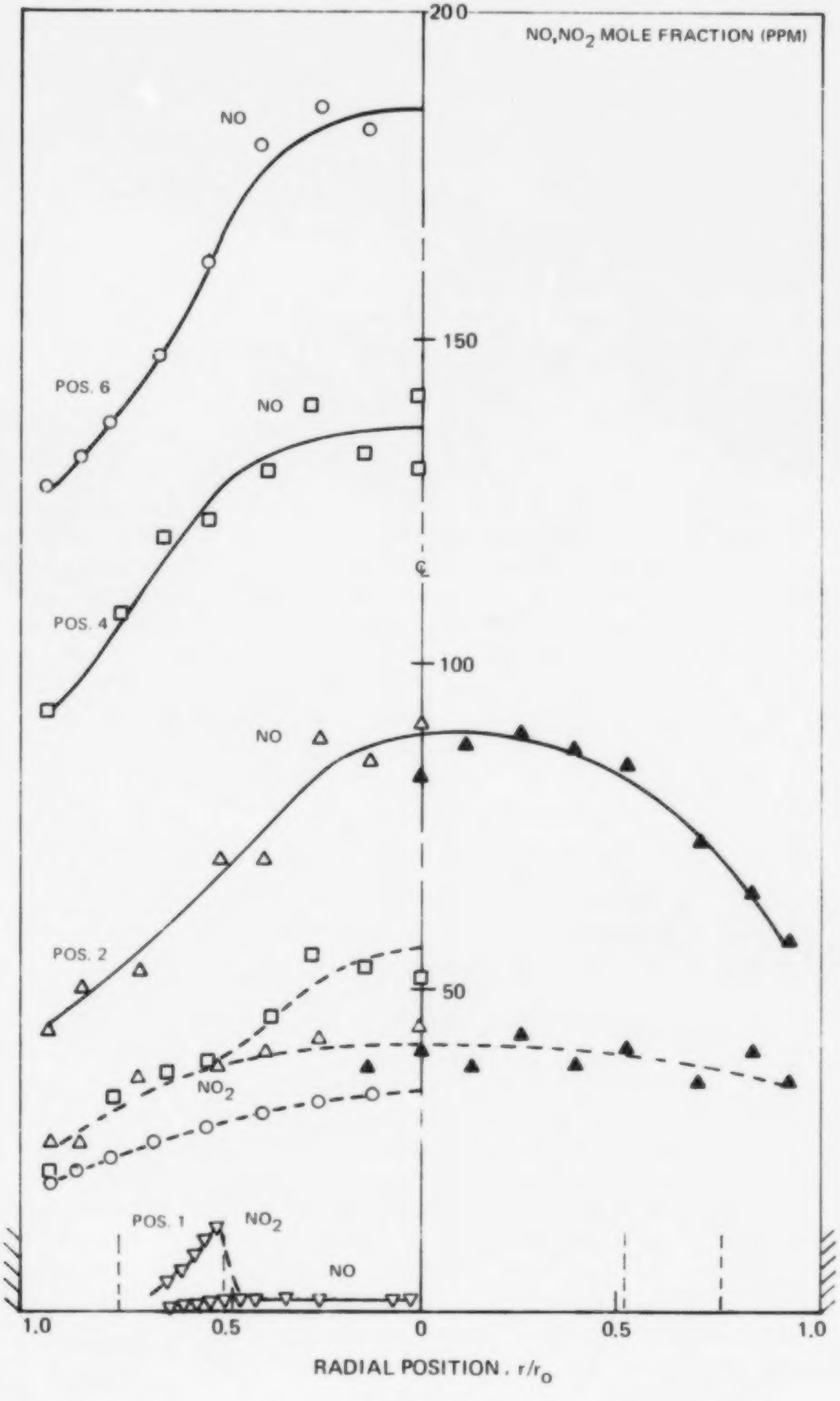

N12-139-4

there are noticeable changes in the velocity, temperature and species concentration distributions in the combustor. In the following sections, these differences will be discussed in detail.

1. Effect of Overall Equivalence Ratio

Decreasing the overall fuel/air equivalence ratio from the baseline value of 0.9 (~ 11 percent excess air) to 0.7 (~ 40 percent excess air), with all other inlet conditions remaining the same produces only minor changes in the velocity and temperature distributions shown in Figs. 23 and 24. Observed temperature levels decrease by 100-150 K and the maximum flow velocity decreases to 70±5 m/sec, primarily because of density increases associated with the decreased temperatures.

The O_2 concentration distributions for $\Phi = 0.7$, Fig. 30, are qualitatively similar to those found for the baseline conditions, although the O_2 concentrations generally are larger for the $\Phi = 0.7$ operating condition. The time-mean radial extent of the recirculation zone for the $\Phi = 0.7$ operating condition, as indicated by the region of relatively constant O_2 concentrations, is approximately the same as for the baseline case.

Oxidation of the hydrocarbon fuel to CO is more rapid at the lower overall equivalence ratio, resulting in hydrocarbon levels which are lower, Fig. 31, and initial CO levels which are higher, Fig. 32, than for baseline operation. Although initial CO levels are high for the $\Phi = 0.7$ operating condition, CO burnout rates are rapid and exhaust concentration levels are only about 36% of the levels measured for the baseline case.

At the axial station nearest the injection plane, CO_2 concentrations for the flow with 40 percent excess air are somewhat larger than were measured for the baseline operating condition, Fig. 33. Near the combustor wall, a region of locally high CO_2 concentration is observed, suggesting a region of recirculating flow just downstream from the back-step at the injection plane. Similar evidence of recirculating flow in this region was obtained in the swirling flow experiment. At axial stations further downstream from the injection plane, CO_2 concentrations in the 40 percent excess air flow are generally lower than in the baseline flow, consistent with the equivalence ratio trend of the exhaust CO_2 concentration reported previously, Fig. 8.

Except for the axial station near the injection plane, the NO concentration profiles are not significantly different for the two equivalence ratios investigated. Near the injection plane, NO concentrations near the combustor centerline are somwehat larger for $\Phi = 0.7$ than for $\Phi = 0.9$. These differences appear to correlate with the temperature measurements, in that the measured temperatures near the centerline are larger for $\Phi = 0.7$ than for $\Phi = 0.9$. The above observations, together with the fact that the exhaust NO concentrations for the two overall equivalence ratios are approximately the same, suggest that there are no significant differences in the NO formation rate. This conclusion is consistent with the observation that there are only very slight differences in the temperature and O_2 concentration profiles in the regions of maximum NO formation in the combustor.

FIG. 30

Comparison of the O_2 Concentration Distributions at the Baseline Condition (Φ=0.9) with Those at Φ=0.7. At the Lower Equivalence Ratio, Natural Gas (307°K) is Burned with 0.136 kg/sec of 754°K Air, V_a/V_f=29.2, Φ= 0.68, S=0 at 1 atm.

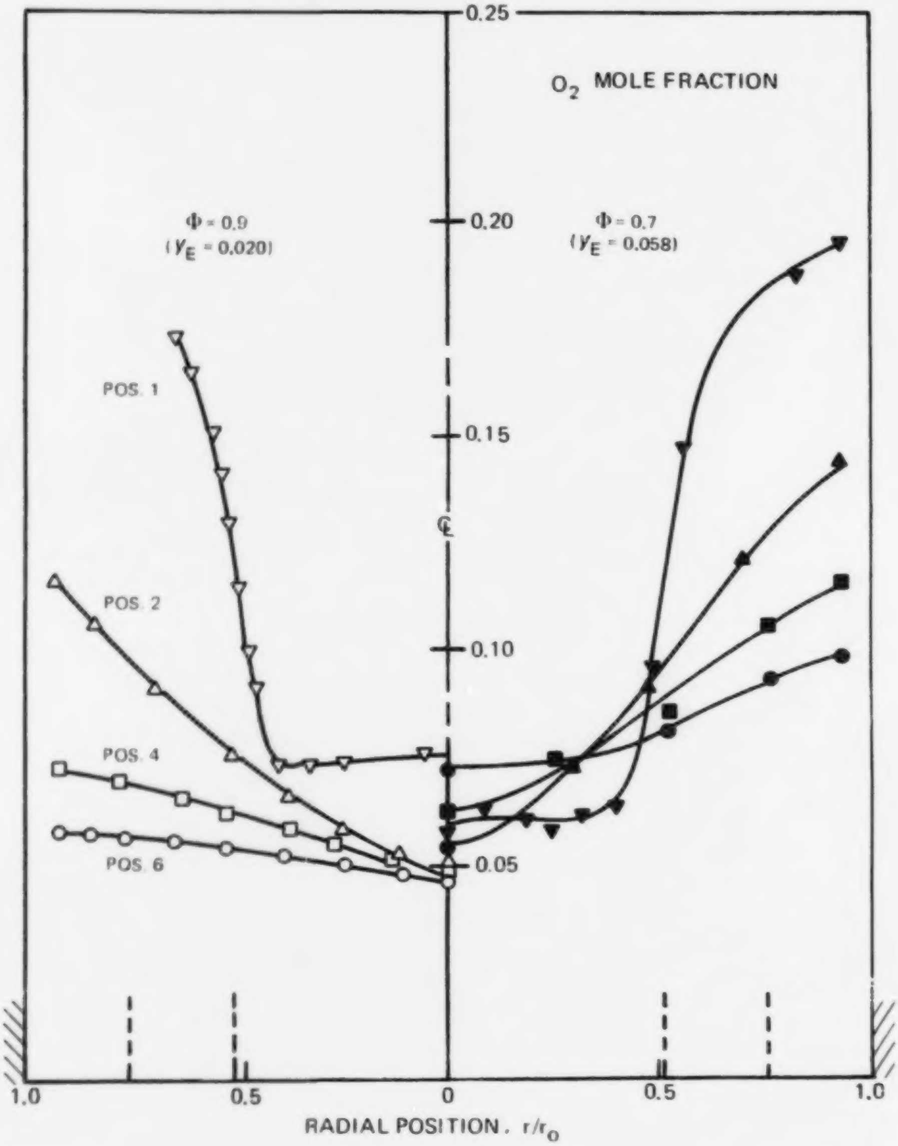

FIG. 31

Effect of Overall Equivalence Ratio on THC Concentration Map. Operating Conditions Identical to Fig. 30.

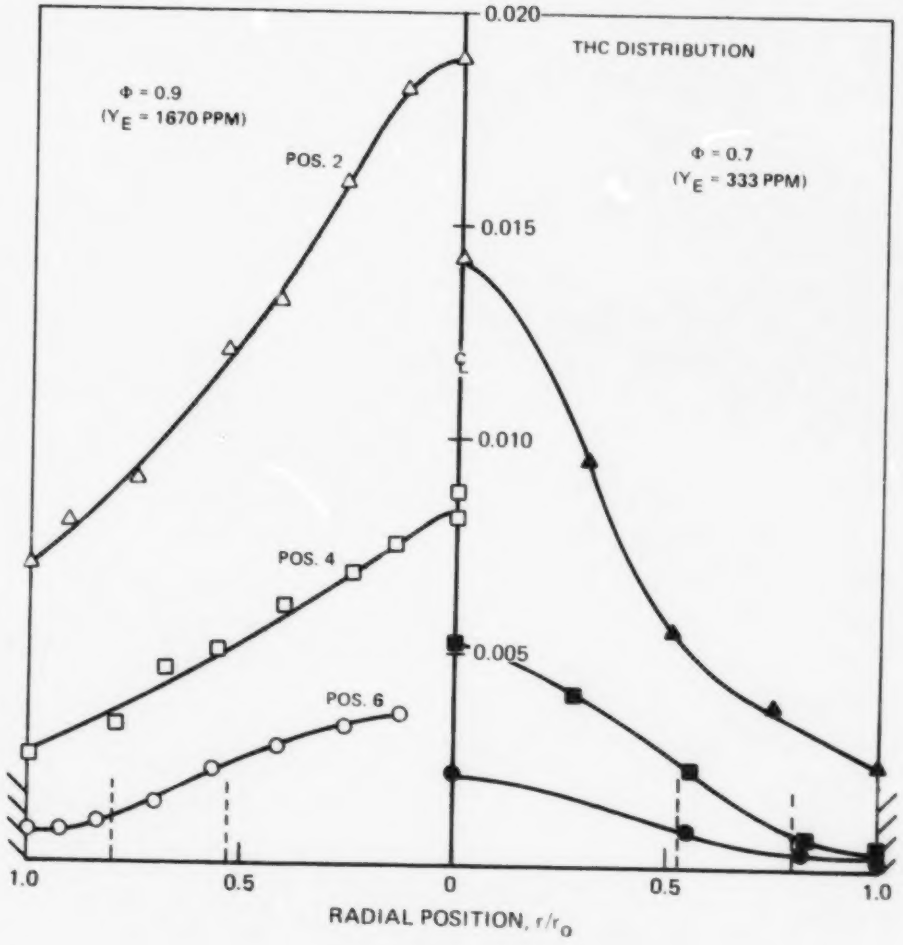

FIG. 32

Effect of Overall Equivalence Ratio on CO Concentration Map. Operating Conditions Identical to Fig. 30.

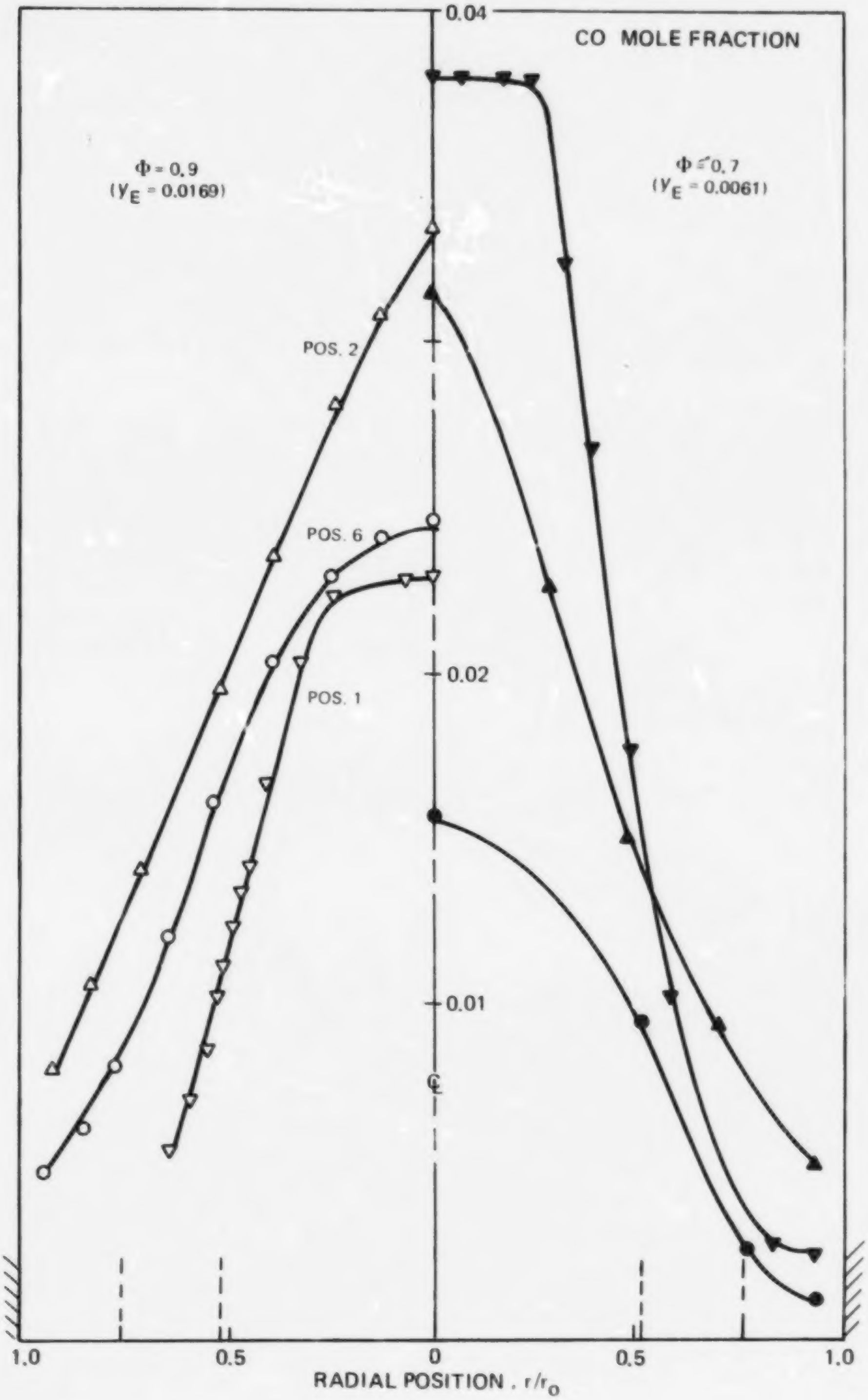

N12–153–16

FIG. 33

Effect of Overall Equivalence Ratio on CO_2 Concentration Map. Operating Conditions Identical to Fig. 30.

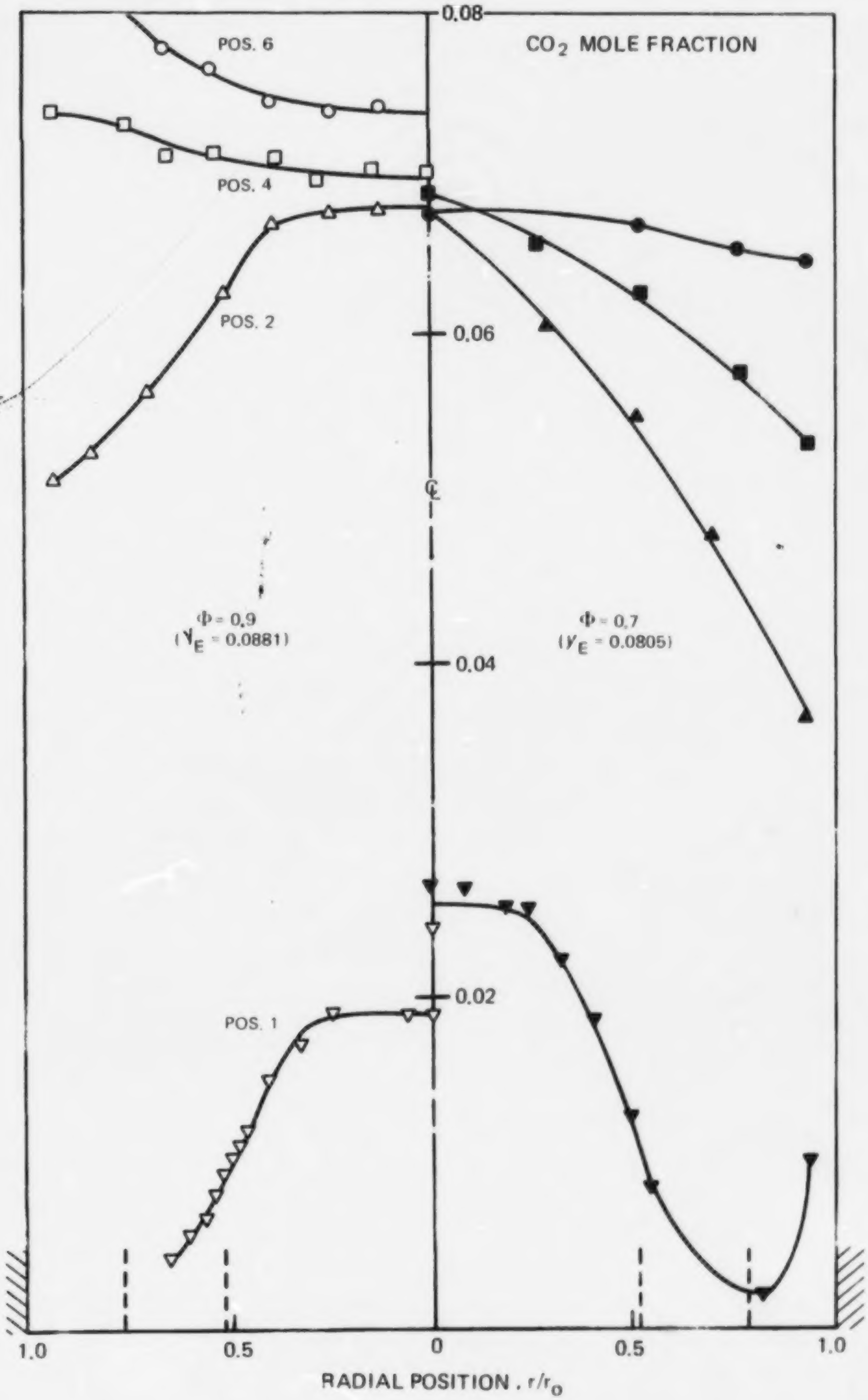

N12–153–1

ii. Effect of Fuel Composition

Substitution of the synthesized fuel ($CH_4/CO/H_2$) for natural gas in the baseline case lowers the heating value by about 24% and, more significantly, reduces the air-fuel velocity ratio from 22.1 to 15.4. This last change brings the air-fuel momentum flux ratio uncomfortably close to the minimum value necessary to sustain an aerodynamic flameholding capability. The recirculation region for these conditions undergoes large scale displacements which leads to a flow field with major three-dimensional features. In particular, the centrally-located, highly mobile recirculation region may merge with other recirculation regions, e.g., the annular region associated with the injector back-step. Detailed maps for the synthesized fuel-burning combustor support these remarks. Large distortions of the velocity distribution at x=31.6 cm, Fig. 34, testify to the unsettled flow situation which exists. The peculiar temperature distribution, Fig. 35, at that same station creates the impression that the recirculation region is located off-center and that the fuel stream has been channeled toward the combustor wall. These observations are consistent with the central recirculation region merging with or establishing intermittant contact with a portion of the recirculation region associated with the injector step. In this event, the recirculation zone may occupy a large, irregular region encompassing the centerline and extending to cover a portion of the combustor wall. The fuel stream is forced away from the central portion of the combustor to move around the recirculation region. All symmetry is destroyed in the initial portion of the combustor and three-dimensional effects persist for a significant distance downstream. As indicated in Figs. 34 and 35, three-dimensional effects are extreme at 5 combustor radii, but only minor at 10.7 radii.

In spite of the quite different composition of the synthesized fuel versus natural gas (Appendix F), and the major nonuniformities described earlier, measured species concentration levels and profile shapes for the two fuels are remarkably similar. Figs. 36 and 37 show comparisons of the concentration distributions of CO_2 and NO, respectively, for the two fuels. For the synthesized fuel, the CO_2 concentrations in the combustor are somewhat larger than for natural gas, reflecting the increased effective carbon/hydrogen ratio of the synthesized fuel. Immediately donwstream from the injector, relatively large CO_2 concentrations near the wall and depleted concentrations in the center of the combustor are consistent with the three-dimensional flow behavior discussed above. NO also appears in larger concentrations adjacent to the wall than in the center of the combustor at the first axial location. At axial locations further downstream, the NO concentration profiles are nearly identical for the synthesized fuel and natural gas, and the exhaust concentrations are approximately the same for these two fuels. These observations suggest that there is no significant difference between the NO formation rates for these two fuels for the set of operating conditions investigated. This conclusion is consistent with the temperature and O_2 concentration profiles measured in the combustor for the two fuels. One additional observation (not shown) is the presence of NO_2 in the vicinity of the air-fuel shear layer at x=1.93 cm at levels exceeding the local NO concentrations; a similar situation was noted earlier for the baseline case.

FIG. 34

Velocity Profiles for Combustion of Synthesized Fuel (T_f=309°K) with 0.132 kg/sec of 730°K Air, V_a/V_f=14.6, S=0, Φ=0.87, at 1 atm.

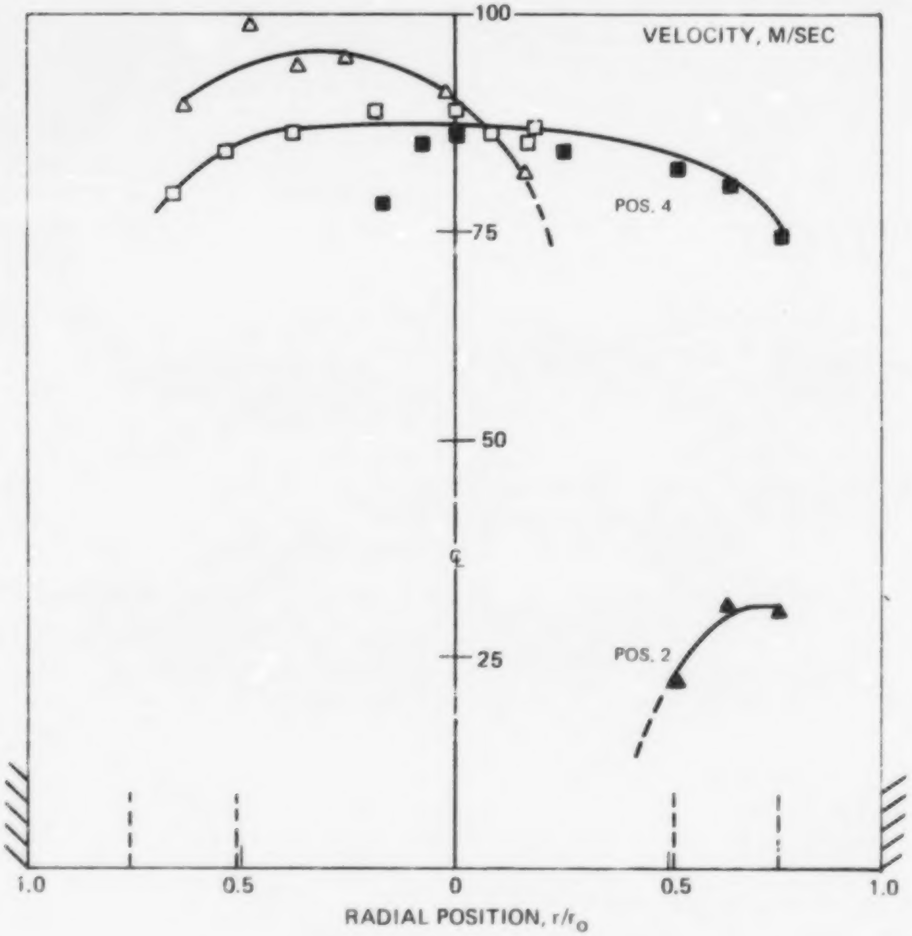

Temperature Profiles for Synthesized Fuel Combustion Test.

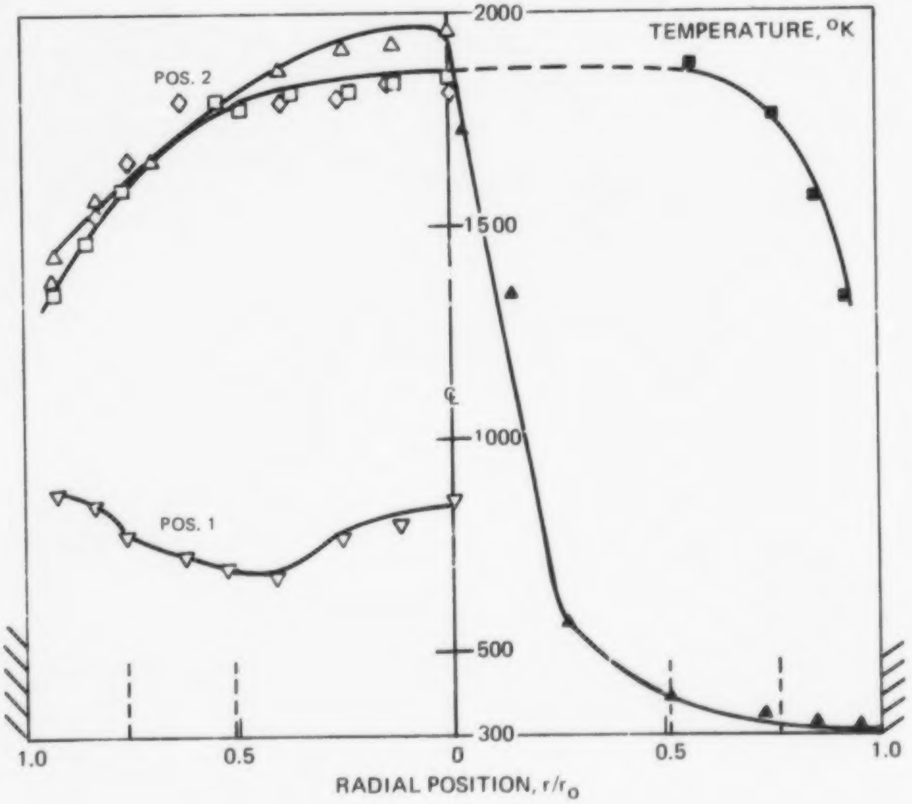

R1-60-1

FIG. 36

CO_2 Concentration Maps for Synthesized Fuel and Baseline (Natural Gas) Combustion Tests.

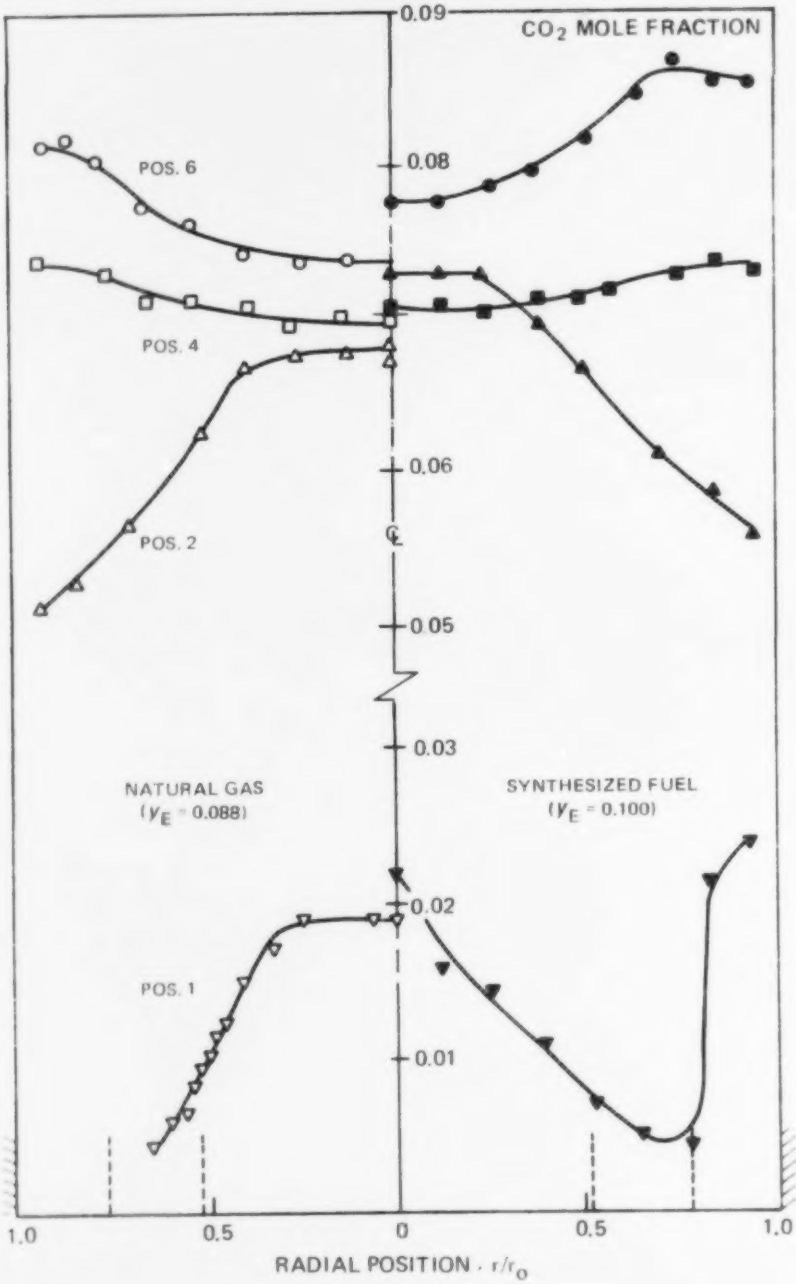

N12-153-1

FIG. 37

NO Concentration Maps for Synthesized Fuel and Baseline (Natural Gas) Combustion Tests.

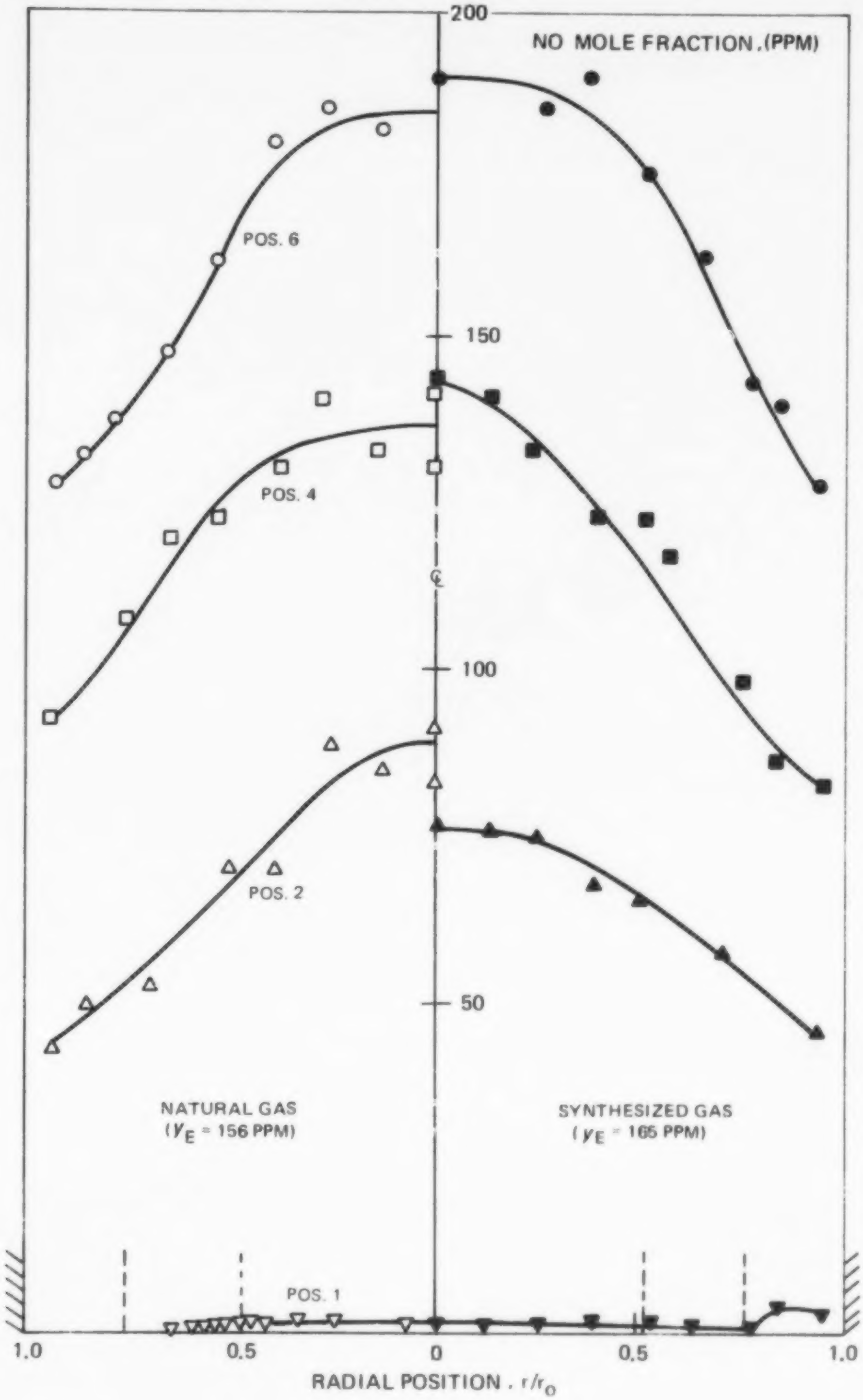

N12–153–14

iii. Effect of Swirl

In mapping experiments discussed so far, the flame is stabilized on a recirculation region produced as the result of a momentum flux deficit between the fuel and air streams, without imparting swirl to either flow. The great mobility of the recirculation zone results in rapid transport of heat, mass and momentum and the formation of an essentially completely mixed flow. The mixed flow downstream of the recirculation zone contains reactive species which continue to undergo chemical changes. Distributions of temperature, velocity and species concentrations in such flows are characteristically flat in the center portion of the combustor and the maximum (or minimum) is at the centerline. These chemical-reaction-limited systems display relatively low NO levels and high THC levels.

When a swirl component is introduced on the inlet air flow, the appearance of the combustion zone in the vicinity of the injector changes dramatically. High-speed motion pictures reveal that the extent of the axial movement of the ignition location is reduced and that the ignition location rotates around the injector lip with a frequency of approximately 150 Hz. Syred and Beér (Ref. 18) have reported similar periodic instabilities in swirl combustors, resulting from a precession of vortices about the axis of symmetry. In the flow fields investigated in Ref. 18, the precessing vortex core (PVC) was located between the boundary of the recirculation zone and the zero streamline, corresponding to a region near the fuel injector lip in the present experimental configuration. Syred and Beér have correlated the PVC frequency, f, in terms of a non-dimensional frequency parameter, fd^3/Q, and the Reynolds number of the inlet air stream for a range of fuel injection geometries and overall fuel/air equivalence ratios. The frequencies of the rotational instabilities observed in the present experiments can be expressed in terms of the Syred and Beér correlation, suggesting that the observed instability is a PVC. Associated with the PVC, Syred and Beér report a radial-axial instability resulting from eddy shedding from the PVC. A similar axial instability is observed in the present experiments. Hence, in the vicinity of the injection plane, the flow is not axisymmetric and steady, but instead is a three-dimensional, time-dependent turbulent flow. The axial extent of the PVC in the present experiments is not known, however Syred and Beér report that the PVC dissipates rapidly in the axial direction $(x/d \sim 1)$.

Although there are substantial time-dependent, three dimensional effects, at the $S=0.3$ condition investigated, the time-mean flow appears to resemble a classical axisymmetric diffusion flame. High temperatures develop off centerline, Fig. 38, by virtue of a separation of the air and fuel streams, resulting in a mixing-limited situation. In the extreme mixing-limited case of a "flame sheet", oxygen moving toward the centerline and fuel moving away from the centerline react exclusively within a very narrow, high temperature annular region, thereby sustaining the local temperature. Reaction products display sharp concentration peaks in the combustion region, while reactant species concentrations fall off abruptly at the boundary of

FIG. 38

Temperature Profiles in Swirling Flow Combustion Test. Combustion of Natural Gas (T_f=360°K) with 0.134 kg/sec of 750°K Air Having a Swirl Number of 0.3, V_a/V_f=23, Φ=0.885, 1 atm.

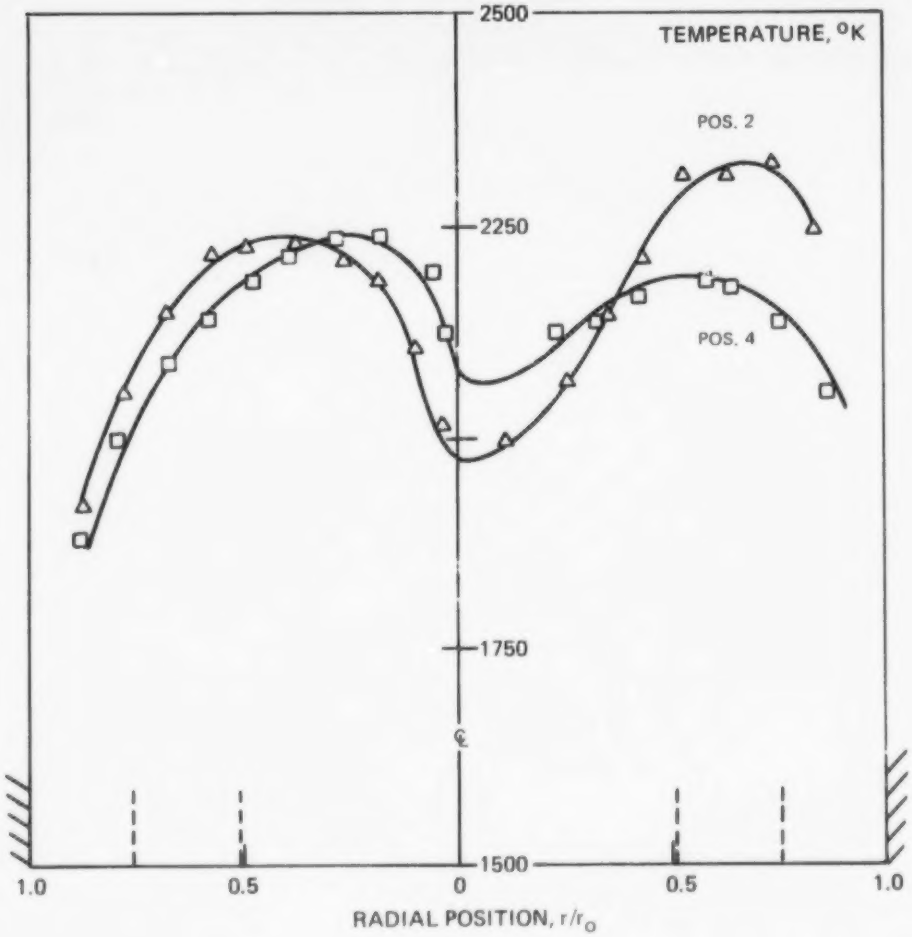

the flame. In this manner, the flame sheet acts as a sink for reactants and a source of products.

Mixing-limited behavior is clearly manifested in the species concentration data acquired for the swirling flow. Figs. 39 and 40 contrast the separation of the fuel and air streams at initial axial locations ($x/r_o \leq 5.17$) for the swirling flow with the non-swirling baseline case. Similar radial distributions of fuel and air in turbulent diffusions flames have been reported by Bilger (Ref. 19). The increase in hydrocarbons near the combustor wall at $x/r_o = 5.17$ is probably due to entrainment of fuel in the recirculating flow in the vicinity of the back-step at the injection plane. Fig. 41 compares the CO concentration distributions for the swirling and non-swirling flow. The initial rate of CO formation in the swirling flow is substantially larger than for the non-swirling flow. This observation, together with the rapid disappearance of hydrocarbons and oxygen in the swirling flow, Figs. 39 and 40, suggests that swirl significantly increases the rate of oxidation of the fuel to CO. Since the exhaust CO levels are lower for the swirling flow than for the non-swirling flow, it appears that swirl also results in an increased rate of CO burnout.

The radial concentration distributions of CO_2 and NO, Figs. 42 and 43, for the swirlin flow are significantly different from those in the non-swirling baseline case. Imparting swirl to the inlet air stream results in CO_2 and NO concentration profiles which exhibit peaks off the combustor centerline, at approximately the same radial position as the maximum temperature. The CO_2, NO and temperature peaks (and, hence, unmixedness) persist for long distances in the combustor, and spread at an angle of approximately 5.5 deg. This angle is consistent with spreading rate data obtained for unconfined turbulent diffusion flames (Ref. 20).

Combustion in the swirling flows resembles the classical turbulent diffusion flame. These flows are characterized by substantial unmixedness, higher combustion rates and locally higher temperatures in the flow field, resulting in increased rates of NO formation. In swirling flows, the region of maximum energy release occurs off the combustor centerline, as evidenced by the temperature and concentration profiles. Evidently, the unmixedness increases with an increase in the swirl number from 0.3 to 0.6, since results from the input-output experiments show that exhaust levels of NO rise and THC levels decrease as the swirl number is increased.

The persistance of swirl-induced effects is evident from the concentration and temperature distributions and also from the axial velocity and flow direction distributions. Axial velocity profiles for the S=0.3 flow Fig. 44 are found to be symmetric and to vary in a nearly linear fashion with radial distance in the central portion of the combustor, i.e., $(V-V_{\mathbb{C}})/r=$ constant. The acceleration rate of the flow in the center of the combustor decreases with axial distance, and a substantial velocity deficit still exists at the centerline at 16.3 combustor radii (x=99.57 cm).

Oxygen Concentration Maps for Swirling (S=0.3) and Baseline (S=0) Combustion Tests.

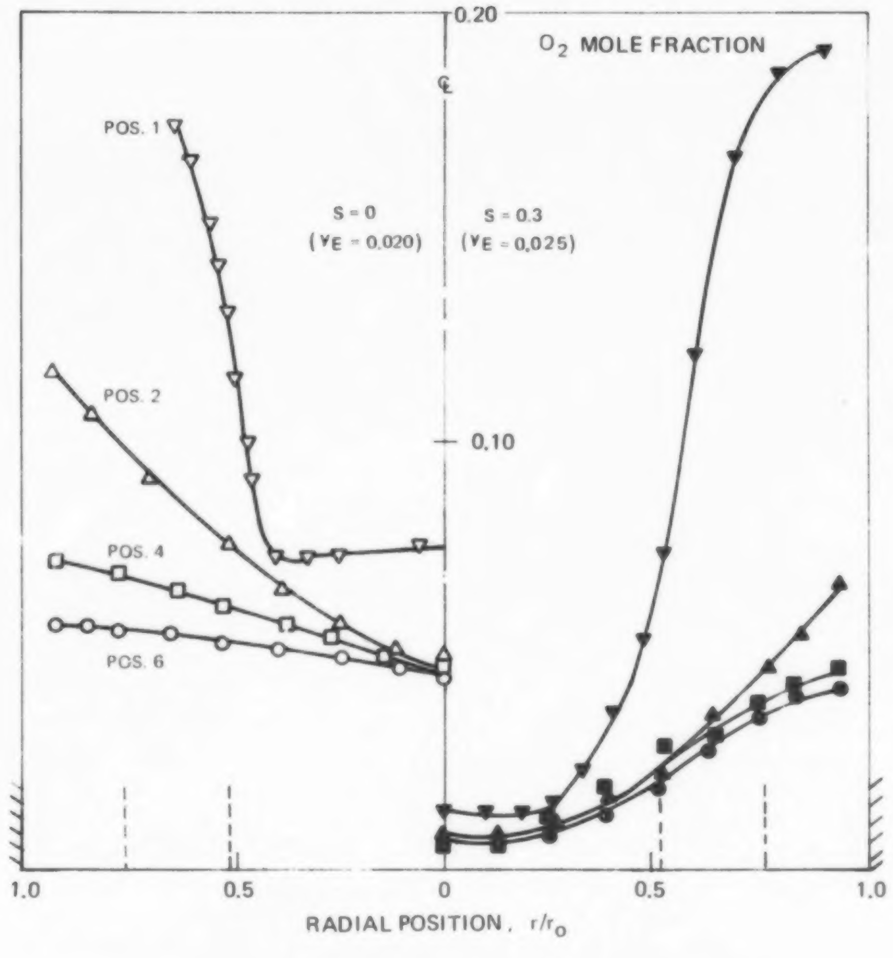

FIG. 40

Total Hydrocarbon Concentration Maps for Swirling (S=0.3) and Baseline (S=0) Combustion Tests.

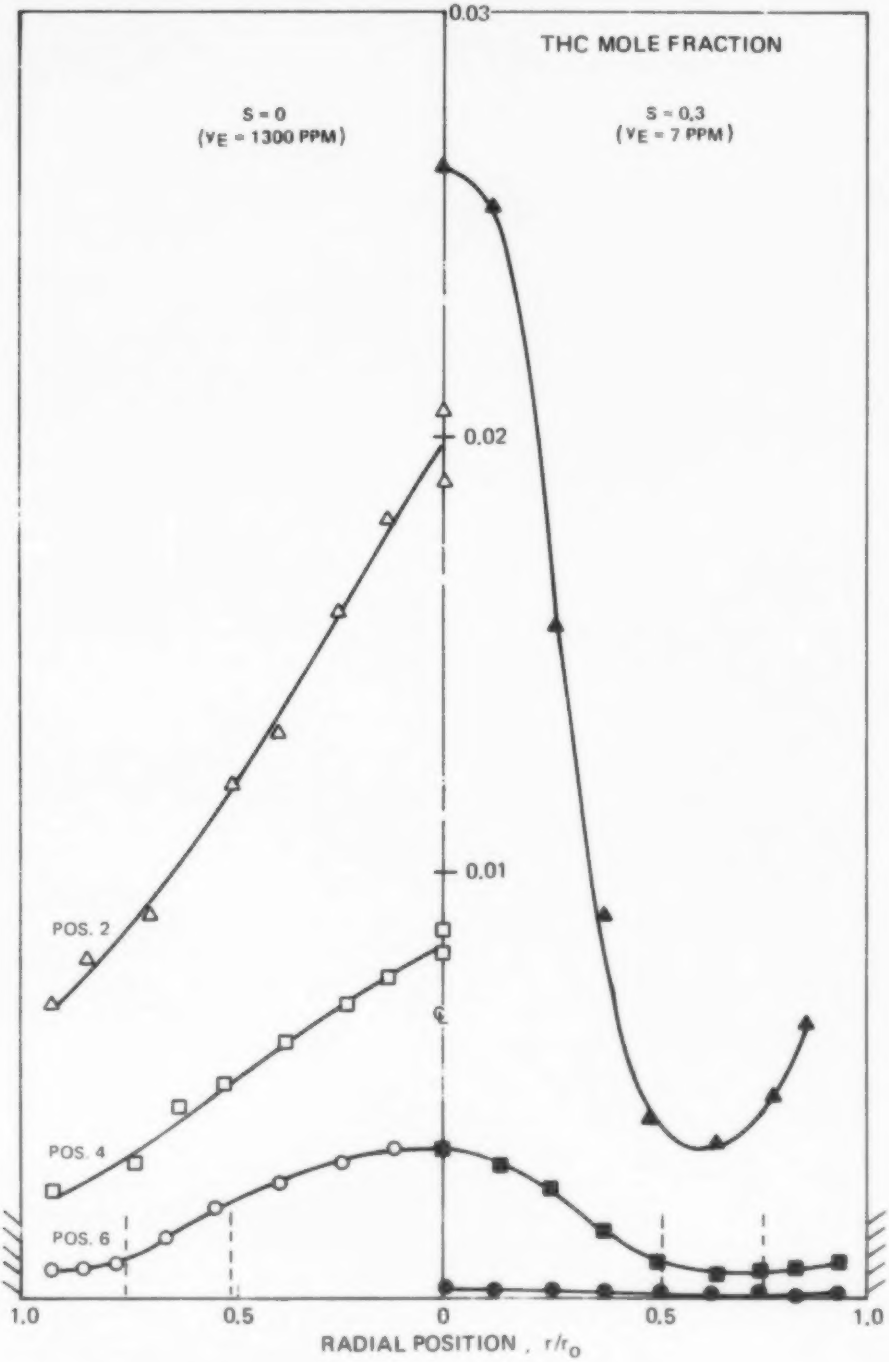

N12-153-1

FIG. 41

CO Concentration Maps for Swirling (S=0.3) and Baseline (S=0) Combustion Tests.

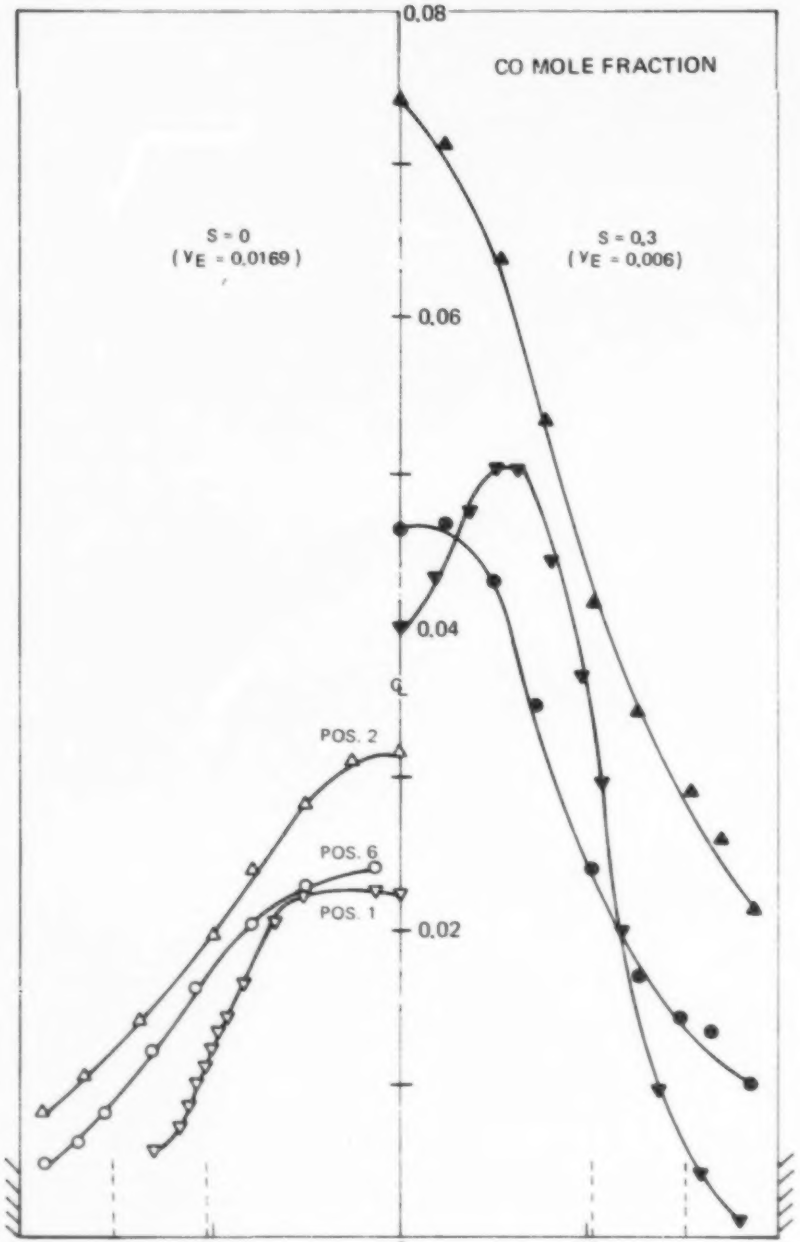

CO_2 Concentration Maps for Swirling (S=0.3) and Baseline (S=0) Combustion Tests.

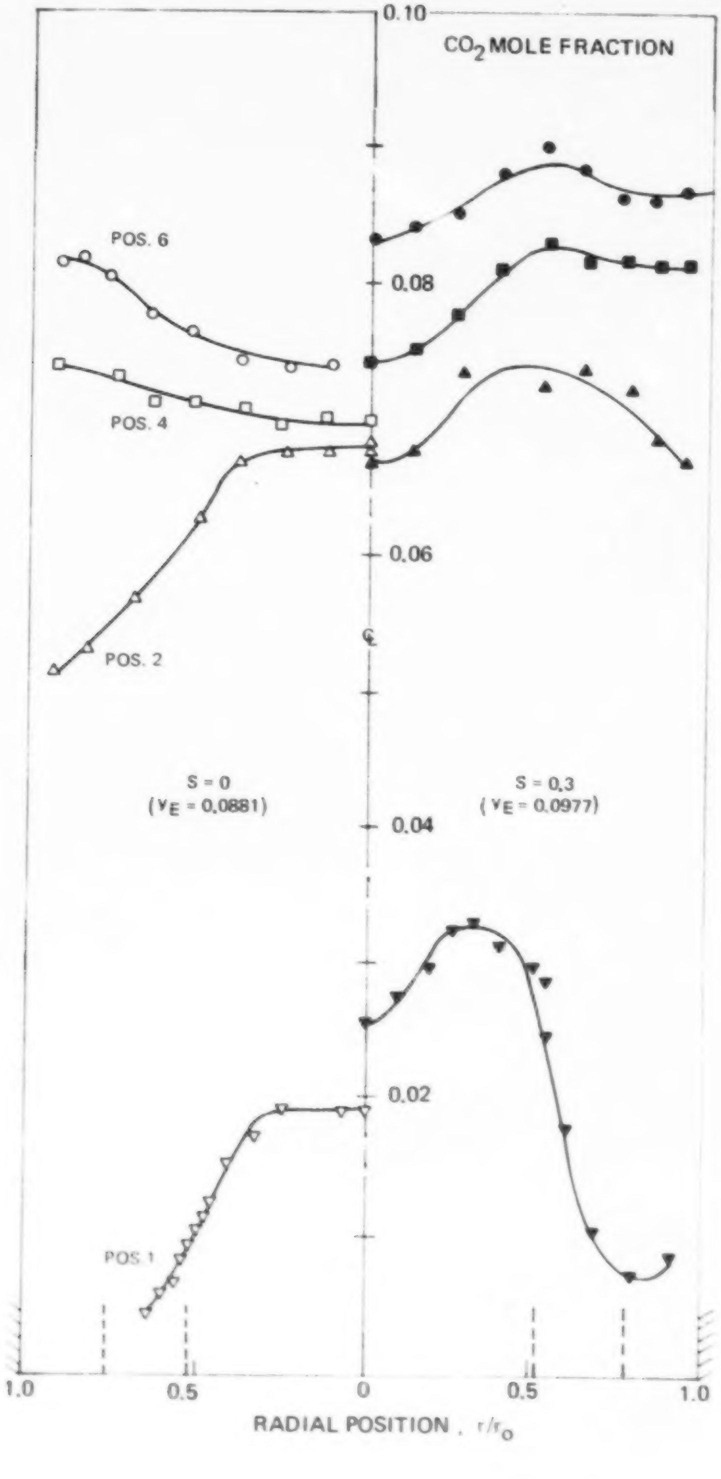

FIG. 43

NO Concentration Maps for Swirling (S=0.3) and Baseline (S=0) Combustion Tests.

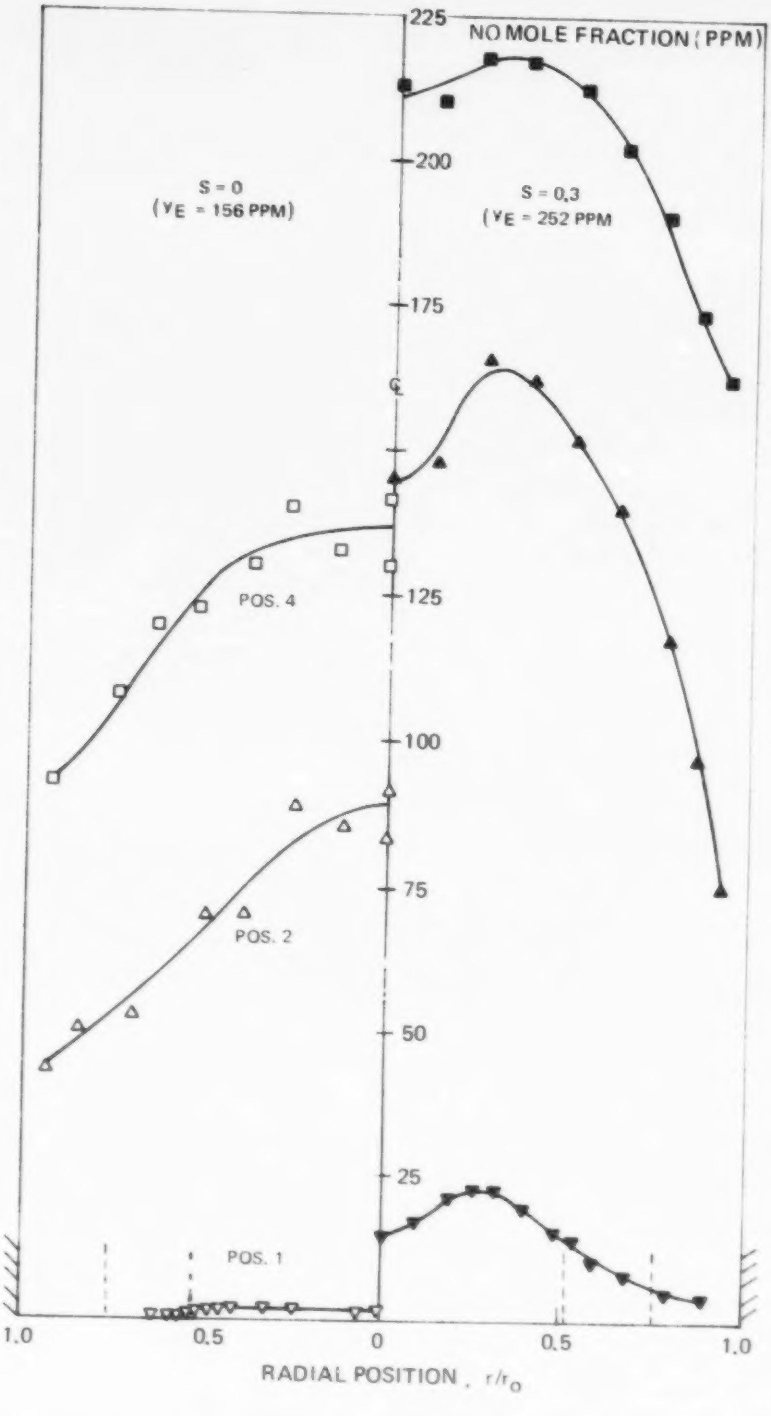

N12-153-6

Velocity Profiles in Swirling Combustor Flow (S=0.3).

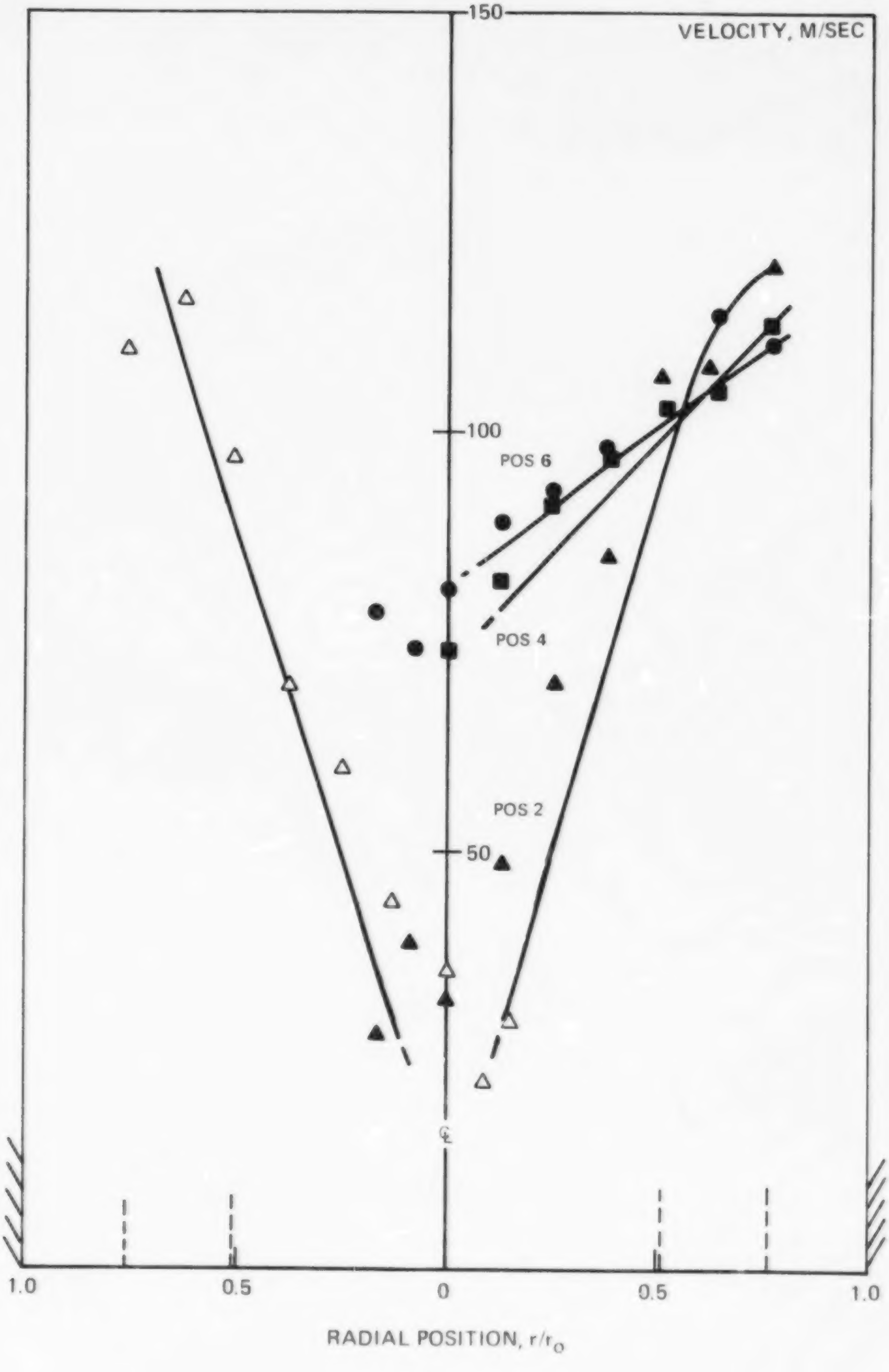

Measured flow angles are given in Fig. 45. With the impact-static probe moving toward the combustor centerline in the horizontal plane, pitch angles are measured in the horizontal plane, and yaw angles are measured in the vertical plane which is parallel to the main flow direction. Pitch angles, α, are positive (negative) for flow moving towards the probe from the wall (centerline). In the S=0.3 flow, pitch angles are small, $\alpha \leq 10$ deg. The flow in the pitch plane is directed toward the wall for $0.5 \leq r/r_o \leq 1.0$ and toward the centerline for radial locations less than $r/r_o \approx 0.5$. Yaw angles, β, are small near the centerline of the combustor and increase as the wall is approached. For typical yaw angles of 25-30 deg, the tangential velocity is approximately one-half of the axial velocity. The tangential current moves down one side of the combustor and up the other in a spiral fashion along the entire combustor length. Total flow angles, θ in Fig. 41, where $\theta = \cos^{-1} [(\cos \alpha)(\cos \beta)]$, (approximately equal to the yaw angle in the present case), provide further verification of the persistance of swirl-induced effects. Thus, for example, maximum total flow angle is only reduced 8 deg between the x=31.6 cm and the x=82.6 cm axial locations.

iv. Effect of Combustor Pressure

Increased pressure leads to enhanced reaction rates and a shift from chemistry-limited to mixing-limited conditions. It may be anticipated, therefore, that temperature and concentration profiles will develop off-axis peaks as the pressure level is raised, and that NO production will increase relative to the baseline case, and THC concentrations will decrease. This diffusion flame behavior is indeed displayed by the temperature map of Fig. 46 and the various concentration maps presented in Figs. 47-51, for combustor operation at about 3.6 atm with all other fuel and air input conditions being the same as the baseline case.

Oxygen and THC concentration profiles, Figs. 47 and 48, for 3.6 atm reflect significant separation of the air and fuels stream, and resemble profiles encountered in classical diffusion flames. As in the swirling flow, combustion is concentrated in an off-axis annular region, characterized by maxima in temperature and in the concentrations of CO, Fig. 49, CO_2, Fig. 50, and NO, Fig. 51. At the elevated pressure the rate of oxidation of hydrocarbons to CO is rapid due to the combination of high peak temperatures and longer residence times. Centerline CO concentration levels at 3.6 atm are very high relative to the 1 atm baseline case in the first meter of combustor length, reflecting the rapid initial hydrocarbon oxidation and the limited availability of oxygen in the central portion of the combustor due to unmixedness. Ultimately, far downstream in the extender section, oxygen is more thoroughly diffused throughout the flow and CO oxidation proceeds unhindered. At the exhaust sampling station, therefore, average CO and CO_2 concentrations are comparable for 1.0 and 3.6 atm.

Increased temperatures and longer residence times associated with the high pressure operating conditions result in an appreciable increase in the NO formation rates

FIG. 45

Direction of Flow in Combustor with S=0.3.

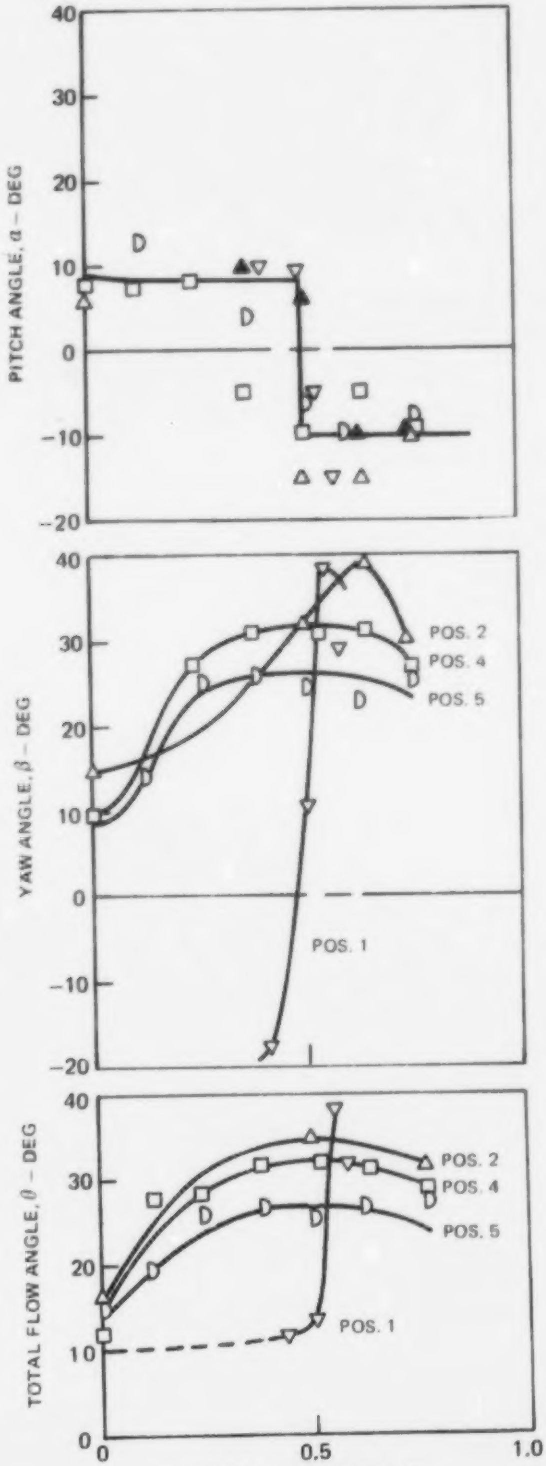

FIG. 46

Temperature Profiles for Baseline (P=1 atm) Combustion Test and for High Pressure (P=3.6 atm) Combustion of Natural Gas (T_f=305°K) with 0.137 kg/sec of 750°K Air, V_a/V_f=22.9, ϕ=0.87, S=0.

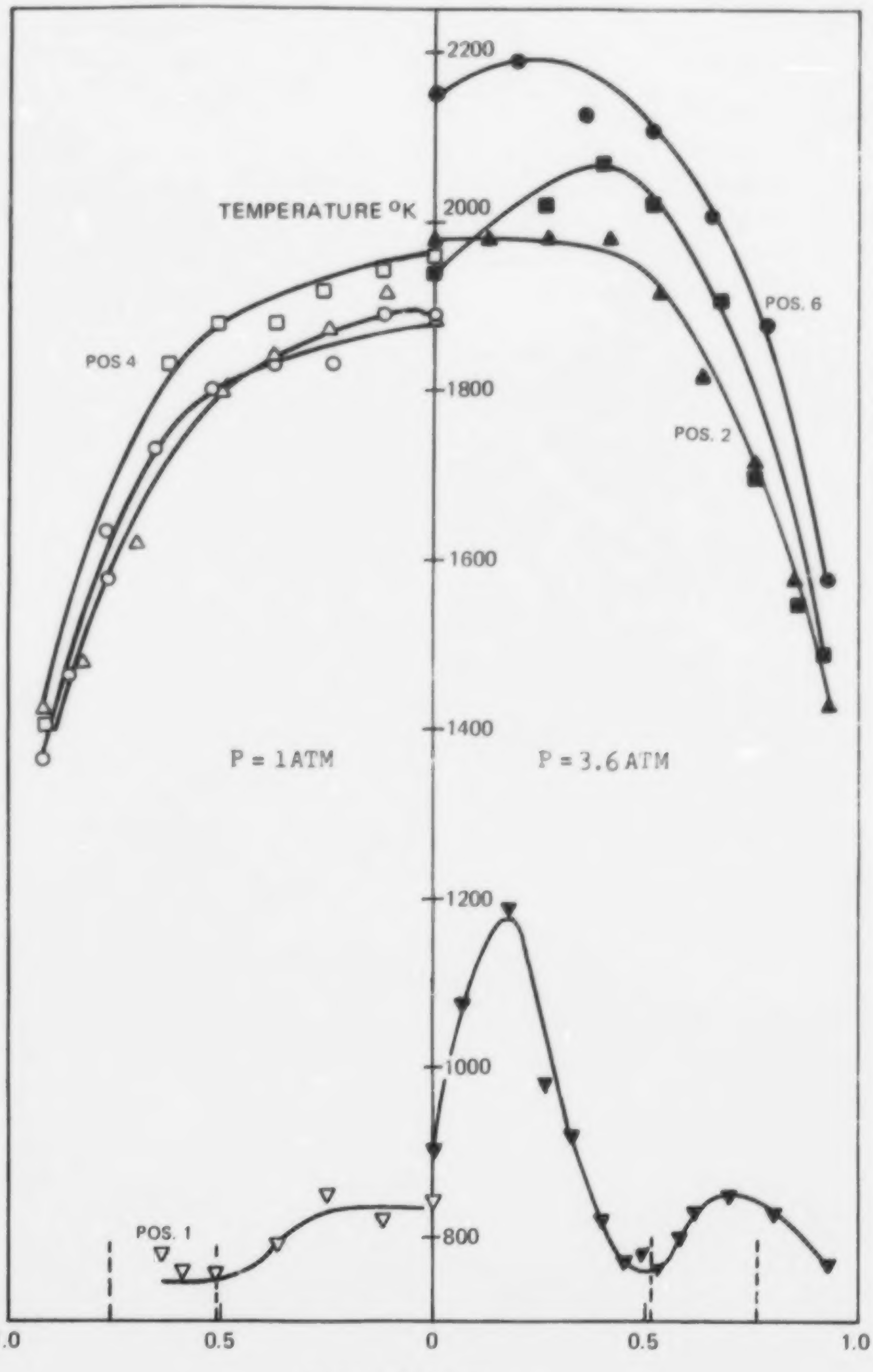

FIG. 47

Oxygen Concentration Maps for High Pressure (P=3.6 atm) and Baseline (P=1 atm) Combustion Tests.

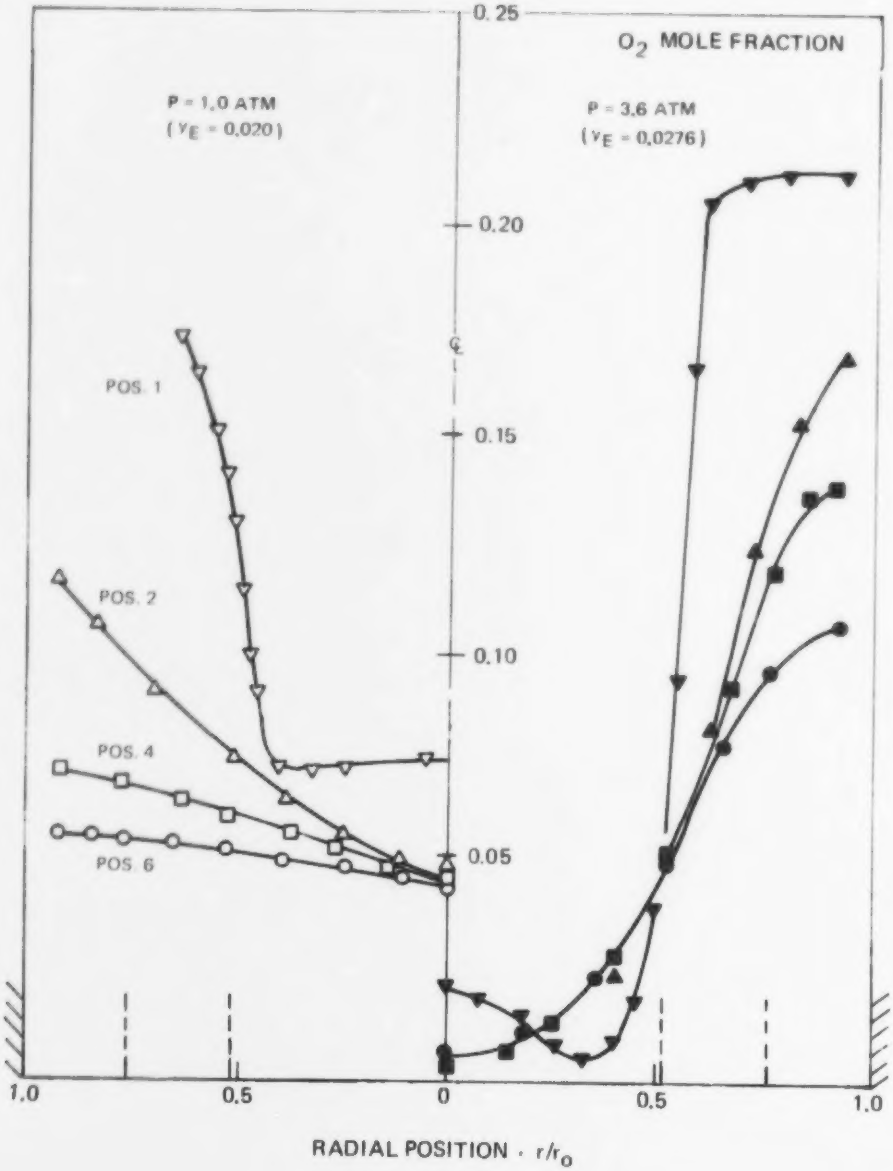

N12–153–8

FIG. 48

Total Hydrocarbon Concentration Maps for High Pressure (P=3.6 atm) and Baseline (P=1 atm) Combustion Tests.

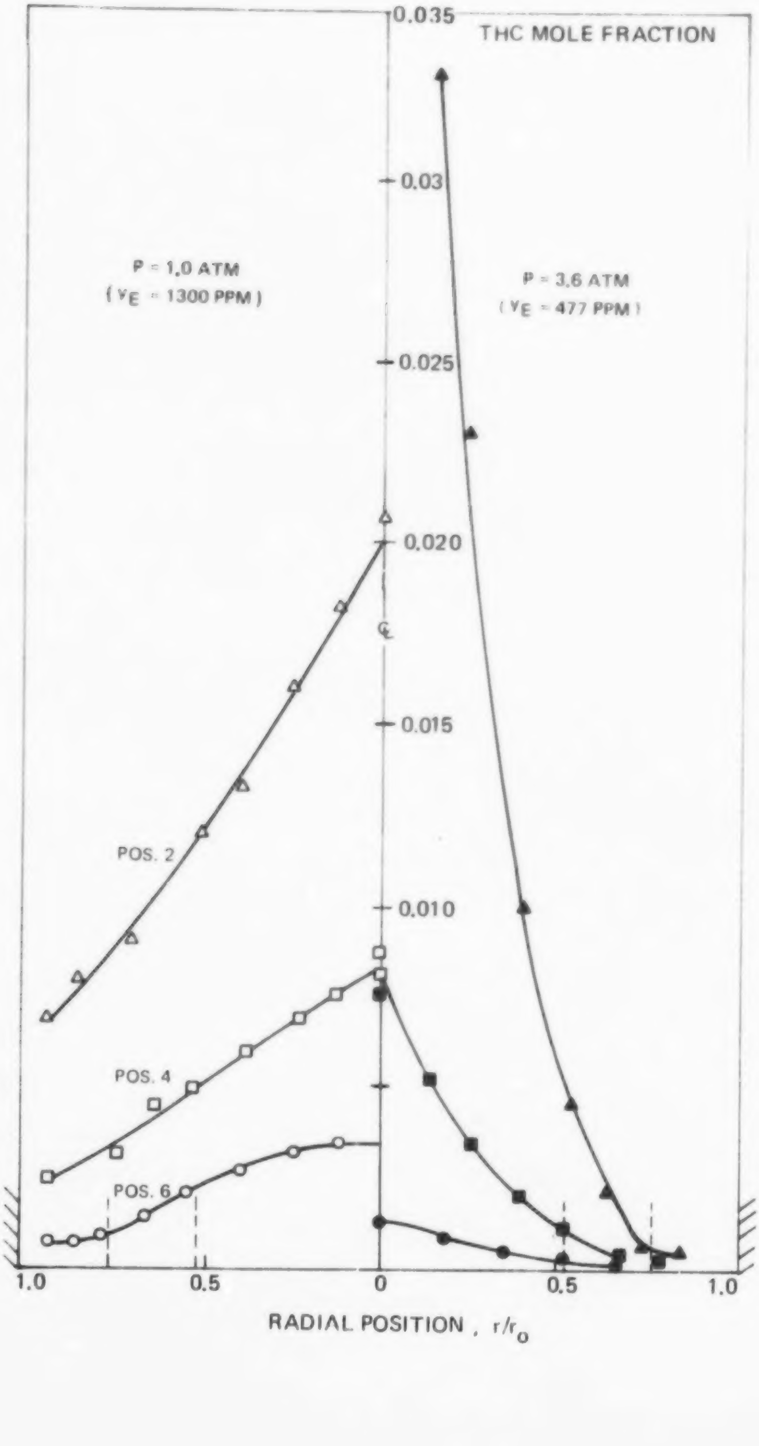

N12–153–15

CO Concentration Maps for High Pressure (P=3.6 atm) and Baseline (P=1 atm) Combustion Tests.

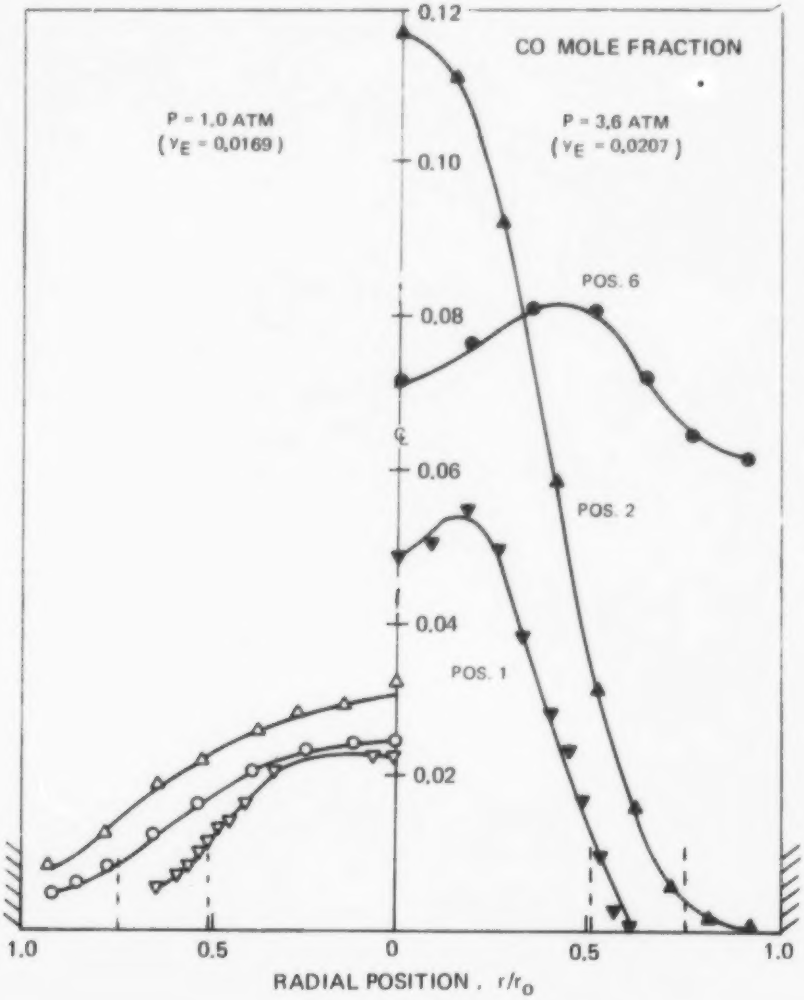

FIG. 50

CO$_2$ Concentration Maps for High Pressure (P=3.6 atm) and Baseline (P=1 atm) Combustion Tests.

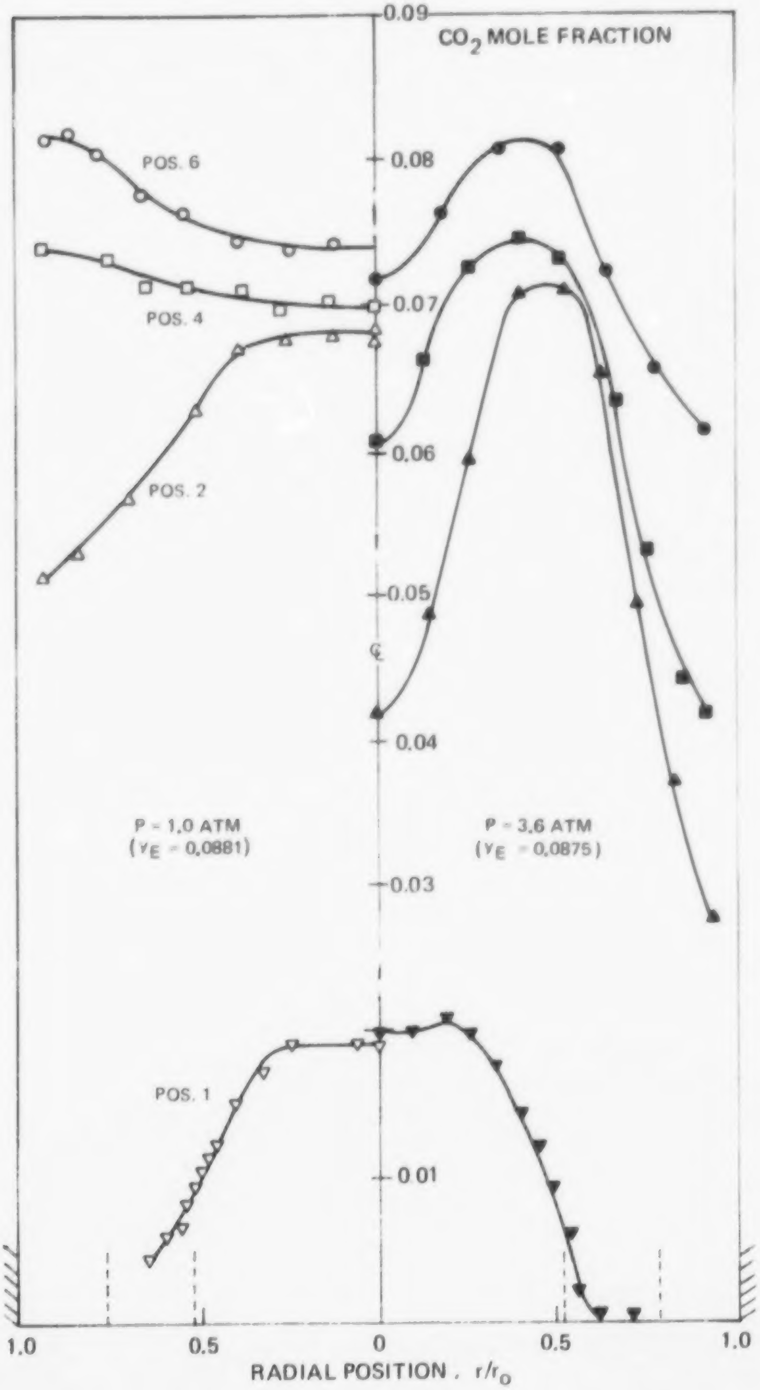

N12-153-9

FIG. 51

NO Concentration Maps for High Pressure (P=3.6 atm) and Baseline (P=1 atm) Combustion Tests.

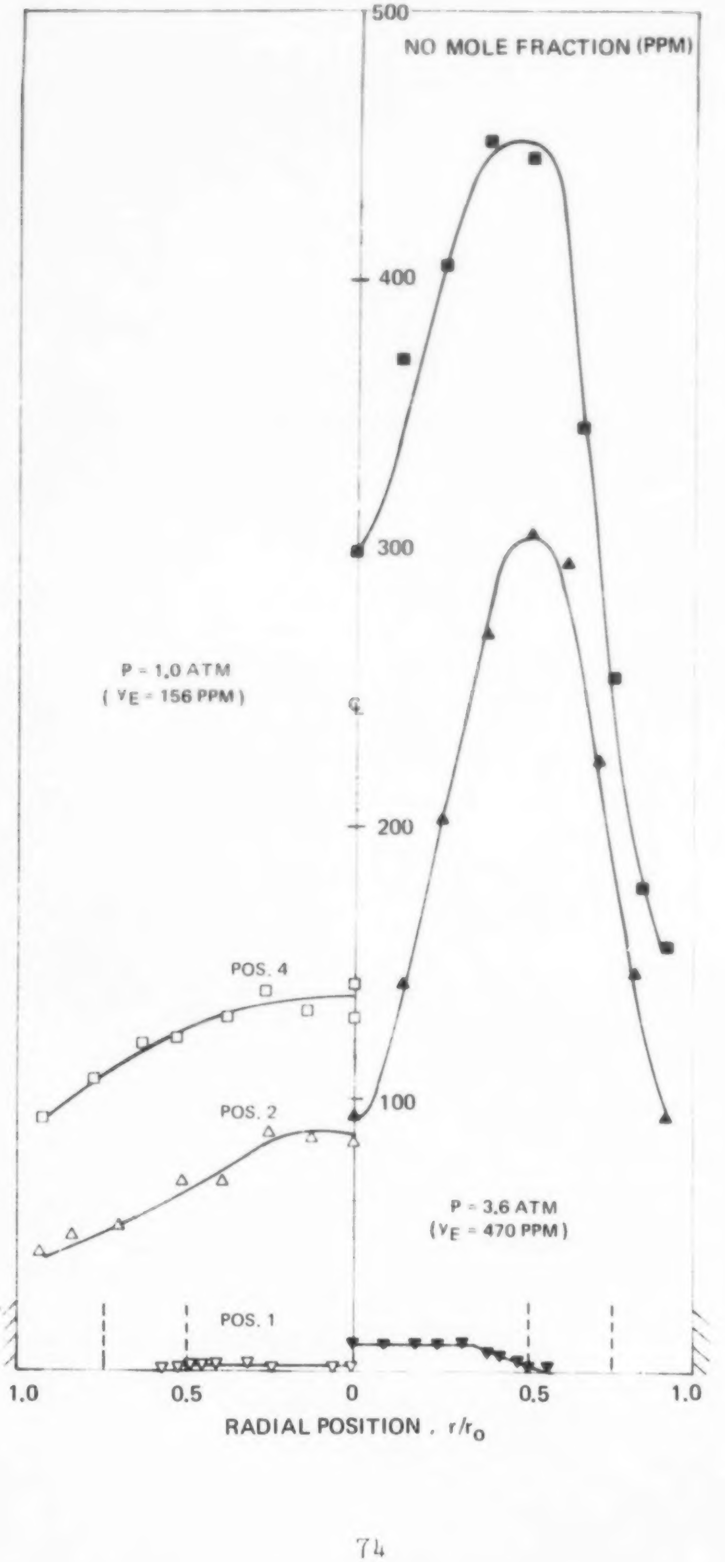

N12–153–5

relative to baseline operation (Fig. 51). Introduction of swirl has only a minor effect on exhaust NO levels (see results from input-output experiments) at the elevated pressure, suggesting that swirl produces only minor changes in the flow field.

NO_2 levels measured at 3.6 atm were much smaller than those at 1 atm. No NO_2 was found in the shear region near the lip of the fuel injector, in contrast to the results of the 1 atm tests.

v. Liquid Propane Tests

Results from the input-output experiments indicate that operation of the combustor on liquid propane produces variations in pollutant emissions levels with input parameters which differ from those found with gaseous fuels. To gain some preliminary understanding of the flow field when burning liquid fuels and to evaluate experimental problems encountered when probing two-phase reacting flows, two mapping tests were carried out with the combustor operating on liquid propane. Nominal test conditions for these experiments are listed in Table II.

High-speed motion pictures of the reacting flow field in the vicinity of the injection plane reveal that the fuel-spray is surrounded by a light blue-orange flame (at one atmosphere pressure) rotating at a frequency which correlates approximately with the tangential velocity of the swirling air stream. In addition, a significant axial movement of the ignition location is observed, and the fuel spray pattern downstream from the injector appears to be non-steady.

Although time-dependent, three-dimensional effects are evident in the swirling flow liquid propane tests, the time-mean flow resembles a classical axisymmetric diffusion flame (except, perhaps, in the vicinity of the spray) and is qualitatively similar to that observed in the swirling natural gas flame. The temperature profiles for the liquid propane tests, Figs. 52 and 53, exhibit peaks off-centerline. Peak temperature levels in the liquid propane tests were approximately the same as found in the swirling natural gas flame, although lower centerline temperatures were found in the propane tests. The O_2 and THC concentration maps for liquid propane combustion, Figs. 54 and 55, also resemble those found in the swirling natural gas flame, with oxygen being confined, more or less, to an annular region near the combustor wall and fuel being confined near the combustor centerline. The CO and CO_2 concentration maps for liquid propane combustion, Figs. 56 and 57, are qualitatively similar to those found in the swirling natural gas flame, with CO being confined to a region near the centerline and CO_2 exhibiting concentration peaks off-centerline. In the liquid propane tests, hydrocarbon and CO oxidation rates appear to be somewhat slower than in the swirling natural gas flame. These reduced oxidation rates are reflected in the results of the input-output tests which show generally higher THC and CO emissions for the liquid propane tests. Examination of the concentration maps suggests that the

Temperature Profiles for Combustion of Liquid Propane with 0.137 kg/sec of 739 K°Air, S=0.3, at 1 atm. Overall Fuel-Air Equivalence Ratio = 0.92. Data Obtained Using Calibrated Thermocouple Probe.

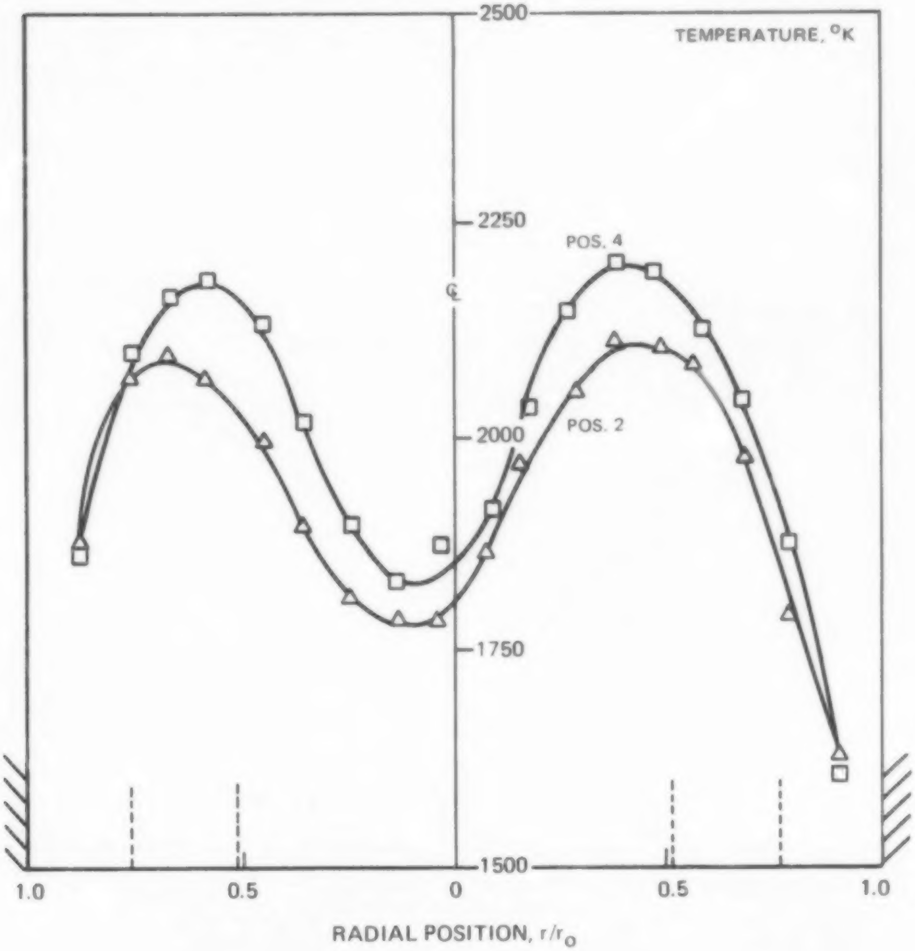

FIG. 53

Temperature Profiles for Combustion of Liquid Propane with 0.137 kg/sec of 739°K Air, S=0.3, at 1 atm. Overall Fuel-Air Equivalence Ratio - 1.04. Data Obtained Using Calibrated Thermocouple Probe.

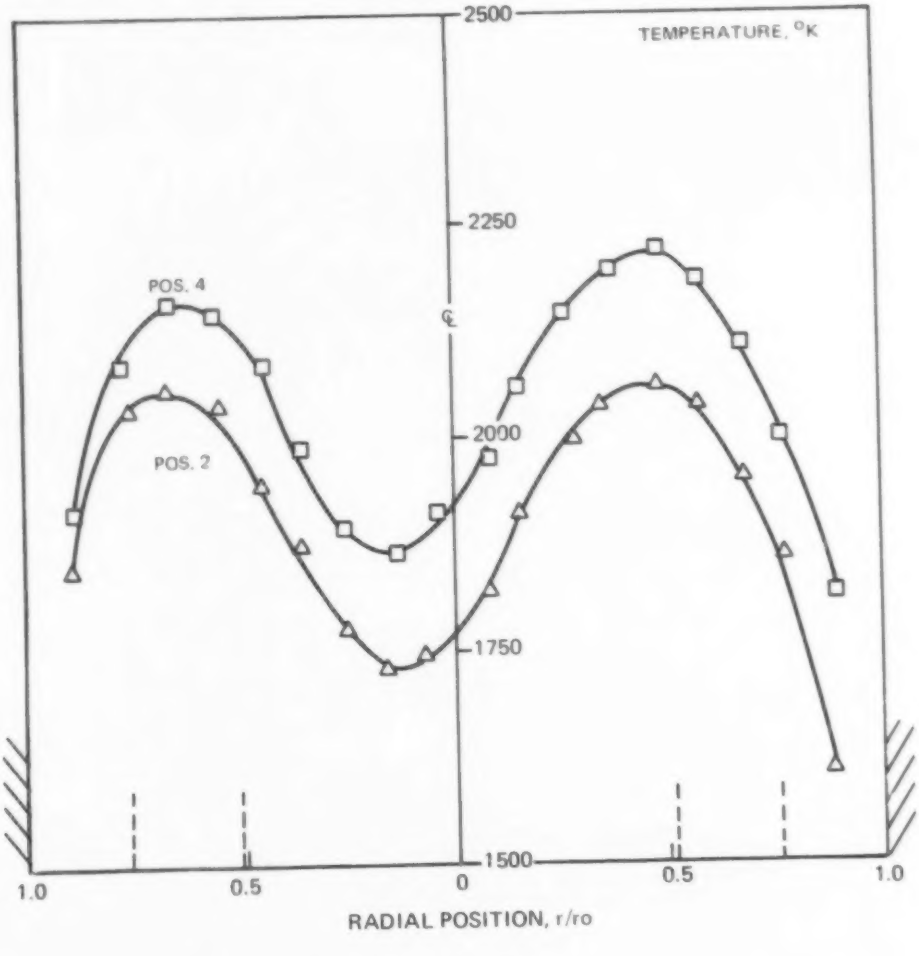

RO2-29-2

FIG. 54

Oxygen Concentration Maps for Liquid Propane Combustion Tests.

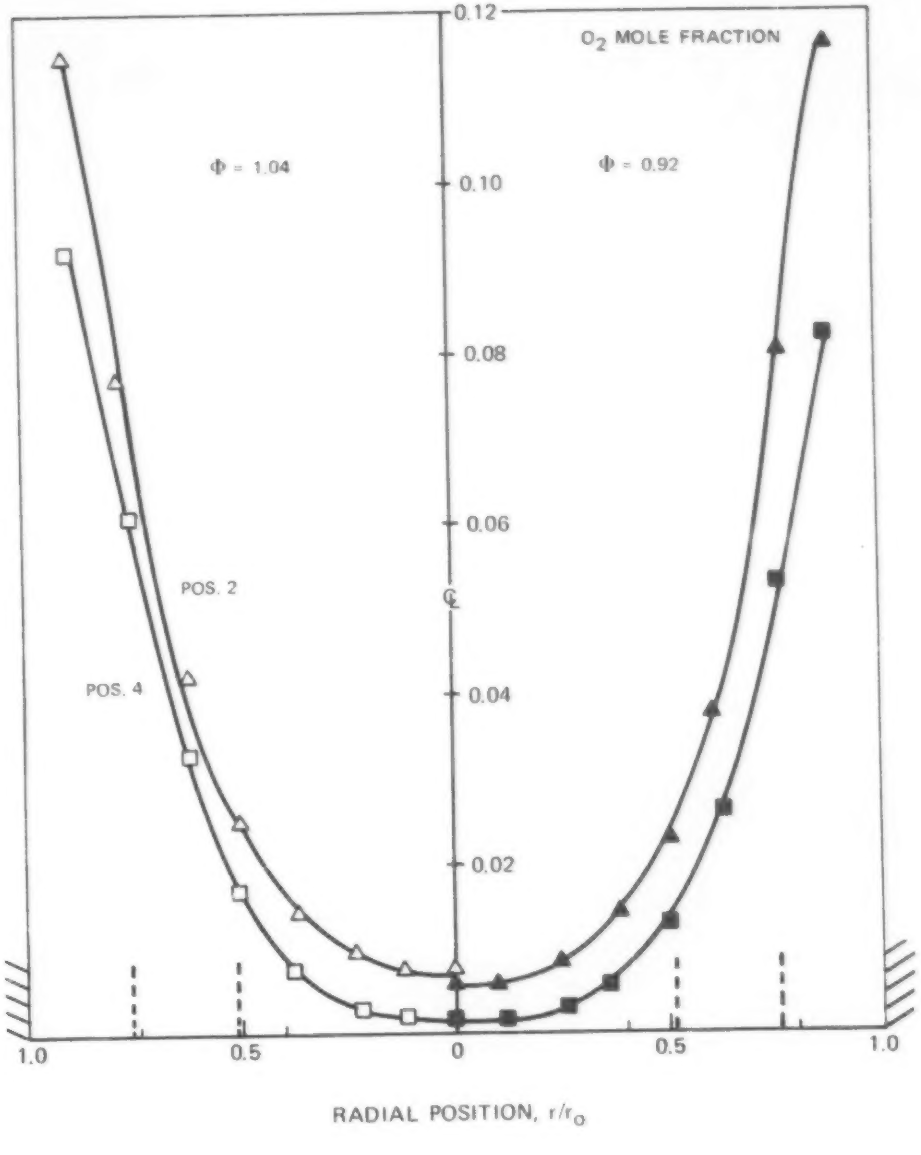

R02-29-1'

Total Hydrocarbon Maps for Liquid Propane Combustion Tests.

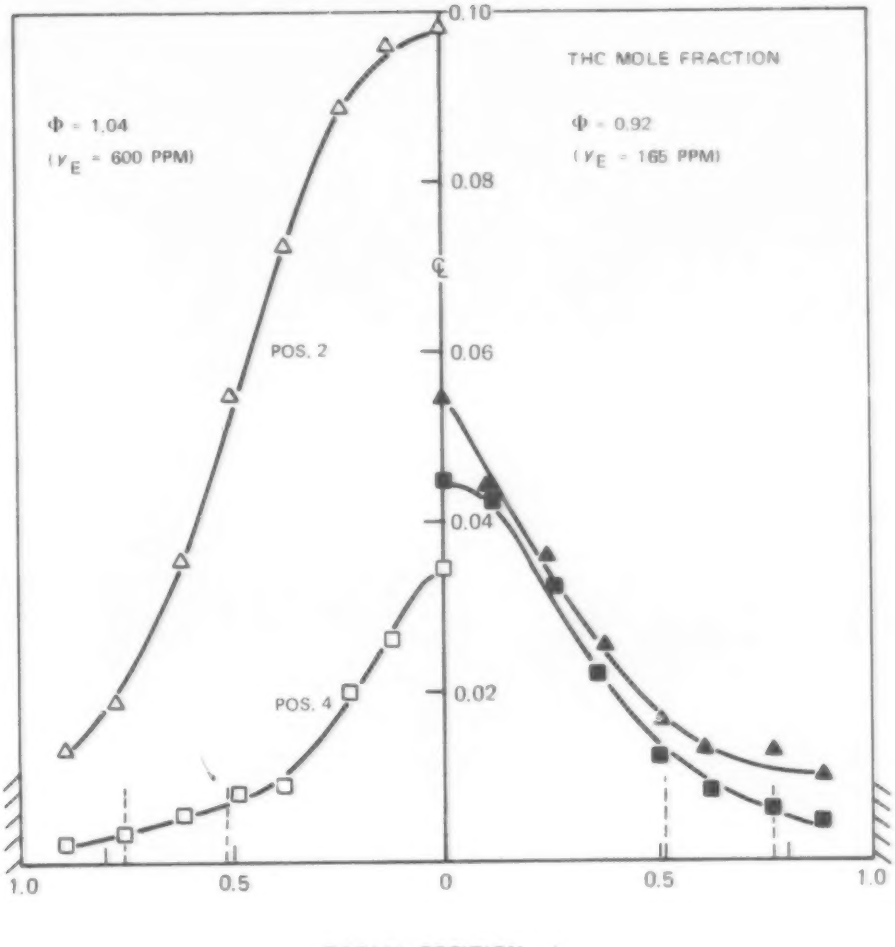

CO Concentration Maps for Liquid Propane Combustion Tests.

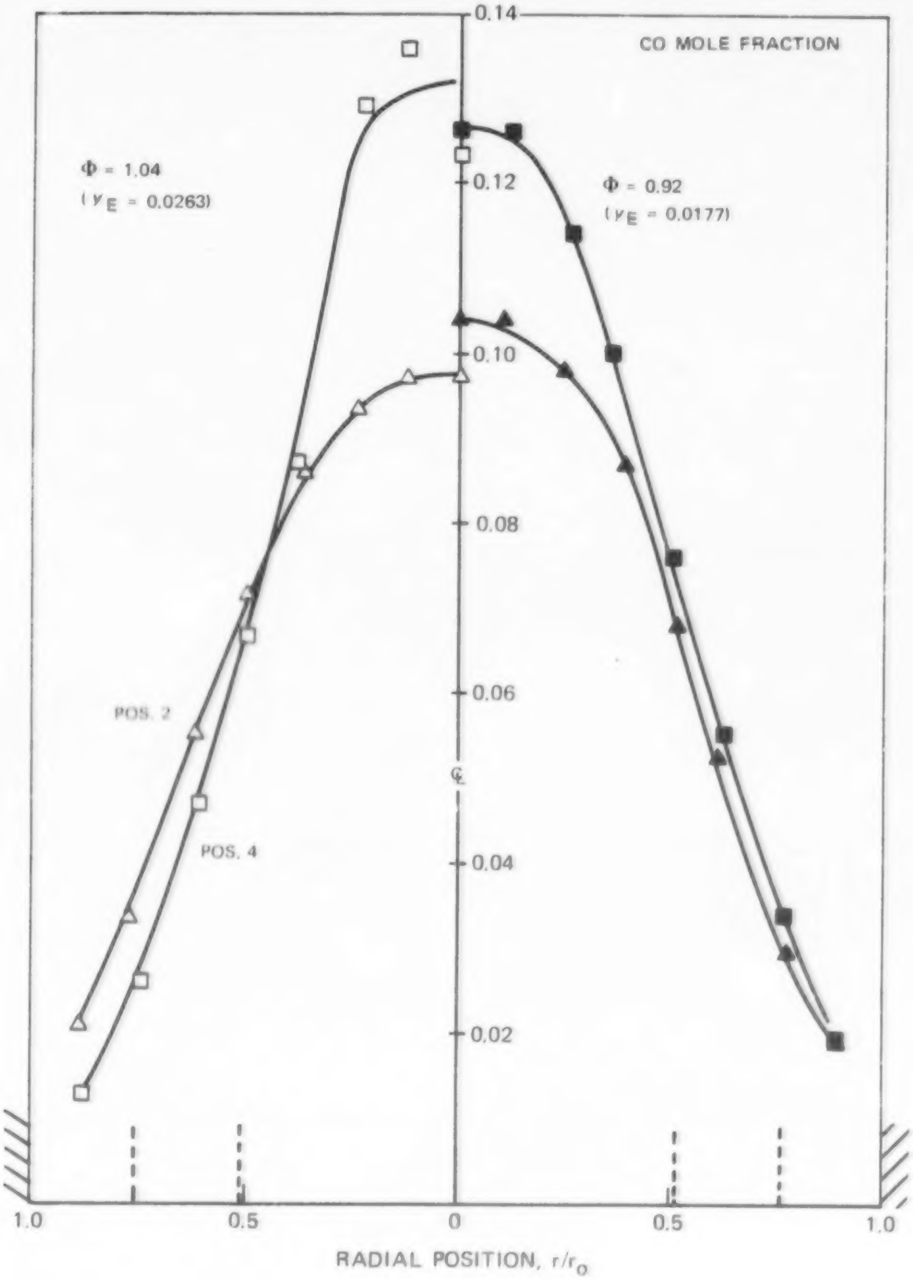

CO_2 Concentration Maps for Liquid Propane Combustion Tests.

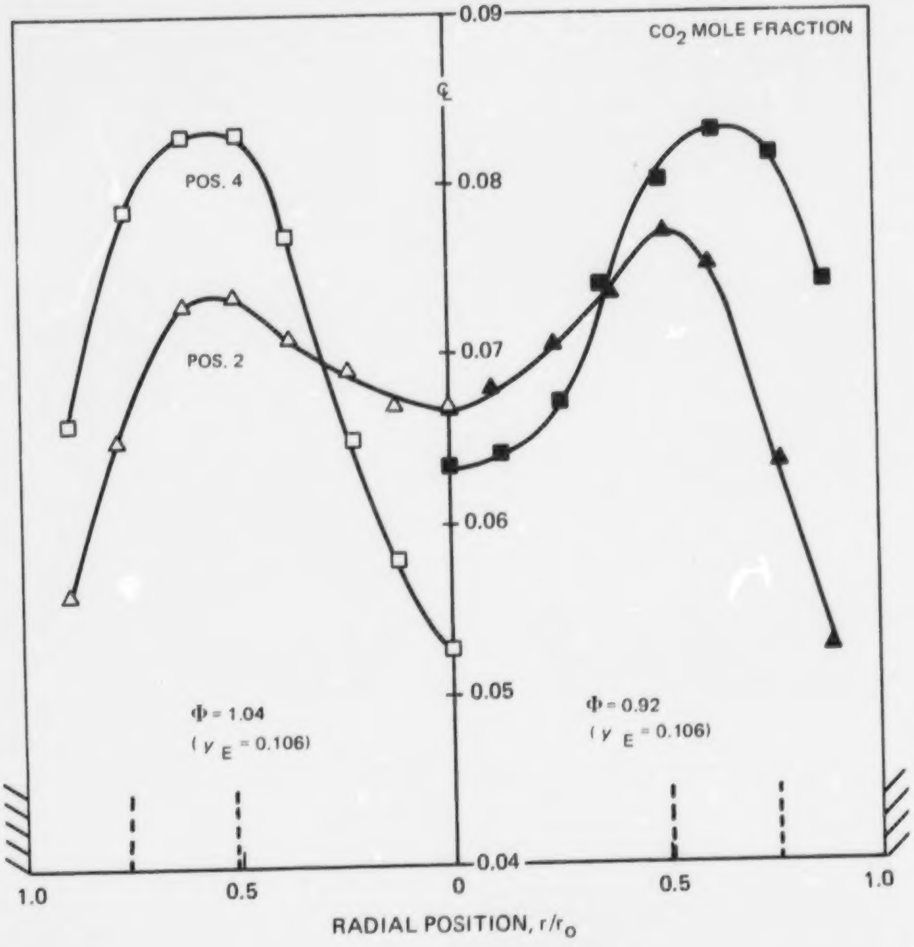

slower oxidation rates primarily are the consequence of a greater separation of the fuel and air streams (i.e. decreased availability of O_2 near the centerline) in the liquid fuel tests. The NO concentration profiles, Fig. 58, in the liquid propane tests also exhibit off-centerline peaks. The radial locations of these peaks correspond approximately with the maximum temperatures. NO concentrations in the liquid propane tests generally are lower than measured in the swirling natural gas flame. The lower NO levels in the liquid fuel tests probably result from a reduction in the high-temperature, O_2-rich volume in the combustor.

The temperature and concentration distributions presented above document the diffusion-flame character of the flow in the liquid propane combustion tests. In these tests, unmixedness, which persists for long distances in the combustor, has a significant influence on hydrocarbon and CO oxidation rates and on NO formation. It can be anticipated that spray characteristics (in particular, spray cone angle) will significantly influence radial temperature and concentration gradients in the flow. As combustor operating pressure increases, the spray cone angle decreases (Ref. 13), and the region of maximum temperature will be somewhat closer to the combustor centerline, encompassing a somewhat smaller volume. Hence, it is reasonable to expect lower NO emissions than found in the atmospheric pressure tests. This observation is in agreement with the trend established in the input-output tests.

Certain difficulties were encountered in probing the two-phase regions of the flow field. The relatively cold exterior probe surfaces served to quench chemical reactions and, in the vicinity of the fuel spray, substantial deposits of soot were formed on the probe. These deposits frequently blocked the probe inlets, hence it was not possible to obtain flow field data at the x=1.92 cm location.

NO Concentration Maps for Liquid Propane Combustion Tests.

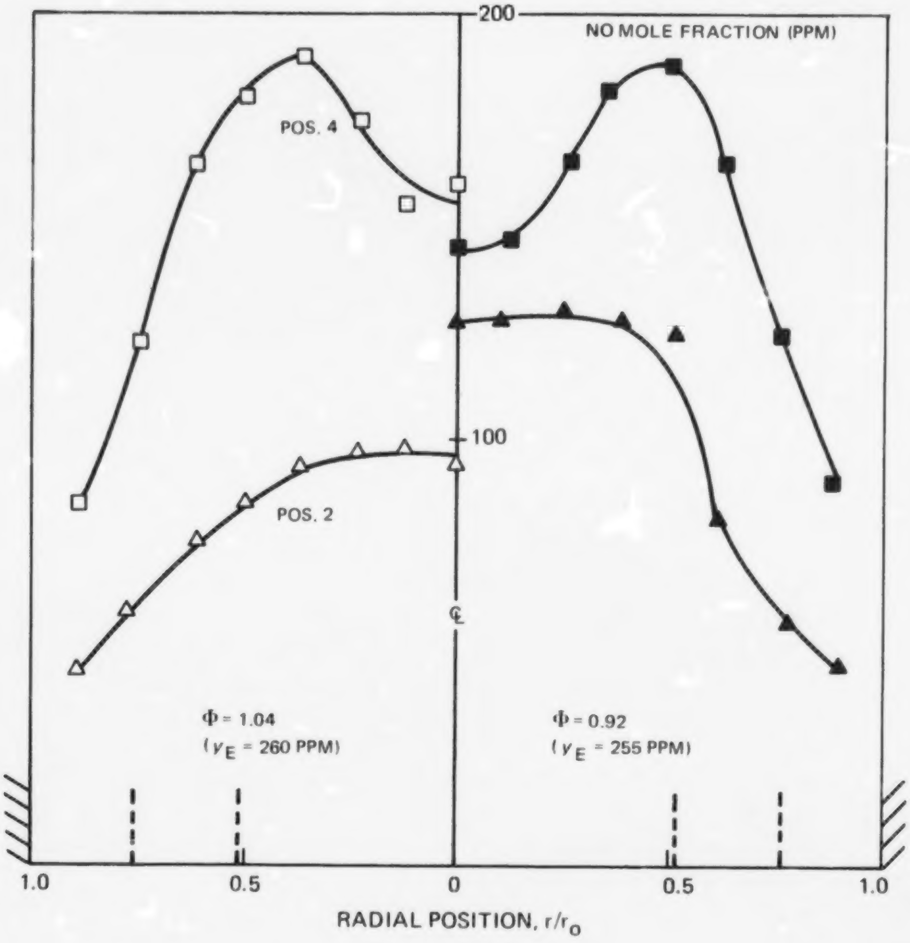

III. CONCLUDING REMARKS

From the results of the flow-field mapping experiments, several general observations can be made concerning the interaction between the flow field and the pollutant formation and destruction processes. For the range of conditions investigated, the primary hydrocarbon combustion zone, where most of the hydrocarbon fuel reacts to form CO, is located relatively close to the injector, i.e., within an axial length of about 5 combustor radii. In this zone which contains the stabilizing recirculation zone, a significant fraction of the total available chemical energy is released, and high levels of CO and NO are established. Peak CO levels in the primary zone are significantly larger than equilibrium levels,calculated based on inlet conditions. Measured NO_2 concentrations in the primary combustion zone are relatively large. Near the injection plane, NO_2 concentrations in excess of the NO concentrations were measured in the shear region separating the inner and outer flows. Downstream from the primary combustion zone, the remaining hydrocarbon fuel and the CO oxidize. There are no significant increases in temperature in this post-combustion zone; however, because of the relatively high temperatures, significant additional NO formation occurs. In the post-combustion zone, the NO_2/NO ratio decreases, primarily because of the increasing NO concentration.

In the present experiments, the reacting flows can be roughly characterized as chemistry-limited or mixing-limited, depending on the relative rates of chemical reaction and mixing. In the non-swirling, atmospheric pressure flames, the large scale fluctuations of the stabilizing recirculation zone enhance mixing of the fuel and air streams and result in a primary combustion zone which resembles a stirred reactor. Downstream from the primary zone, the flow resembles plug flow. These flows appear to be chemistry-limited in that mixing rates are rapid relative to chemical reaction rates. As a result of the well-mixed nature of the flow, temperatures are moderated so that hydrocarbon and CO oxidation rates and NO formation rates are relatively slow. Hence, chemistry-limited flows are characterized by relatively high THC and CO emissions and relatively low NO emissions.

Increasing combustor pressure or imparting swirl to the inlet air streams results in a shift from chemistry-limited to mixing-limited behavior. In mixing-limited flows, the time-mean flow field exhibits the characteristics of a diffusion flame, with separation of the fuel and air streams and with chemical reaction occuring principally in an annular region surrounding the combustor centerline. Maximum temperatures in the region are considerably larger than found in the chemistry-limited flows, resulting in increased hydrocarbon and CO oxidation rates and NO formation rates. Hence, mixing-limited flows are characterized by relatively low THC and CO emissions and relatively high NO emissions.

High-speed motion pictures of the reacting flow field in the vicinity of the injection plane reveal significant fluctuations in the flame structure, and several different types of flow instabilities have been identified. Although there are substantial time-dependent, three-dimensional effects, for most of the experimental conditions investigated the time-mean flow is nearly axisymmetric.

Present experimental results indicate that much of the interesting fluid dynamic and chemical phenomena occur in a region very near the injection plane, containing the stabilizing recirculation zone. More detailed information on the velocity, temperature and species concentration distributions are required in the near-injector region if the significant features of the flow field and the interaction with the pollutant formation process are to be understood. Of particular importance are velocity and flow direction measurements in the recirculation zone. An effort is required to characterize the unsteadiness in the flow field and the subsequent effect on pollutant formation. In the present experiments, penetration of the recirculation zone in the gaseous fuel injector was observed for a range of experimental conditions. This penetration made identification of the inlet conditions difficult, and, hence, introduced an additional uncertainty in the comparison of the experimental data with results from the combustor flow analysis. Some effort should be devoted to the characterization of the injector flow upstream from the penetration region of the recirculation zone.

APPENDIX A

COMPUTATION OF THE SWIRL NUMBER

The derivation to follow is taken from Ref. 21 where a swirl number, S, which is used to characterize swirling flows, is defined in terms of the nozzle torque, τ, the jet thrust, ξ, and an effective nozzle diameter, $d_e \equiv d\,(1-Z^2)^{\frac{1}{2}}$, i.e.,

$$S = \tau/\xi \cdot d_e \tag{A-1}$$

For the swirl generator in Fig. 3, vanes of constant chord and angle are mounted on a hub of diameter, d_h, and extend to the wall of the nozzle tube, of diameter d. In passing over the vanes the air at velocity, V, is accelerated to $V/\cos\eta$, where η is the blade angle. The axial and tangential components of the air velocity issuing from the blades are V and $V\tan\eta$, respectively. If the air-fuel momentum flux ratio is large with respect to unity and/or the hub diameter is small with respect to the outer diameter, the components of the momentum associated with the fuel stream can be ignored. This is the case for the present experiments.

Considering an elemental annulus the torque is

$$d\tau = 2\pi\rho V\,(V\tan\eta)\int_{d_h}^{d} r^2\,dr \tag{A-2}$$

or

$$\tau = \xi\left[\frac{d}{3}\left(\frac{1-Z^3}{1-Z^2}\right)\right]\tan\eta \tag{A-3}$$

Then

$$S = \frac{1}{3}\;\frac{(1-Z^3)}{(1-Z^2)^{3/2}}\tan\eta \tag{A-4}$$

verifying that the swirl number is dependent exclusively on nozzle and blade geometry.

APPENDIX B

COMBUSTOR PROBE DESIGNS AND CALIBRATION PROCEDURES AND REDUCTION OF PROBE DATA

The probing devices employed in the current investigation included: (1) a five-probe rake for exhaust flow sampling, (2) a calibrated conduction heat-loss thermocouple probe and (3) a multi-purpose rake consisting of a double-sonic orifice probe and a flow field measuring probe. All of the probes were designed specifically for operation within the severe environments that are characteristic of the EPA combustion rig. Since these designs contain several unique features and since the application of the various probes to combustion measurements is somewhat complicated, each probe type is described in detail and calibration and data reduction procedures are discussed.

Exhaust Gas Sampling Rake

The five-probe, exhaust gas sampling rake is placed just downstream of the second spool piece, approximately 1.8 m from the plane at which fuel and air are brought into initial contact, to aspirate the combustion gases for subsequent analysis. Placement of the five probes was determined by dividing one-half of the combustor circular cross-section into five equal concentric area segments and noting the radial distances to the mid-point of each area segment. A probe was then located at each mid-point along a diameter, or its corresponding position 180 deg away as dictated by packaging constraints. With this arrangement, each probe aspirates sample with a composition which is approximately an average for the segment in which it is located. An identical choke is placed in each probe to insure that equal mass flows are aspirated for every segment. Gas from all five probes enters a common chamber where mixing occurs to produce a fluid with the same area-averaged composition as that at the combustor exhaust. It is this fluid which is analyzed using a time-of-flight mass spectrometer or Scott Analyzer.

Quenching of the gas sample and cooling of the stainless steel probes is accomplished using high pressure, hot water which flows in jackets surrounding the sample flow passage (Fig.59). Operation of the rake at gas temperatures to 2500 °K and pressures from 1 to 7 atm is permissible for 1.8 kg/sec of cooling water at 4 atm and an inlet temperature of about 400°K. The internal design of the probes was achieved through a one-dimensional analysis of the governing geometric and flow parameters for the most severe environmental conditions expected. Area variations, wall friction and heat transfer were accounted for in the analysis through the use of influence coefficients (Ref. 22). It was desired in the design of the probes to: (1) inhibit chemical reaction of the material captured, by the combined effects of aerodynamic expansion and convective cooling, (2) minimize wall catalytic activity by keeping wall temperature below about 520°K, (3) prevent condensation of water by maintaining a minimum wall temperature of 400°K throughout, and (4) delay shocking down of the flow downstream of the choke until the flow total temperature was less than the auto-ignition limit, i.e., about 1000°K. The resulting probe design, Fig.59, has a length of 15.88 cm and an inlet hole diameter of 0.16 cm. A minimum area section located 4.61 cm from the probe entry chokes the flow. The question of chemical reaction of material within the probe was assessed by following the growth of an ignition parameter in the probe. This parameter, defined as the ratio of gas

Exhaust Gas Sampling Probe.

ALL DIMENSIONS IN CM

NOT TO SCALE

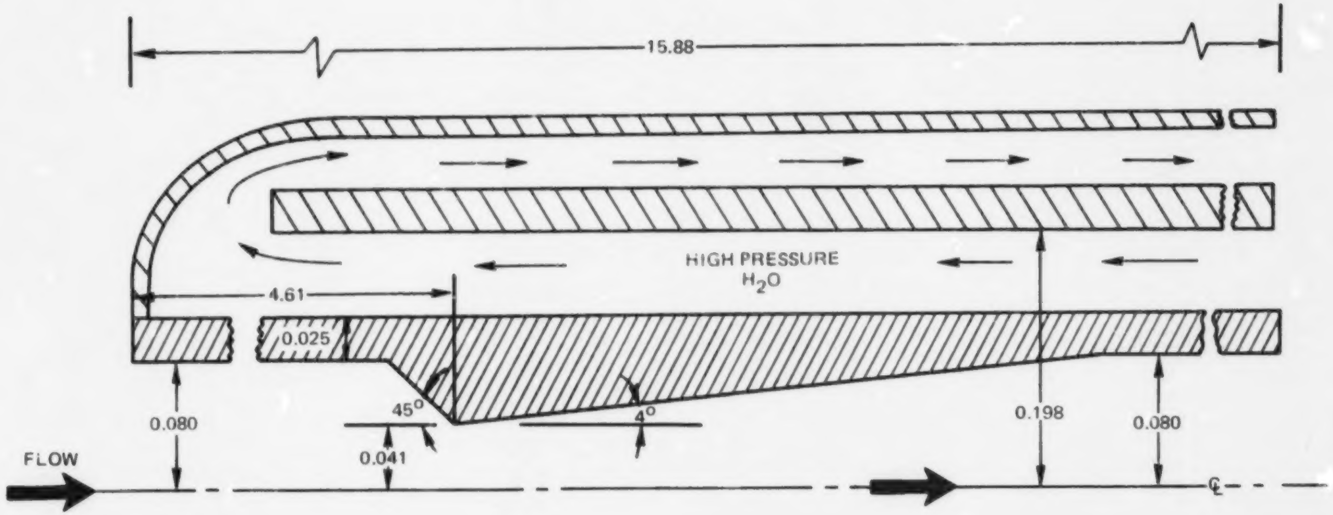
15.88
HIGH PRESSURE H_2O
4.61
0.025
0.080
45°
0.041
4°
0.198
0.080
FLOW
℄

FIG. 59

residence time to chemical ignition delay time (Ref.20), signifies ignition when its value is equal to or greater than unity. For gas samples initially at conditions which are representative of the most severe thermal environments of interest, e.g., $T=2500^{\circ}K$, $P=7$ atm, no ignition occurs in the probe according to the one-dimensional analysis. At the aft end of the probe the flow which was accelerated to supersonic speeds in the 4 deg divergent section, must shock down and rise to the stagnation temperature. Chemical reaction will not occur, however, since the stagnation temperature is reduced significantly below 1000°K in this probe design. The total volumetric flow for the five probe rake is in excess of 0.65 std m^3/hr at 1 atm, which is the minimum flow required by the Scott Analyzer.

Calibrated Heat-Loss Conduction Probe

This water-cooled thermocouple probe is designed to measure temperatures in excess of the platinum-rhodium and iridium-rhodium melting points which usually limit the use of thermocouples. The basic design philosophy is to deliberately apply a known error (heat loss) to the sensing thermocouple and to measure its subsequent temperature. The amount of heat loss used is sufficient to cool the thermocouple below the melting point.

The probe consists of three thermocouples including an iridium-60% rhodium/iridium thermocouple which protrudes from a copper base into the stream to record a temperature, T_A, and two platinum-10% rhodium/platinum thermocouples installed on the base to record base temperature, T_B. In order to obtain the true local stream temperature, T_T, the measured stream thermocouple temperature must be increased by the conduction and radiation heat-loss corrections, T_C and T_R, respectively:

$$T_T = T_A + T_C + T_R \qquad \text{(B-1)}$$
$$= 0.556\,(t_A + t_C + t_R)$$

where the small t denotes the measured temperature. Manipulation of corrections (supplied by the manufacturer) yields

$$T_T = 0.556\left[(1 + A)\,t_A - A t_B + B t_A^{3.75}\right] \qquad \text{(B-2)}$$

where for combustor weight flow, $\dot{w}$,

$$A \equiv \operatorname{sech}(0.59\dot{w})$$
$$B \equiv 33.6 \times 10^{-12}/\dot{w}^{0.5} \qquad \text{(B-3a,b)}$$

In typical situations, conduction and radiation heat loss corrections account for about a 25% reduction in the stream temperature measurement.

Multi-Purpose Rake

I. Impact-Static Probe

The impact-static probe, Fig. 6, consists of a cylinder with a hemispherical tip having a impact tap at its center and four symmetrically-located static pressure taps on a circle 40 deg back from the center. A static tap also is located 2.12 cm from the probe stagnation point, on the 0.95 cm diameter cylindrical portion. The pressure measured at this location was subtracted from the impact pressure for the calculation of dynamic pressure and, ultimately, axial flow velocity. Water at about $400^{\circ}K$ and 4 atm was used to cool the 5 cm long probe.

Local flow direction in the combustor was determined from the four differential pressures associated with the four static pressure taps on the hemispherical tip and the impact pressure, using suitable calibration information. Calibration data were acquired in the UARL 4-in.x 4-in. continuous (cold) flow wind tunnel for free stream dynamic pressures of 2-5 in. H_2O corresponding to Reynolds numbers based on the tunnel width of $0.5\text{-}1.3 \times 10^5$. These cold flow dynamic pressures approximate the levels found within the combustor. The Reynolds numbers are 3 to 6 times greater; however, no important variations in the calibration data were discovered over the range of Reynolds numbers tested.

Prior to installation of the probe, the uniformity of the tunnel flow field was verified by means of a traversing impact rake available with the facility. Subsequently, the probe was inserted into a rotatable disk, Fig. 60, in the tunnel sidewall. A range of probe yaw angles ($-20 \text{ deg} \leq \beta \leq +40 \text{ deg}$) relative to the known flow direction was set by rotating the disk. In addition, the probe mounting disk was fitted with angled brackets such that the probe could be pitched ($-40 \text{ deg} \leq \alpha \leq +40 \text{ deg}$) relative to the main flow direction. In this fashion flow angles comprised of both pitch and yaw components could be studied.

Differential pressures were measured between the probe impact tap and each of the static taps for several combinations of pitch and yaw angles. Read-out capability was provided with Magnehelic pressure gages (accuracy-better than 2% of full scale for 2 in. H_2O and 10 in. H_2O gages). It was found convenient for data reduction purposes to display this cold flow calibration information as shown in Figs. 61 and 62. The ordinate in each case is the difference between the differential pressures measured for static taps 180 deg apart, normalized by the dynamic pressure, q, e.g., $\left[(P_{T_1}-P_1)-(P_{T_1}-P_3)\right]/q$. If the impact-static probe is visualized as moving toward the combustor centerline in a horizontal plane, then the pitch plane is the horizontal plane and the yaw plane is vertical. Static taps nos. 3 and 1 are in the pitch plane, with tap no. 3 closest to the centerline for most of the traverse during the course of a typical test. Pitch angles, α, are positive (negative) for flow moving towards the probe from the wall (centerline). Static taps nos. 4 and 2 are in the yaw plane, with tap no. 4 over tap no. 2. Yaw angles, β, are positive (negative) for flow moving towards the probe from above (below).

Examination of Fig. 62 reveals that the yaw plane pressure factor is only a weak function of pitch angle for $-20 \leq \alpha < +20$. Within this range, therefore, a good esti-

FIG. 60

Calibration Set-up for Impact-Static Probe.

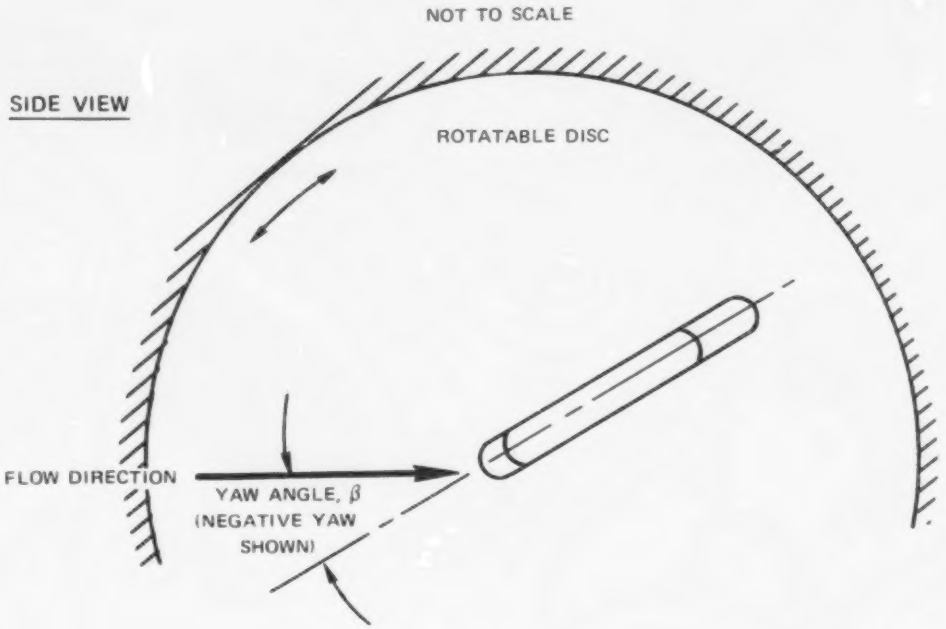

SIDE VIEW

NOT TO SCALE
ROTATABLE DISC
FLOW DIRECTION
YAW ANGLE, β
(NEGATIVE YAW
SHOWN)

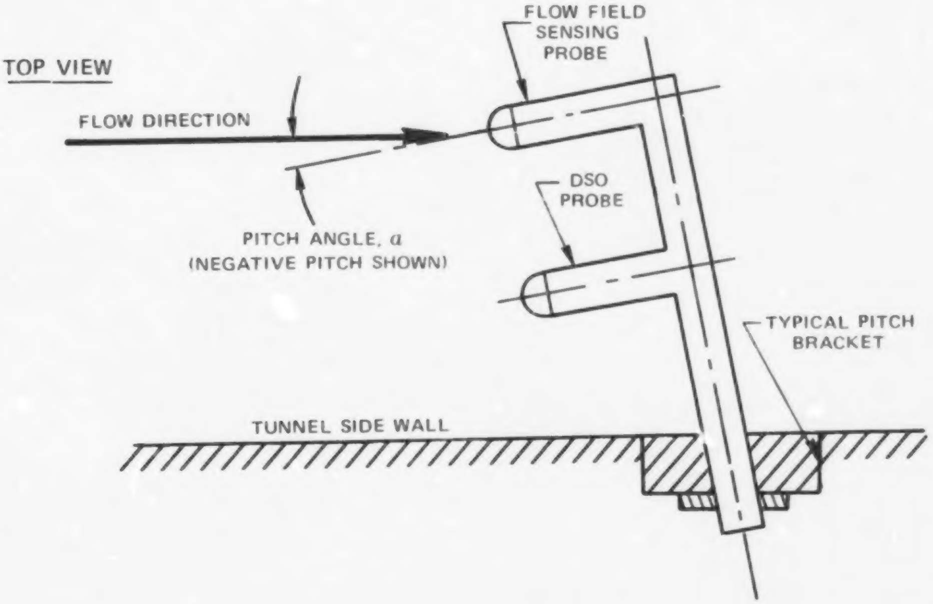

TOP VIEW

FLOW FIELD
SENSING
PROBE
FLOW DIRECTION
DSO
PROBE
PITCH ANGLE, α
(NEGATIVE PITCH SHOWN)
TYPICAL PITCH
BRACKET
TUNNEL SIDE WALL

P1-27-3

Impact-Static Probe Pitch Plane-Angle Calibration Data.

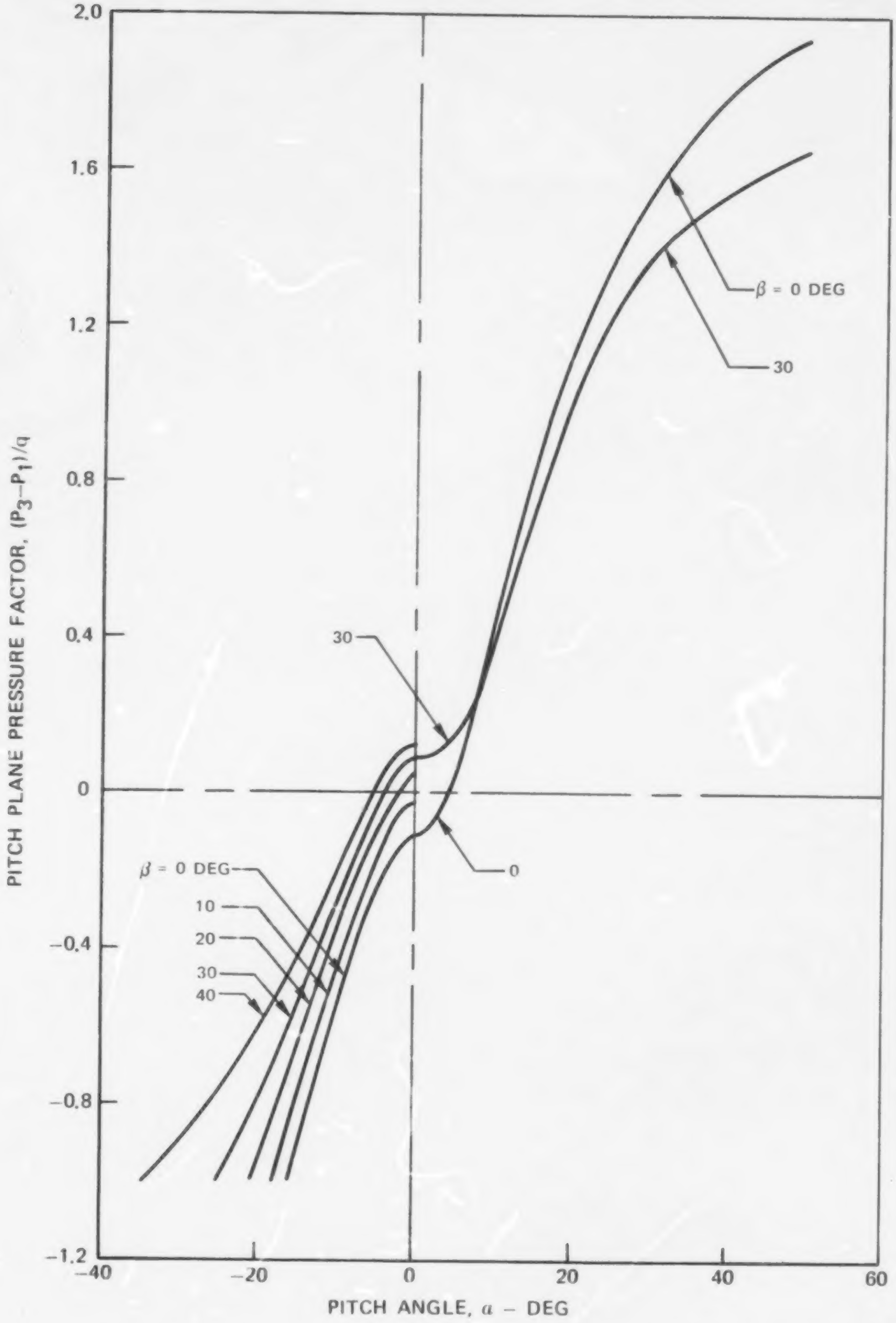

P1-27-2

Impact-Static Probe Yaw Plane-Angle Calibration Data.

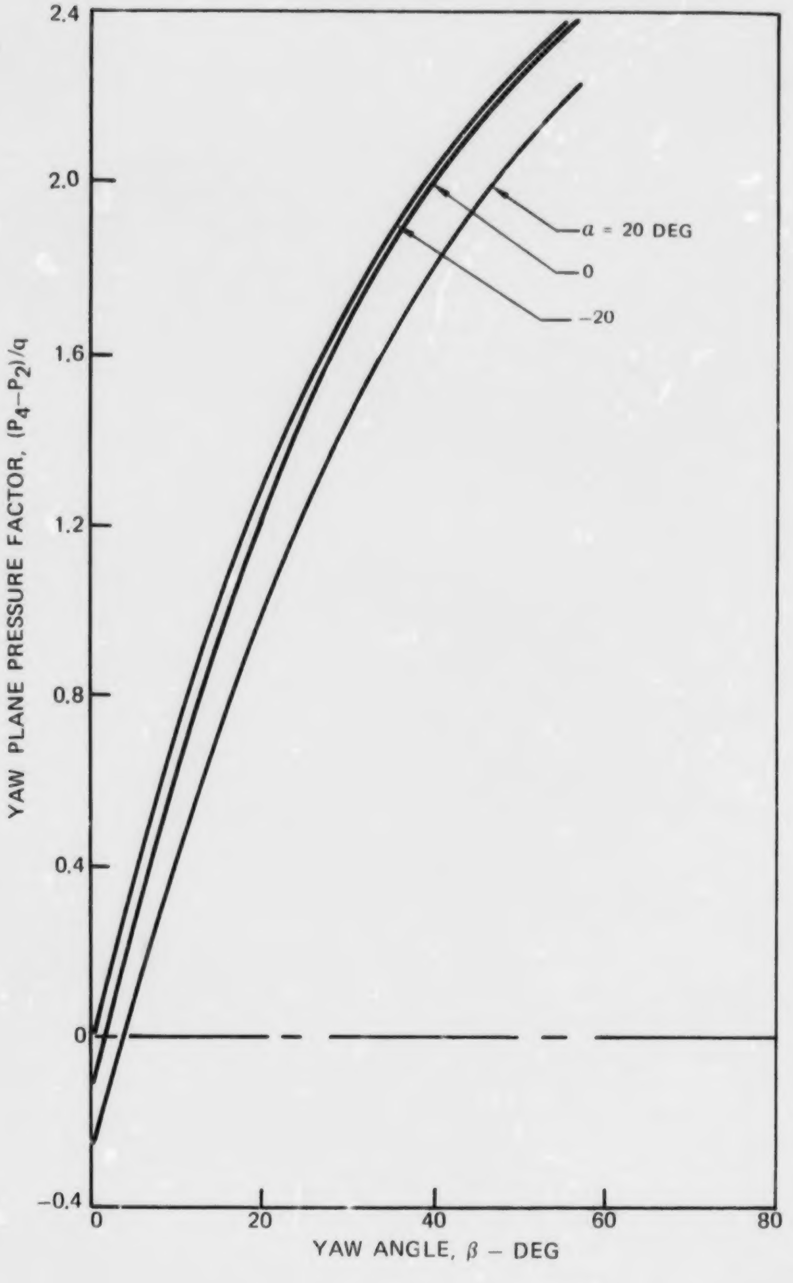

P1–27–1

mate of yaw angle can be determined for entry into Fig. 61 to establish a pitch angle. A minimal amount of iteration between Figs. 61 and 62 is then required to refine the values of α and β. Finally, a total flow angle, θ, can be computed from,

$$\theta = \cos^{-1}\left[(\cos\alpha)\ (\cos\beta)\right] \qquad \text{(B-4)}$$

This parameter is found to correlate with the geometric average pressure,

$$\frac{\overline{\Delta P}}{q} = \left[\left(\frac{P_{T_1} - P_1}{q} - \frac{P_{T_1} - P_3}{q}\right)^2 + \left(\frac{P_{T_1} - P_2}{q} - \frac{P_{T_1} - P_4}{q}\right)^2\right]^{1/2} \qquad \text{(B-5)}$$

as shown in Fig. 63.

II. Double-Sonic-Orifice (DSO) Probe

The DSO probe, Fig. 6, contains a nominal 0.127 cm diameter choked orifice integrated with the tip and a second orifice, 0.168 cm in diameter, at some distance downstream of the first orifice. The orifices are sized so that choking occurs at both orifices when gas is aspirated through the probe.

In principle, by measuring the stagnation pressure and temperature upstream of the second orifice during aspiration, P_{T_2} and T_{T_2}, respectively, and the stagnation pressure of the first orifice, i.e., the impact pressure obtained by "dead-ending" the probe, P_{T_1}, the stagnation temperature of the stream can be determined. That is, for a constant mass flow, and assuming that no significant molecular weight or ratio of specific heat changes occur in the flow between the two orifices, the desired local stream temperature, T_{T_1}, is given by

$$T_{T_1} = T_{T_2}\left[\frac{(C_D A^*)_1}{(C_D A^*)_2} \cdot \frac{P_{T_1}}{P_{T_2}}\right]^2 \qquad \text{(B-6)}$$

In order to use Eq. (B-6) for stream temperature determination, suitable calibration information for orifice flow coefficients must be available. These coefficients, which reflect boundary layer effects, depend on throat Reynolds number and the ratio of wall temperature to flow stagnation temperature. As Reynolds numbers are increased and/or wall temperature ratios are decreased, boundary layer displacement thickness decreases and the flow coefficient approaches unity.

DSO calibration data were obtained by placing the probe in uniform streams of high temperature air and natural gas-air combustion products. Local stream temperatures were measured using calibrated thermocouples and the calibrated heat-loss conduction probe. A summary of the calibration data is provided in Fig. 64. Also shown are analytical results for various first orifice wall temperature ratios, $(T_W/T_T)_1$, computed using an integral boundary layer code (Ref. 22). It should be noted that the flow coefficient correction for Reynolds numbers of interest is approximately 10%. At high Reynolds numbers, where $C_{D_1} \cong C_{D_2} \cong 1$, the actual throat area ratio, A_1^*/A_2^*, is found to be about 0.662 versus a nominal value of $(0.127/0.168)^2 = 0.572$.

Correlation of Total Flow Angle.

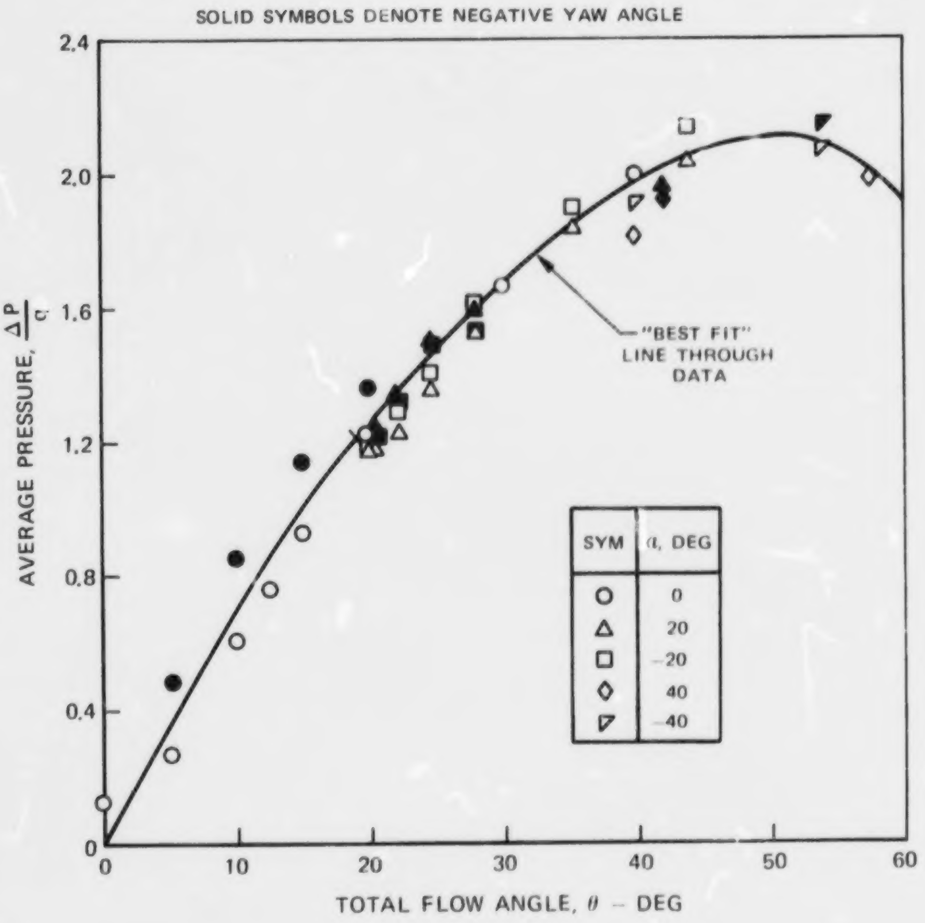

Double Sonic Orifice (DSO) Calibration.

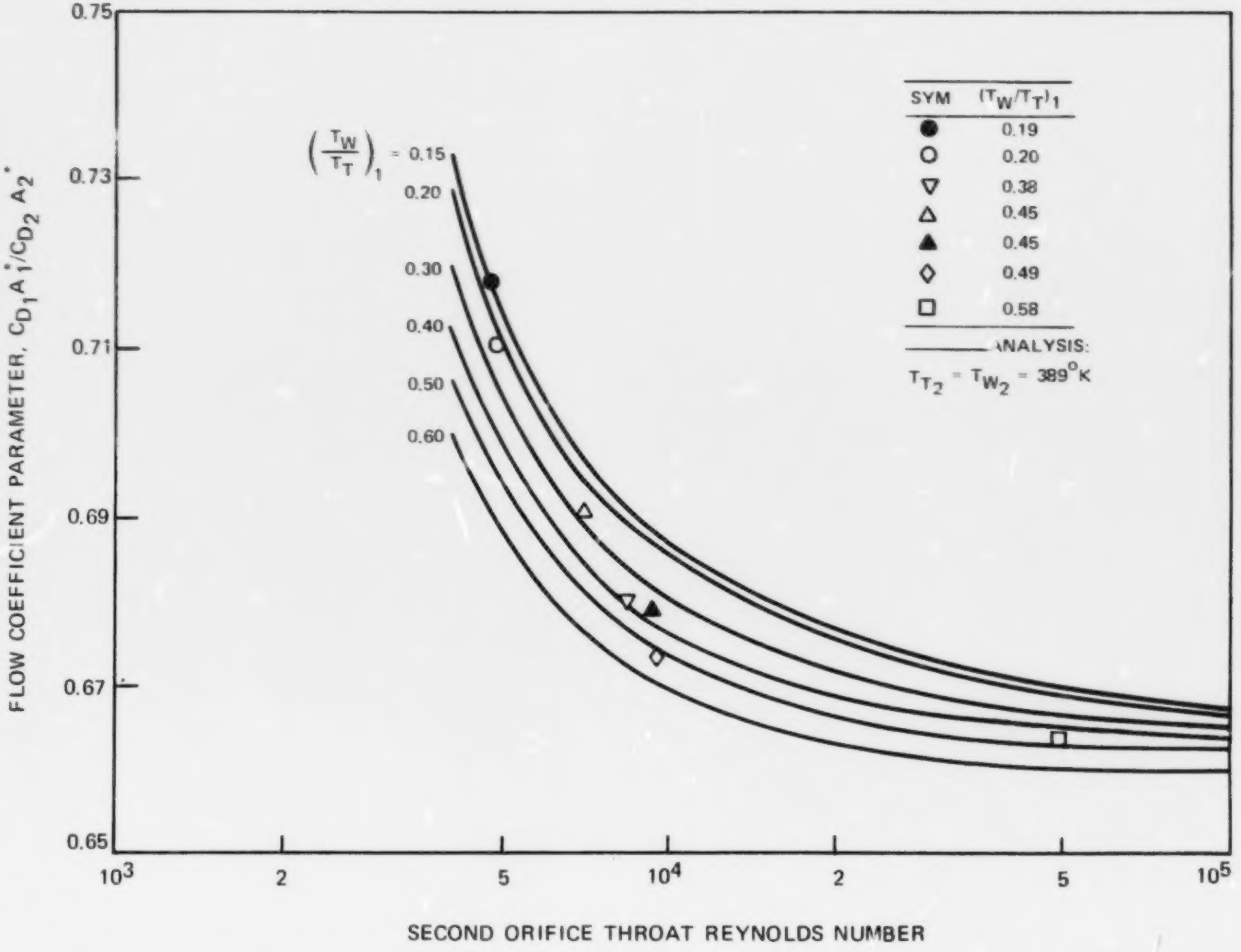

FIG. 64

R1-223-2

APPENDIX C

GAS SAMPLING SYSTEM, CALIBRATION PROCEDURES AND DATA REDUCTION TECHNIQUES

The gas samples withdrawn through the five probe exhaust rake or the combustor DSO probe are analyzed on-line for the time-averaged concentration of a number of species. The sampling system, the various pieces of analytical instrumentation, the calibration procedures and the data reduction techniques used to obtain species concentration data are discussed herein.

Sampling System

A schematic diagram of the sampling system used in the present investigation is shown in Fig. 7. The gas samples withdrawn by the hot-water-cooled sampling probe pass into an electrically-heated (~400°K), teflon-coated, stainless-steel manifold. The sample pressure in this manifold is maintained at approximately 300 torr by means of a mechanical vacuum pump (not shown in Fig. 7). A portion of the gas sample in the manifold is directed through an electrically-heated, teflon-coated, stainless-steel line to the inlet of a time-of-flight mass spectrometer. The sample pressure at the inlet of the mass spectrometer is maintained at approximately 10 torr by means of a remotely-actuated micrometer valve. The TOF mass spectrometer was located close to the probe assembly. In all of the experiments, the distance from the sample probe inlet to the mass spectrometer inlet was less than 60 cm. The mass spectrometer was used to measure the concentration (mole fraction) of CO_2, O_2 and NO, prior to removal of water vapor from the sample. The remainder of the gas sample passed through a short electrically-heated, teflon-coated, aluminum line to a condensate trap (~277°K), where most of the water vapor in the sample was removed. The gas sample then passed through an unheated, teflon-coated, aluminum line and a stainless-steel bellows pump to a Scott Model 119 Exhaust Analyzer. The stainless steel bellows pump increased the sample pressure from sub-atmospheric levels to 1 atm as required by the Exhaust Analyzer. The Analyzer was used to measure the concentration (mole fraction) of CO, CO_2, O_2, NO, NO_2 and unburned hydrocarbons (THC) in the "dry" gas sample. The Exhaust Analyzer was located in the combustion facility control room, approximately 10 m from the combustor. The redundant sampling instrumentation provided a measure of the influence of the long line (and condensate trap) connecting the sampling probe to the Exhaust Analyzer on the sample received by the Analyzer. In a limited number of the input-output tests, the formaldehyde concentration in the exhaust gas was measured using the MBTH wet chemical method. Gas samples for these measurements were withdrawn from the heated manifold via an unheated pyrex line and passed through the reagent solution.

Time-of-Flight Mass Spectrometer

The time-of-flight (TOF) mass spectrometer used in the present investigation was developed at United Aircraft Research Laboratories under the direction of Dr. M. F. Zabielski. The instrument is portable and rugged, and was specifically designed for the harsh environments encountered in combustion facility test cells. The mass spectrometer consists of two separate packages: (1) a portable vacuum station housing the spectrometer, to which the electronics associated with the ion source and ion detector are attached, and (2) a small control unit. This configuration not only permits the spectrometer to be coupled to the sampling device by an extremely short gas inlet, but also allows control by an operator in a remote location.

The vacuum station consists of a 304 stainless steel tee-type chamber connected via a liquid-nitrogen cooled baffle to a 6-inch oil diffusion pump, backed by a mechanical pump. The vacuum chamber can be pumped to a pressure in the low 10^{-8} torr range, and has a typical operating pressure of 1×10^{-6} torr. The inlet system consists of a stainless steel tube with the flow in the inlet line controlled by a remotely-actuated micrometer valve.

In the present investigation, the TOF mass spectrometer was used to scan the m/e range of 12-44. The output signal from the TOF mass spectrometer was sent to on-line data storage and processing equipment. A description of the data storage and processing equipment, the data processing techniques and the procedures used in calibration of the mass spectrometer are discussed later.

Scott Exhaust Analyzer

The Scott Model 119 Exhaust Analyzer used in the present investigation provides for the simultaneous analysis of CO, CO_2, NO or NO_2, O_2 and total hydrocarbons (THC). The Exhaust Analyzer, Fig.65, is an integrated system, with flow controls for sample, zero and calibration gases conveniently located on the control panel. The incoming gas sample passes through a refrigeration condenser (~275°K), to remove residual water vapor. As the sample passes from the condenser, it is filtered to remove particulate matter. The Exhaust Analyzer is comprised of five different pieces of analytical instrumentation. Beckman Model 315B Non-Dispersive Infrared (NDIR) Analyzers were used to measure the CO and CO_2 concentations (mole fractions) in the gas sample. Concentration ranges available on the CO analyzer were from 0-200 ppm to 0-15 % on several scales. Concentration ranges available on the CO_2 analyzer were 0-4% and 0-16%. The accuracy of the NDIR analyzers is nominally ±1% of full scale. A Scott Model 125 Chemiluminescence Analyzer was used to measure the NO and NO_2 concentrations in the gas sample. Concentration ranges available with this instrument were from 0-1 ppm to 0-10,000 ppm on several scales, with a nominal ±1% of full scale accuracy. The thermal converter used in the chemiluminescent analyzer was stainless steel, and was operated at a temperature of approximately 1000°K. A Scott Model 150 Paramagnetic Analyzer was used to measure the O_2 concentration in the gas sample. Concentration ranges available with this instrument were from 0-1% to 0-25% on several scales, with a nominal accuracy of ±1% of full scale. A Scott Model 116 Total Hydrocarbon Analyzer was used to measure the hydrocarbon concentration in the gas sample. This analyzer utilizes an unheated flame ionization detection system to provide for measurement of hydrocarbons (as carbon) in concentration ranges from 0-1 ppm to 0-10%, with a nominal accuracy of ±1% of full scale. Output signals from the various analyzers are displayed on chart recorders and also are sent to the on-line data storage and processing equipment.

Exhaust Gas Analytical System.

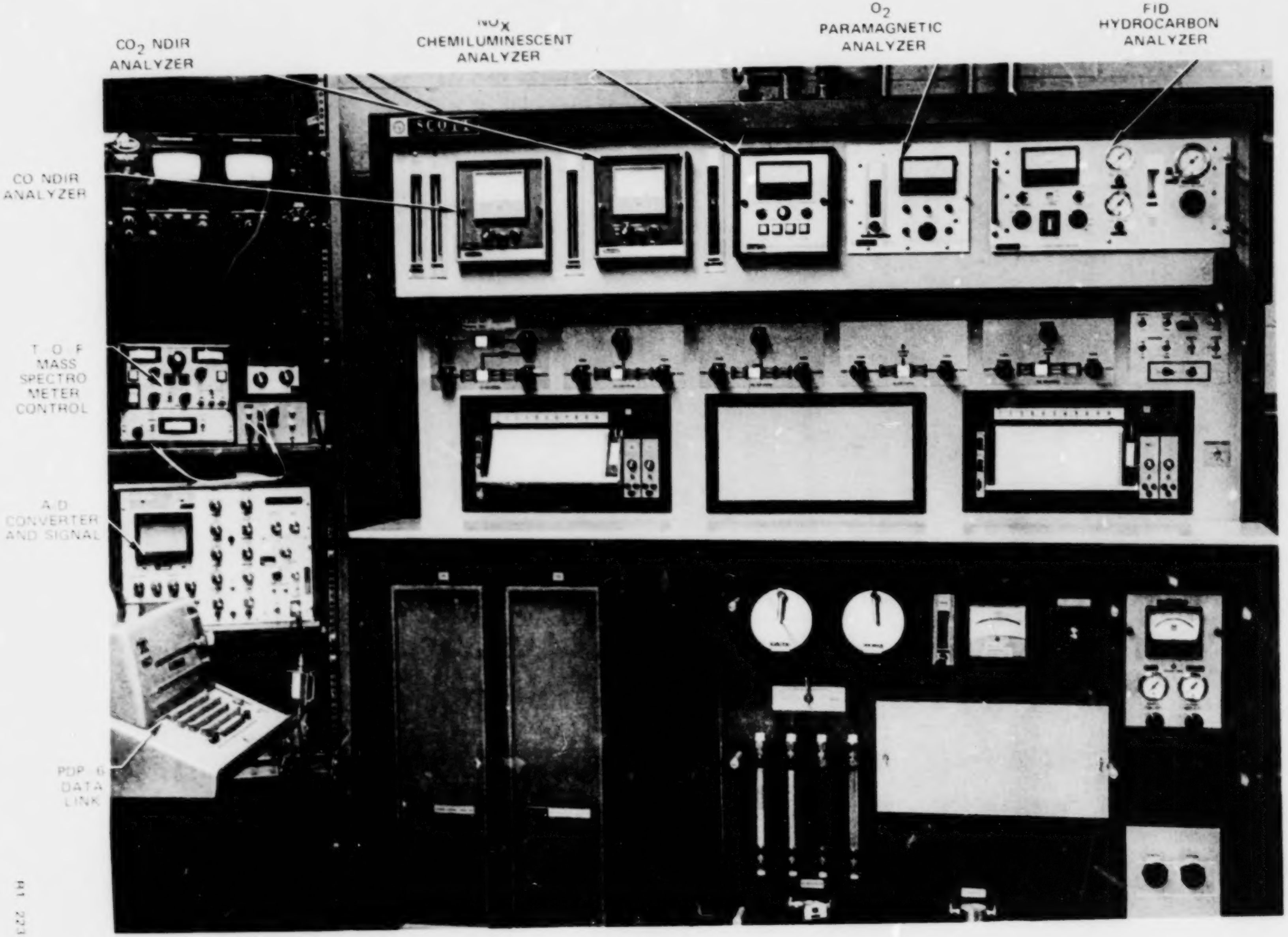
CO_2 NDIR ANALYZER
NO_x CHEMILUMINESCENT ANALYZER
O_2 PARAMAGNETIC ANALYZER
FID HYDROCARBON ANALYZER
CO NDIR ANALYZER
T O F MASS SPECTRO METER CONTROL
A/D CONVERTER AND SIGNAL
PDP 6 DATA LINK

FIG. 65

R1 223 1

Data Storage and Processing Equipment

Output signals from the TOF mass spectrometer and from the various components of the Exhaust Analyzer were recorded on chart recorders and also sent through a multiplexer to a Northern NS-575 analog-digital converter and signal averager, Fig. 7. Averaging of the output signals of the various analytical instruments was required because of low-amplitude, low-frequency fluctuations in the sample line pressure. These fluctuations were the result of temperature and density fluctuations in the reacting flow field. Typically, at each test condition, sampling data were acquired for a period of 2-3 min. Upon completion of the test, the stored data were dumped directly into a PDP-6 computer for processing. Data from the Scott Exhaust Analyzer were processed immediately by the computer, and the processed data were transmitted to the test operators via teletype for verification prior to initiation of the next test. Output from the TOF mass spectrometer was stored in the computer, for later analysis via several data reduction computer codes. A typical mass spectrum of an exhaust gas sample as stored in the computer is shown in Fig. 66.

MBTH Formaldehyde Analysis

In a limited number of the input-output experiments, the formaldehyde concentration in the exhaust gas was measured using the MBTH (3- methyl-2-benzothiazolone hydrazine hydrochloride) wet chemical method. This method is discussed in detail in Ref.24 and only a brief summary of the technique will be given here. A schematic diagram of the apparatus is shown in Fig. 67. A gas sample is continuously withdrawn from the heated manifold and bubbled through a 0.05% aqueous solution of MBTH. The volume of gas sample passed through the reagent solution depended on the formaldehyde concentration in the sample. Typically, gas samples of 1-2 liters (STP) were used, requiring a collection time of 5-10 min. Water soluble aliphatic aldehydes in the gas sample react with MBTH to form an azine. After collecting a gas sample, the reagent solution was taken to the UARL Analytical Chemistry Laboratory where the resulting azine is oxidized by a ferric chloride-sulfuric acid solution to form a blue cationic dye in acid media. The concentration of this dye, which is related to the aldehyde concentration, is determined by measuring the absorptivity of the solution at 628 nm. There are no significant interferences of other gaseous, water-soluble compounds with the MBTH method.

Calibration Procedures

The TOF mass spectrometer and the components of the Exhaust Analyzer were calibrated using various mixtures of methane, carbon dioxide, carbon monoxide, oxygen, nitric oxide, nitrogen dioxide in nitrogen or air. The calibration gases were supplied by Scott Research Laboratories, Plumsteadville, Pa. The specified tolerances of the calibration gas composition were ±2% of the cylinder analysis as supplied by the manufacturer. Spot checks of the gas composition were made at UARL, and the compositions were found to be within the specified tolerances.

The TOF mass spectrometer was calibrated by measuring the mass spectra of various calibration gas mixtures. From the known mixture composition and the observed mass spectra, mass discrimination effects in the inlet and the fragmentation patterns

FIG. 66

Typical Mass Spectrum of Exhaust Gas Sample.

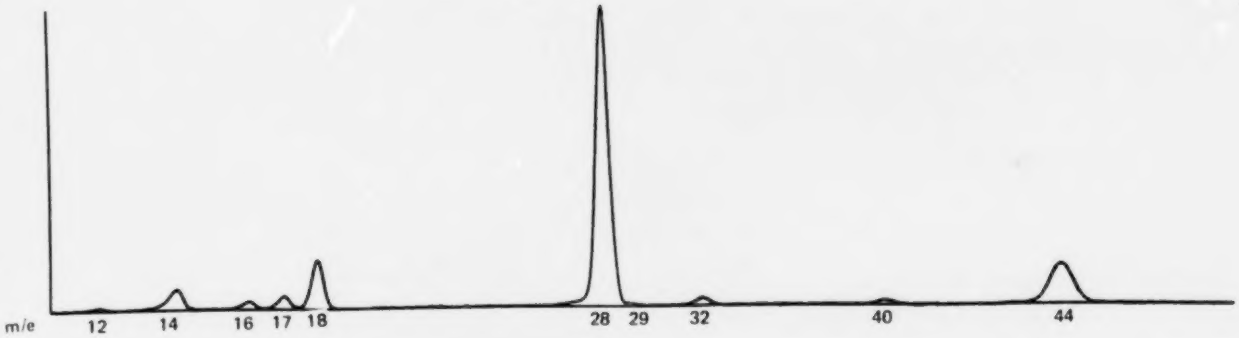

N12-139-1

MBTH Formaldehyde Analysis Apparatus.

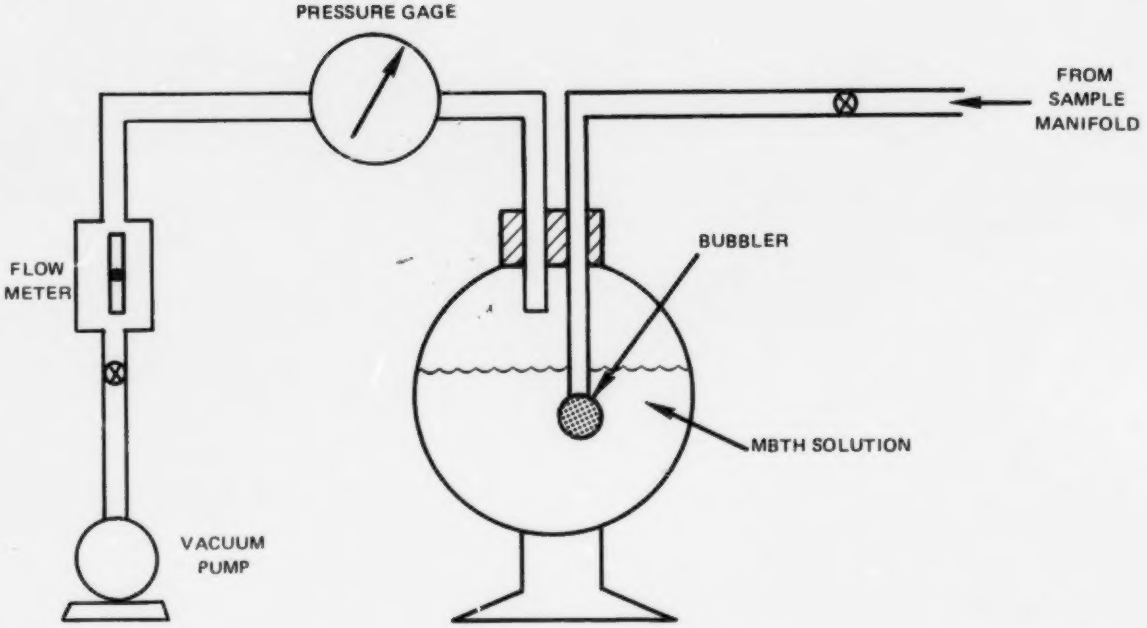
PRESSURE GAGE
FROM
SAMPLE
MANIFOLD
BUBBLER
FLOW
METER
MBTH SOLUTION
VACUUM
PUMP

N12-161-2

for various species of interest were determined. Mass discrimination effects and fragmentation patterns are required if a unique determination of gas sample composition is to be obtained from the measured mass spectra. The Scott Exhaust Analyzer was calibrated prior to each test by flowing a zero gas (hydrocarbon-free N_2) and a calibration gas through each of the instruments in the Analyzer. As part of the calibration procedure of the Exhaust Analyzer, the converter efficiency was determined as a function of converter temperature by flowing known mixtures of NO_2/air mixtures through the converter. A converter efficiency, defined in terms of percent NO_2 dissociation, greater than 98% was obtained for the converter operating at a temperature of 1000°K.

Sampling System Effects

To evaluate the effect of the sample line, condensate traps and particulate filters on the composition of the gas sample, calibration gas mixtures were flowed through the entire sampling system and the composition of the gas was measured using both the TOF mass spectrometer and the Exhaust Analyzer. These experiments served two purposes: (1) to determine if the sampling system served as a source or sink for any of the gaseous species of interest and, (2) to establish the time required to attain a steady-state measurement of the composition. When various N_2-diluted mixtures of CH_4, CO, CO_2, O_2 and NO were flowed through the sampling system, both the TOF mass spectrometer and the Exhaust Analyzer gave essentially the gas analysis indicated on the gas cylinders. A steady-state measurement of concentration was attained at the TOF mass spectrometer in less than 30 sec and at the Scott Exhaust Analyzer in less than 60 sec. When various NO_2-air mixtures were flowed through the sampling system, approximately 120 sec were required to establish a steady-state measurement at the Exhaust Analyzer approximating the cylinder analysis. Sawyer, et al. (Ref.16) and Mellor, et al. (Ref.15) have reported NO_2 losses in sample line condensate traps and on particulate filters with soot deposits. In the present study, noticeable losses in NO_2 were observed in flowing NO_2-air mixtures through dirty particulate filters. In experimental studies of nitrogen oxide formation in premixed laminar flames (Ref. 25 and 26), significant levels of NO_2 were found in the flame zone. One investigator (Ref. 26) has attributed these observations to the conversion of NO to NO_2 in the sampling probe. In a recent analytical study of nitrogen oxide reactions in probes (Ref. 27), it was found that there could be significant interconversion of NO and NO_2 within stainless steel and quartz probes, particularly in regions of the flow with relatively large O-atom concentrations (i.e. in hot, O_2-rich regions). Considering the potential sources (oxidation of NO in a sample containing O_2) and sinks of NO_2 in the probe and sampling system and the difficulty in using a chemiluminescent analyzer to measure NO_2 in gas samples containing appreciable concentrations of hydrocarbons, the reported levels of NO_2 in combustion gas samples must be viewed as having a high degree of uncertainty. This uncertainty, together with the possibility of the conversion of some of the NO in the gas sample to NO_2, suggests that reported levels of NO also are uncertain. However, it is believed that the reported nitrogen oxide levels, which are uncertain, do provide a valid qualitative measure of the variations of nitrogen oxide concentrations with changes in combustor operating conditions.

TABLE D-1. EXHAUST CONCENTRATION DATA - NATURAL GAS FUEL, S = 0

Φ	P (atm)	T_a (°K)	V_a/V_f	$\dot{w}_a$ (kg/sec)	$\dot{w}_f$ (kg/sec)	NO (ppm)	NO_2 (ppm)	THC (ppm)	CO (%)	O_2 Mass Spec. (%)	CO_2 (%)	
											Ex. Anal.	Mass Spec.
0.719	1.01	750	27.4	0.132	0.00567	163	20	333	0.61	5.08	8.05	8.24
0.797	1.00	744	24.9	0.133	0.00637	151	37	537	1.14	4.15	8.59	8.85
0.823	0.99	738	23.9	0.131	0.00645	163	27	782	1.35	3.95	8.50	8.65
0.892	1.00	738	22.1	0.133	0.00708	156	30	1310	1.69	2.99	8.81	9.06
0.915	1.00	738	21.5	0.132	0.00725	155	35	1670	1.91	2.02	8.58	8.70
0.967*	1.00	742	20.3	0.132	0.00763	166	30	1904	2.19	2.00	8.41	8.59
1.058	1.01	740	18.4	0.132	0.00835	154	-	3130	2.96	1.31	8.69	8.52
1.164	1.00	735	16.6	0.131	0.00916	157	-	4770	3.91	0.55	8.74	8.37
0.752	3.58	749	26.6	0.134	0.00604	500	31	60	0.77	4.03	8.72	9.12
0.875	3.65	745	22.9	0.134	0.00703	470	10	477	2.07	2.76	8.75	9.24
0.969	3.79	739	20.6	0.134	0.00777	423	-	1010	3.76	1.68	8.36	8.85
1.068	3.76	750	19.0	0.134	0.00855	402	-	1400	4.88	0.89	8.43	8.86
0.778	1.00	860	29.4	0.132	0.00616	302	45	128	0.78	3.94	8.56	9.01
0.871	1.00	859	26.6	0.132	0.00689	284	50	424	1.37	2.54	8.46	9.03
0.980	0.98	860	23.4	0.133	0.00778	281	22	1380	2.39	1.69	8.39	8.87
1.068	1.00	863	21.6	0.133	0.00851	274	-	3410	3.71	1.14	8.20	8.67
0.803	1.00	740	24.2	0.087	0.00420	196	37	357	0.912	3.80	9.35	9.40
0.886	1.00	733	21.8	0.088	0.00468	190	20	711	1.352	2.64	8.94	9.40
0.987	1.00	742	19.8	0.088	0.00523	221	-	1620	2.374	1.28	8.79	9.12
1.047	0.99	739	18.6	0.088	0.00554	200	-	2400	3.292	0.80	8.93	9.07

Note: All species concentrations (mole fractions) are reported on a dry basis.

* H_2CO = 0.5 ppm

TABLE D-2. EXHAUST CONCENTRATION DATA - NATURAL GAS FUEL, $S = 0.3$

Φ	P (atm)	T_a (°K)	V_a/V_f	$\dot{w}_a$ (kg/sec)	$\dot{w}_f$ (kg/sec)	NO (ppm)	NO_2 (ppm)	THC (ppm)	CO (%)	O_2 (%)		CO_2 (%)	
										Ex. Anal.	Mass Spec.	Ex. Anal.	Mass Spec.
0.785	0.99	751	26.1	0.134	0.00631	260	19	3	0.21	3.55	3.88	9.12	9.46
0.876	0.99	743	23.4	0.134	0.00704	252	16	7	0.60	2.56	2.73	9.77	9.91
0.964*	0.99	744	21.2	0.135	0.00778	226	-	18	1.50	1.23	1.13	9.89	10.1
1.079	0.99	742	19.4	0.134	0.00867	195	-	74	3.52	0.61	0.35	8.11	8.33

Note: All species concentrations (mole fractions) are reported on a dry basis.
*H_2CO = 0.6 ppm

TABLE D-3. EXHAUST CONCENTRATION DATA - NATURAL GAS FUEL, S = 0.6

Φ	P (atm)	T_a (°K)	V_a/V_f	$\dot{w}_a$ (kg/sec)	$\dot{w}_f$ (kg/sec)	NO (ppm)	NO_2 (ppm)	THC (ppm)	CO (%)	O_2 Ex. Anal. (%)	O_2 Mass Spec. (%)	CO_2 Ex. Anal. (%)	CO_2 Mass Spec. (%)
0.795	0.99	739	25.6	0.132	0.00627	299	-	4	0.142	3.43	3.79	9.18	9.46
0.876	0.99	737	23.1	0.133	0.00698	280	-	4	0.614	1.66	1.85	9.70	10.3
0.983	0.99	734	20.7	0.134	0.00788	269	-	10	1.79	0.58	0.73	9.73	10.0
1.078	1.00	736	19.4	0.134	0.00866	246	-	44	3.98	0.06	0.12	8.91	9.44
0.774	3.42	747	26.0	0.133	0.00618	518	-	8	0.100	-	3.76	9.55	9.63
0.878	3.60	742	23.2	0.135	0.00710	438	-	5	0.371	1.76	1.82	9.78	10.4
0.980	3.59	736	20.7	0.134	0.00784	413	-	11	1.59	0.15	0.25	9.52	10.3
1.080	3.55	761	19.5	0.134	0.00864	351	-	65	4.00	0.10	-	8.86	8.92
0.778	1.02	744	10.8	0.131	0.00609	276	21	3	0.092	3.73	-	9.96	-
0.824	1.02	746	10.3	0.131	0.00645	288	20	3	0.162	3.52	3.47	-	9.38
0.862	1.01	754	9.9	0.132	0.00682	303	-	4	0.257	2.26	2.21	9.79	10.1
0.927	1.02	741	9.1	0.131	0.00727	273	22	3	0.467	1.61	-	9.82	-
0.955*	1.01	756	9.0	0.132	0.00755	320	-	5	1.41	0.61	-	9.95	-
1.02	1.02	753	8.3	0.132	0.00805	273	-	4	1.70	0.68	-	9.49	-
1.056	1.01	748	8.0	0.132	0.00832	266	-	19	4.19	0.09	-	8.76	-
1.11	1.02	743	7.6	0.132	0.00879	233	-	17	3.74	0.44	-	8.49	-
0.511	1.01	740	0.30	0.137	0.00425	117	18	20	0.67	9.60	-	5.92	-
0.616	1.01	740	0.25	0.137	0.00507	108	22	95	1.04	9.40	-	6.30	-
0.714	1.01	739	0.21	0.137	0.00589	117	33	240	1.2	8.02	-	6.53	-
0.817	1.01	740	0.19	0.137	0.00671	131	32	435	1.07	6.02	-	7.64	-
0.917	1.01	742	0.17	0.137	0.00754	145	32	525	1.11	4.30	-	8.52	-
1.02	1.01	772	0.16	0.137	0.00836	194	-	780	1.75	1.86	-	9.54	-
1.11	1.01	770	0.14	0.137	0.00915	203	-	1250	2.64	0.63	-	9.70	-
1.22	1.01	769	0.13	0.136	0.00993	169	-	5100	5.83	0.28	-	7.98	-
1.33	1.01	770	0.12	0.136	0.0109	131	-	7850	7.67	0.05	-	6.94	-

Note: All species concentrations (mole fractions) are reported on a dry basis.

*H_2CO = 0.5 ppm

TABLE D-4. EXHAUST CONCENTRATION DATA - SYNTHESIZED FUEL, S = 0

Φ	P (atm)	T_a (°K)	V_a/V_f	$\dot{w}_a$ (kg/sec)	$\dot{w}_f$ (kg/sec)	NO (ppm)	NO_2 (ppm)	THC (ppm)	CO (%)	O_2 (%)	CO_2 (%)
0.779	1.02	728	16.9	0.137	0.00867	165	25	170	0.90	4.62	9.50
0.874	1.02	740	15.4	0.137	0.00976	165	15	425	1.40	3.62	10.0
0.972	1.02	732	13.8	0.137	0.0109	165	28	1125	2.15	2.75	10.0
1.063	1.02	735	12.7	0.137	0.0119	115	20	2500	3.00	2.12	9.40

Note: All species concentrations (mole fractions) are reported on a dry basis.

TABLE D-5. EXHAUST CONCENTRATION DATA - SYNTHESIZED FUEL, S = 0.6

Φ	P (atm)	T_a (^oK)	Va/Vf	$\dot{w}_a$ (kg/sec)	$\dot{w}_f$ (kg/sec)	NO (ppm)	NO_2 (ppm)	THC (ppm)	CO (%)	O_2 (%) Ex. Anal	O_2 (%) Mass Spec.	CO_2 (%) Ex. Anal.	CO_2 (%) Mass Spec.
0.791	1.00	745	18.0	0.137	0.00881	241	28	3	0.162	4.16	4.08	9.76	9.6
0.889	1.00	741	16.0	0.137	0.00989	240	26	3	0.666	2.64	2.27	10.4	10.8
0.991	1.00	741	14.5	0.136	0.0110	221	44	3	1.72	1.29	1.08	10.5	10.6
0.792	3.59	752	17.7	0.137	0.00879	561	18	4	0.089	3.62	3.51	10.2	10.1
0.892	3.75	749	15.8	0.137	0.00990	567	27	4	0.557	1.76	1.77	11.1	11.3
1.000	3.82	746	14.1	0.137	0.0111	494	-	4	1.85	0.34	0.25	11.0	11.4

NOTE: All species concentrations (mole fractions) are reported on a dry basis.

TABLE D-6. EXHAUST CONCENTRATION DATA - GASEOUS PROPANE

Φ	P (atm)	T_a (°K)	V_a/V_f	$\dot{w}_a$ (kg/sec)	S	NO (ppm)	NO_2 (ppm)	THC (ppm)	CO (mole %)	O_2 (mole %)	CO_2 (mole %)
0.804	1.01	730	41.3	0.137	0	260	15	400	0.94	-	9.30
0.907	1.00	724	36.6	0.137	0	250	18	1425	1.63	-	10.1
0.973	1.00	738	34.8	0.136	0	270	17	1900	2.23	-	10.1
1.115	1.00	738	30.6	0.137	0	255	25	4500	4.10	-	10.1
0.814	1.01	733	39.1	0.136	0.3	350	30	50	0.59	4.45	10.3
0.927	1.01	744	37.5	0.136	0.3	350	25	350	1.24	3.05	10.2
1.033	1.01	744	34.3	0.136	0.3	355	18	600	2.51	1.65	10.5
1.128	1.01	747	30.3	0.136	0.3	325	-	1550	3.75	1.05	10.1

Note: All species concentrations (mole fractions) are reported on a dry basis.

TABLE D-7. EXHAUST CONCENTRATION DATA - LIQUID PROPANE

Φ	P (atm)	T_a (°K)	$\dot{w}_a$ (kg/sec)	S	NO (ppm)	NO_2 (ppm)	THC (ppm)	CO (mole %)	O_2 (mole %)	CO_2 (mole %)
0.824	1.00	728	0.135	0.3	250	30	40	0.79	-	9.80
0.935	1.00	729	0.135	0.3	255	35	165	1.77	-	10.6
1.037	1.00	726	0.135	0.3	260	20	600	2.63	-	10.6
1.153	1.00	730	0.135	0.3	260	-	1850	4.10	-	10.5
0.731	6.27	747	0.136	0.3	170	15	50	0.18	7.00	10.8
0.835	6.95	756	0.136	0.3	150	5	75	0.18	4.10	10.6
0.947	6.99	754	0.136	0.3	165	10	175	0.41	1.70	11.8
1.046	6.44	751	0.136	0.3	185	-	700	1.20	0.25	11.8

Note: All species concentrations (mole fractions) are reported on a dry basis.

TABLE D-8. EXHAUST TEMPERATURE PROFILES FOR NATURAL GAS COMBUSTION AT VARIOUS Φ*

r/r_o	TEMPERATURE, °K		
	$\Phi = 0.80$	$\Phi = 1.0$	$\Phi = 1.2$
1.0 (wall)	1066	1088	1105
0.95	1175	1170	1177
0.89	1332	1320	1340
0.79	1509	1525	1505
0.68	1631	1669	1670
0.58	1716	1755	1754
0.47	1765	1828	1846
0.35	1827	1894	1928
0.17	1855	1919	1994
0.06	1883	1945	1996
0. (℄)	1885	1958	1996
0.10	1890	1953	2029
0.20	1897	1972	2028
0.33	1881	1982	2003
0.45	1881	1935	1966
0.56	1848	1920	1935
0.68	1749	1841	1829
0.77	1635	1738	1702
0.88	1478	1620	1583

*P=1 atm, S=0, T_a=740°K, $\dot{w}_a$=0.132 kg/sec

TABLE D-9. EXHAUST TEMPERATURE PROFILES FOR NATURAL GAS COMBUSTION AT VARIOUS INLET AIR CONDITIONS*

r/r_o	TEMPERATURE, °K	
	T_a = 742°K $\dot{w}_a$ = 0.089 kg/sec	T_a = 860°K $\dot{w}_a$ = 0.132 kg/sec
1.0 (wall)	1093	1183
0.95	1097	1277
0.89	1256	1499
0.79	1422	1650
0.68	1572	1779
0.58	1737	1883
0.47	1760	1927
0.35	1833	2001
0.17	1893	2027
0.06	1893	2044
0.(℄)	1902	2026
0.10	1897	2026
0.20	1891	2028
3	1900	2039
0.45	1825	2017
0.56	1816	1999
0.68	1762	1919
0.77	--	1800
0.88	1532	1667

*P = 1 atm, S = 0, $\Phi \equiv 1.0$

TABLE D-10. EXHAUST TEMPERATURE PROFILES* FOR NATURAL GAS COMBUSTION - S = 0.6

r/r_o	TEMPERATURE, ^oK		
	$\Phi = 0.8$ P = 3.4 atm	$\Phi = 1.0$ P = 3.4 atm	$\Phi = 0.8$ P = 1 atm
1.0 (wall)	1429	1595	1195
0.95	1587	1821	--
0.89	1766	1989	1464
0.79	1900	2238	1633
0.68	1957	2390	1704
0.58	2060	2472	--
0.47	2177	2539	1803
0.35	2246	2550	1873
0.17	2167	2525	1784
0.06	2083	--	--
0. (℄)	2011	2391	1639
0.10	1998	2386	--
0.20	2026	--	1601
0.33	2014	2390	1808
0.45	2244	2486	1901
0.56	2259	2490	--
0.68	2204	2490	1845
0.77	2126	--	1618
0.88	2014	2303	--

*T_a = 740^{o}K, $\dot{w}_a$ = 0.133 kg/sec

TABLE D-11. EXHAUST TEMPERATURE PROFILES FOR SYNTHESIZED GAS COMBUSTION AT VARIOUS Φ^*

r/r_o	TEMPERATURE, ^oK		
	$\Phi = 0.8$	$\Phi = 0.9$	$\Phi = 1.0$
1.0 (wall)	1210	1334	1416
0.96	1283	1413	1445
0.89	1410	1490	1569
0.80	1564	1637	1690
0.69	1717	1821	1887
0.59	1855	2012	2035
0.48	2040	2130	2096
0.37	2168	2190	2110
0.27	2182	2169	2062
0.17	2102	2060	1984
℄–0.06	1934	1927	1859
0.04	1835	2170	1760
0.14	1808	1789	1750
0.25	1902	1790	1838
0.35	2098	2053	2017
0.46	2203	2213	2132
0.56	2157	2213	2146
0.67	2019	2122	2126
0.78	1895	2020	2064
0.87	1807	1916	1989

*P = 1 atm, S = 0.6, $T_a \cong 740^oK$, $\dot{w}_a = 0.137$ kg/sec

TABLE E-1. BASELINE CASE CONCENTRATION DISTRIBUTIONS

Natural Gas-Air
Overall Equivalence Ratio = 0.9
Pressure = 1 atm

Inlet Air Swirl Number = 0
Inlet Air Temperature = 740°K
Air-Fuel Velocity Ratio = 22.1

$x/r_o = 0.32$

r/ro	0 (℄)	0.062	0.254	0.328	0.416	0.462	0.478
Species							
CO (mole%)	2.27	2.27	2.22	2.04	1.66	1.4	1.34
CO_2 (mole%)	1.9	1.9	1.9	1.71	1.51	1.21	1.14
O_2 (mole%)	-	7.6	7.3	7.3	7.3	9.05	10.0
NO (ppm)	-	1.2	1.6	1.5	1.0	1.0	1.0
NO_x (ppm)	-	-	-	-	-	-	-
THC (mole%)	>10	>10	>10	>10	>10	>10	>10

r/ro	0.495	0.516	0.541	0.561	0.599	0.653	
Species							
CO (mole%)	1.23	1.1	1.02	0.85	0.71	0.56	
CO_2 (mole%)	1.04	.94	.84	.66	.60	.44	
O_2 (mole%)	11.5	13.0	14.2	15.1	16.6	17.4	
NO (ppm)	0.7	0.7	0.3	0.4	-	-	
NO_x (ppm)	-	13.0	11.0	9.0	6.0	5.0	
THC (mole%)	>10	>10	>10	>10	>10	>10	

$x/r_o = 5.17$

r/ro	0(℄)	0.125	0.254	0.395	0.495	0.711	0.852	0.944
Species								
CO (mole%)	3.14	3.08	2.8	2.34	1.95	1.4	1.05	0.8
CO_2 (mole%)	6.83	6.75	6.74	6.63	6.25	5.65	5.28	5.13
O_2 (mole%)	5.0	5.1	5.65	6.5	7.55	9.05	10.6	11.6
NO (ppm)	83	85	88	70	70	52	50	43
NO_x (ppm)	127	122	130	110	108	88	76	68
THC (mole%)	1.9	.182	1.60	1.32	1.20	0.9	0.79	0.685

TABLE E-1 (CONT.)

x/r_o = 5.17*

r/ro	0 (℄)	0	0.125	0.262	0.395	0.536	0.719	0.857	0.948
Species									
CO (mole%)	2.9	3.34	3.5	3.58	3.44	3.35	2.84	2.55	2.2
CO_2 (mole%)	6.42	6.76	7.0	6.98	6.90	6.85	6.65	6.46	6.55
O_2 (mole%)	5.95	5.34	4.2	4.15	4.3	4.67	5.5	6.2	6.75
NO (ppm)	83	93	88	90	87	84	72	65	58
NO_x (ppm)	124	128	125	132	125	125	108	105	94
THC (mole%)	1.90	2.07	2.25	2.25	2.32	2.21	2.10	1.95	1.95

* Traverse made in combustor on opposite side of centerline from previous table

x/ro = 7.95

r/ro	0 (℄)	0.133	0.254	0.407	0.553	0.661	0.778	0.948	
Species									
CO (mole%)	3.42	3.3	3.02	2.62	2.22	1.91	1.44	0.83	
CO_2 (mole%)	6.73	6.83	6.77	6.82	6.65	6.62	6.46	6.43	
O_2 (mole%)	4.72	5.0	5.3	5.98	6.95	7.45	8.0	8.7	
NO (ppm)	100	100	102	95	85	80	73	64	
NO_x (ppm)	148	150	-	152	135	128	110	94	
THC (mole%)	1.87	1.72	1.65	1.35	1.10	1.02	0.70	0.47	

x/ro - 10.73

r/ro	0 (℄)	0.141	0.274	0.382	0.536	0.644	0.794	0.944	
Species									
CO (mole%)	3.23	2.93	2.83	2.55	2.17	1.86	1.21	0.77	
CO_2 (mole%)	7.1	7.0	6.95	7.08	7.10	7.10	7.30	7.35	
O_2 (mole%)	4.5	5.05	5.4	5.8	6.1	6.5	6.88	7.2	
NO (ppm)	142	132	140	130	123	120	107	93	
NO_x (ppm)	193	184	195	174	160	156	140	114	
THC (mole%)	0.81	0.75	0.68	0.60	0.50	0.45	0.32	0.25	

x/ro = 13.50

r/ro	0 (℄)	0.141	0.245	0.387	0.516	0.653	0.786	0.869	0.944
Species									
CO (mole%)	3.07	2.96	2.83	2.55	2.18	1.61	1.06	0.8	0.69
CO_2 (mole%)	6.94	7.1	7.12	7.15	7.22	7.4	7.75	7.8	7.83
O_2 (mole%)	5.05	4.9	4.9	5.15	5.5	5.95	6.22	6.2	6.3
NO (ppm)	150	145	150	147	137	130	117	111	112
NO_x (ppm)	190	185	190	186	172	160	144	135	135
THC (mole%)	0.70	0.67	0.62	0.56	0.45	0.31	0.20	0.15	0.135

TABLE E-1 (CONT.)

x/ro = 16.28

r/ro	0.121	0.249	0.395	0.545	0.665	0.790	0.869	0.940	
Species									
CO (mole%)	2.4	2.27	2.03	1.62	1.2	0.81	0.61	0.49	
CO_2 (mole%)	7.4	7.34	7.43	7.63	7.74	8.03	8.15	8.12	
O_2 (mole%)	4.85	5.0	5.11	5.3	5.52	5.55	5.66	5.73	
NO (ppm)	183	186	180	162	147	137	132	128	
NO_x (ppm)	215	219	210	190	173	160	154	148	
THC (mole%)	0.35	0.32	0.27	0.215	0.145	0.09	0.070	0.070	

TABLE E-2. SPECIES CONCENTRATION DISTRIBUTIONS FOR LOW EQUIVALENCE RATIO CASE

Natural Gas-Air
Overall Equivalence Ratio = 0.7
Pressure = 1 atm

Inlet Air Swirl Number = 0
Inlet Air Temperature = 740°K
Air-Fuel Velocity Ratio = 27

x/r_o = 0.32

r/ro	0 (℄)	0.079	0.191	0.245	0.324	0.407	0.491
Species							
CO (mole%)	3.81	3.81	3.81	3.81	3.23	2.68	1.78
CO_2 (mole%)	2.43	2.68	2.62	2.62	2.20	1.82	1.26
O_2 (mole%)	5.60	6.30	6.00	5.65	6.20	6.30	9.55
NO (ppm)	16.2	17.5	17.5	18.5	15.7	14.5	8.70
NO_x (ppm)	33.2	-	-	-	-	-	-
THC (mole%)	>10	>10	>10	>10	>10	>10	>10

r/ro	0.574	0.836	0.944				
Species							
CO (mole%)	1.01	0.28	0.26				
CO_2 (mole%)	0.84	0.47	1.02				
O_2 (mole%)	14.9	18.8	19.0				
NO (ppm)	5.0	2.3	3.3				
NO_x (ppm)	13.8	6.50	6.3				
THC (mole%)	>10	3.60	1.75				

x/ro = 5.17

r/ro	0 (℄)	0.295	0.486	0.707	0.944		
Species							
CO (mole%)	3.14	2.24	1.55	0.95	0.5		
CO_2 (mole%)	6.75	6.1	5.5	4.77	3.67		
O_2 (mole%)	5.42	7.25	9.3	12.1	14.5		
NO (ppm)	82	70	66	79	32		
NO_x (ppm)	125	112	103	75	50		
THC (mole%)	1.42	0.95	0.55	0.32	0.24		

TABLE E-2. (CONT.)

$x/r_o = 5.17$*							
r/ro	0 (℄)	0.146	0.349	0.582	0.719	0.857	0.948
Species							
CO (mole%)	3.24	3.40	3.44	3.00	2.65	2.20	1.82
CO_2 (mole%)	6.75	6.70	6.75	6.35	6.07	5.75	5.61
O_2 (mole%)	5.45	5.10	4.80	6.05	7.05	8.05	8.60
NO (ppm)	92	100	100	78	68	53	42
NO_x (ppm)	144	143	-	130	113	91	80
THC (mole%)	1.37	1.57	1.55	1.65	1.60	1.60	1.68

* Traverse made in combustor on opposite side of centerline from previous table

x/ro = 7.95							
r/ro	0 (℄)	0.287	0.486	0.753	0.948		
Species							
CO (mole%)	3.07	2.50	1.70	1.00	0.36		
CO_2 (mole%)	6.53	6.30	5.85	5.32	4.81		
O_2 (mole%)	5.45	6.90	8.75	11.2	13.0		
NO (ppm)	117	117	97	72	54		
NO_x (ppm)	185	169	140	102	76		
THC (mole%)	1.05	0.70	0.45	0.22	0.15		

x/ro = 10.73							
r/ro	0 (℄)	0.262	0.528	0.786	0.944		
Species							
CO (mole%)	2.60	1.90	1.40	0.55	0.21		
CO_2 (mole%)	6.80	6.56	6.25	5.76	5.32		
O_2 (mole%)	6.05	7.40	8.47	10.5	11.6		
NO (ppm)	147	132	120	88	75		
NO_x (ppm)	190	152	157	113	93		
THC (mole%)	0.52	0.40	0.23	0.07	0.04		

TABLE E-2 (CONT.)

x/r_o = 13.50

r/rc	0 (℄)	0.195	0.382	0.611	0.699	0.944	
Species							
CO (mole%)	2.26	2.13	1.70	0.99	0.41	0.40	
CO_2 (mole%)	6.70	6.61	6.50	6.42	6.24	6.15	
O_2 (mole%)	6.50	6.90	7.55	8.80	10.1	10.7	
NO (ppm)	160	150	143	120	100	87	
NO_x (ppm)	198	185	177	150	122	104	
THC (mole%)	0.35	0.31	0.22	0.10	0.044	0.01	

x/r_o = 16.28

r/ro	0 (℄)	0.520	0.778	0.940			
Species							
CO (mole%)	1.57	0.96	0.21	0.11			
CO_2 (mole%)	6.75	6.70	6.57	6.49			
O_2 (mole%)	7.15	8.25	9.45	9.87			
NO (ppm)	170	140	120	105			
NO_x (ppm)	188	162	135	125			
THC (mole%)	0.21	0.092	0.037	0.03			

TABLE E-3. SPECIES CONCENTRATION DISTRIBUTIONS FOR SYNTHESIZED GAS CASE

Synthesized Fuel-Air	Inlet Air Swirl Number = 0
Overall Equivalence Ratio = 0.9	Inlet Air Temperature = 740°K
Pressure = 1 atm	Air-Fuel Velocity Ratio = 15.8

x/r_o = 0.32									
r/ro	0 (℄)	0.129	0.262	0.407	0.536	0.649	0.778	0.852	0.944
Species									
CO (mole%)	13.7	13.7	14.8	15.0	8.20	4.30	2.10	1.40	1.25
CO_2 (mole%)	2.20	1.60	1.45	1.10	0.70	0.50	0.90	2.15	2.40
O_2 (mole%)	5.64	6.25	5.64	5.37	11.8	15.9	17.5	16.3	16.3
NO (ppm)	0.8	0.6	0.6	0.5	0.4	0.3	0.5	3.2	2.5
NO_x (ppm)	-	-	-	-	-	-	7.5	10.0	5.0
THC (mole%)	>10	>10	>10	>10	>10	8.85	4.10	2.35	1.75

x/r_o = 5.17									
r/ro	0 (℄)	0.121	0.245	0.395	0.511	0.711	0.848	0.944	
Species									
CO (mole%)	4.70	4.45	4.00	3.15	2.65	1.95	1.55	1.20	
CO_2 (mole%)	7.30	7.30	7.30	6.90	6.70	6.10	5.90	5.60	
O_2 (mole%)	5.00	5.12	6.12	7.38	8.13	9.90	10.8	11.5	
NO (ppm)	77	77	75	67	57	57	50	45	
NO_x (ppm)	113	118	115	110	107	90	75	67	
THC (mole%)	1.88	1.75	1.60	1.08	0.87	0.60	0.50	0.37	

x/r_o = 5.17*									
r/ro	0 (℄)	0.141	0.282	0.399	0.524	0.736	0.877	0.956	
Species									
CO (mole%)	4.10	4.40	4.50	4.40	4.50	4.06	3.60	3.40	
CO_2 (mole%)	6.80	6.95	7.00	7.20	6.90	6.90	6.85	6.90	
O_2 (mole%)	6.45	5.80	5.50	5.38	5.70	6.20	6.52	6.66	
NO (ppm)	65	77	83	80	78	72	65	60	
NO_x (ppm)	112	120	125	118	118	107	104	105	
THC (mole%)	1.92	2.15	2.08	2.02	2.15	2.17	2.02	1.90	

* Traverse made in combustor on opposite side of centerline from previous table.

TABLE E-3 (CONT.)

x/r_o = 7.95

r/ro	0 (℄)	0.129	0.279	0.411	0.532	0.661	0.790	0.857	0.956
Species									
CO (mole%)	5.45	5.25	4.65	4.10	3.45	2.90	2.10	1.45	1.15
CO_2 (mole%)	7.00	7.00	7.00	6.90	6.90	6.90	7.00	7.00	6.90
O_2 (mole%)	4.87	5.00	5.62	6.25	7.00	7.65	8.37	8.88	9.38
NO (ppm)	115	107	105	100	96	93	83	77	65
NO_x (ppm)	147	150	153	152	141	132	115	99	87
THC (mole%)	1.92	1.75	1.44	1.19	0.94	0.75	0.47	0.38	0.29

x/r_o = 10.73

r/ro	0 (℄)	0.125	0.245	0.383	0.516	0.578	0.769	0.857	0.944
Species									
CO (mole%)	-	-	-	-	-	-	-	-	-
CO_2 (mole%)	7.05	7.05	7.00	6.95	7.10	7.16	7.27	7.38	7.27
O_2 (mole%)	4.83	4.96	5.46	6.21	6.62	7.18	7.66	8.00	8.42
NO (ppm)	145	141	132	123	124	116	97	86	83
NO_x (ppm)	190	188	171	160	163	145	130	107	97
THC (mole%)	1.53	1.39	1.20	0.95	0.62	0.56	0.33	0.26	0.21

x/r_o = 10.73

r/ro	0 (℄)	0.125	0.378	0.578	0.769	0.857	0.944		
Species									
CO (mole%)	-	-	-	-	-	-	-		
CO_2 (mole%)	7.00	7.00	7.35	7.45	8.27	8.80	8.65		
O_2 (mole%)	4.39	4.15	3.82	3.68	3.08	3.00	3.25		
NO (ppm)	142	145	152	126	105	99	88		
NO_x (ppm)	-	-	-	-	-	132	124		
THC (mole%)	1.40	1.40	1.57	1.50	1.32	1.25	1.20		

* Traverse made in combustor on opposite side of centerline from previous table.

TABLE E-3 (CONT.)

x/r_o = 16.28									
r/ro	0 (℄)	0.129	0.266	0.387	0.520	0.653	0.782	0.865	0.952
Species									
CO (mole%)	4.40	4.10	3.80	3.40	2.50	1.60	0.90	0.65	0.60
CO_2 (mole%)	7.80	7.80	7.90	8.00	8.20	8.50	8.90	8.80	8.80
O_2 (mole%)	4.73	4.88	5.13	5.38	5.85	6.13	6.25	6.38	6.50
NO (ppm)	190	190	185	192	175	162	143	140	127
NO_x (ppm)	238	235	220	228	212	192	172	165	140
THC (mole%)	0.735	0.660	0.580	0.455	0.267	0.127	0.048	0.0350	0.0265

TABLE E-4. SPECIES CONCENTRATION DISTRIBUTIONS FOR SWIRLING FLOW CASE

Natural Gas - Air	Inlet Air Swirl Number = 0.3
Overall Equivalence Ratio = 0.9	Inlet Air Temperature = 740 °K
Pressure = 1 atm	Air-Fuel Velocity Ratio = 22

$x/r_o = 0.32$

r/r_o	0 (℄)	0.099	0.187	0.266	0.328	0.412	
Species							
CO (mole%)	3.94	4.31	4.75	5.01	5.00	4.42	
CO_2 (mole%)	2.57	2.74	2.97	3.25	3.28	3.13	
O_2 (mole%)	1.38	1.27	1.24	1.57	2.32	3.70	
NO (ppm)	14.0	17.0	21.0	22.0	22.0	19.0	
NO_x (ppm)	-	-	-	-	-	-	
THC (mole%)	>10.0	>10.0	>10.0	>10.0	>10.0	>10.0	

r/r_o	0.495	0.536	0.599	0.702	0.807	0.923	
Species							
CO (mole%)	3.67	2.97	1.99	0.97	0.43	0.21	
CO_2 (mole%)	2.94	2.47	1.80	1.12	0.76	0.85	
O_2 (mole%)	5.37	7.44	12.0	16.7	18.7	19.1	
NO (ppm)	14.0	10.0	8.0	4.0	3.0	3.0	
NO_x (ppm)	-	-	26.0	15.0	10.0	9.0	
THC (mole%)	>10.0	>10.0	>10.0	5.1	2.2	0.7	

$x/r_o = 5.17$

r/r_o	0 (℄)	0.125	0.270	0.391	0.524	0.644	0.786	0.869	0.944
Species									
CO (mole%)	7.40	7.13	6.37	5.33	4.13	3.44	2.90	2.58	2.12
CO_2 (mole%)	6.68	6.76	6.76	7.34	7.25	7.39	7.23	6.83	6.68
O_2 (mole%)	80	0.77	1.03	1.65	3.18	3.65	4.66	5.50	6.87
NO (ppm)	145	148	166	162	151	140	118	97	75
NO_x (ppm)	-	-	-	-	-	-	-	125	98
THC (mole%)	2.64	2.55	1.57	0.90	0.42	0.36	0.46	0.84	1.54

TABLE E-4 (CONT.)

x/r_o = 13.50									
r/r_o	0 (℄)	0.146	0.262	0.383	0.516	0.657	0.782	0.852	0.944
Species									
CO (mole%)	5.63	5.33	4.68	3.57	2.42	1.77	1.40	1.26	0.93
CO_2 (mole%)	7.98	8.1	8.33	8.57	8.65	8.59	8.51	8.48	8.45
O_2 (mole%)	0.7	0.74	0.99	1.88	2.8	3.74	4.35	4.61	4.98
NO (ppm)	247	255	253	250	235	216	197	190	176
NO_x (ppm)	-	-	-	-	-	216	198	189	177
THC (mole%)	0.097	0.082	0.060	0.054	0.049	0.044	0.047	0.040	0.041

x/r_o = 16.28									
r/r_o	0 (℄)	0.125	0.258	0.378	0.520	0.636	0.761	0.848	0.949
Species									
CO (mole%)	4.62	4.66	4.27	3.47	2.41	1.74	1.43	1.36	0.96
CO_2 (mole%)	8.33	8.42	8.54	8.85	9.05	8.87	8.64	8.59	8.73
O_2 (mole%)	0.85	0.87	0.80	1.20	1.92	2.78	3.64	4.07	4.30
NO (ppm)	285	289	289	280	263	242	225	215	205
NO_x (ppm)	-	-	-	-	-	-	220	206	200
THC (mole%)	0.032	0.029	0.0245	0.019	0.012	0.007	0.006	0.007	0.005

TABLE E-4 (CONT.)

x/r_o = 5.17*									
r/r_o	0 (℄)	0.166	0.254	0.382	0.557	0.636	0.765	0.857	0.915
Species									
CO (mole%)	7.21	7.03	6.15	5.30	4.49	3.94	3.45	3.08	2.80
CO_2 (mole%)	6.37	6.66	7.04	7.39	7.48	7.36	7.24	6.97	6.52
O_2 (mole%)	1.3	0.93	1.35	1.57	2.5	3.32	4.29	5.33	6.37
NO (ppm)	131 .0	139.0	149.0	151.0	150.0	141.0	121.0	103.0	88.0
NO_x (ppm)	-	-	-	-	-	-	-	134.0	116.0
THC (mole%)	3.25	2.9	1.9	.1.	0.54	0.33	0.31	0.44	0.66

*Traverse made in combustor on opposite side of centerline from previous table

x/r_o = 7.95									
r/r_o	0 (℄)	0.121	0.262	0.387	0.516	0.640	0.765	0.857	0.940
Species									
CO (mole%)	7.12	6.19	5.19	3.92	3.14	2.36	2.20	1.93	1.54
CO_2 (mole%)	6.31	6.31	6.99	7.08	7.56	7.47	7.18	6.68	6.74
O_2 (mole%)	4.15	2.65	2.47	2.68	3.72	4.47	5.42	6.83	7.10
NO (ppm)	163.0	159.0	180.0	182.0	178.0	150.0	141.0	124.0	95.0
NO_x (ppm)	-	-	-	190.0	200.0	148.0	151.0	135.0	101.0
THC (mole%)	1.25	0.92	0.48	0.19	0.11	0.12	0.14	0.17	0.32

x/r_o = 10.73									
r/r_o	0 (℄)	0.129	0.254	0.387	0.528	0.649	0.773	0.865	0.944
Species									
CO (mole%)	6.60	6.37	5.42	3.82	2.77	2.24	1.98	1.80	1.51
CO_2 (mole%)	7.42	7.52	7.80	8.14	8.27	8.19	8.20	8.17	8.19
O_2 (mole%)	0.67	0.6	1.22	2.10	3.05	3.58	3.95	4.24	4.73
NO (ppm)	213.0	210.0	218.0	218.0	212.0	202.0	190.0	173.0	163.0
NO_x (ppm)	-	-	-	-	-	200.0	190.0	173.0	164.0
THC (mole%)	0.35	0.31	0.25	0.16	0.092	0.06	0.075	0.069	0.087

TABLE E-5. SPECIES CONCENTRATION DISTRIBUTIONS FOR HIGH PRESSURE CASE

Natural Gas-Air	Inlet Air Swirl Number = 0
Overall Equivalence Ratio = 0.9	Inlet Air Temperature = 740 °K
Pressure = 3.6 atm	Air-Fuel Velocity Ratio = 22.0

x/ro = 0.32

r/ro	0 (℄)	0	0.079	0.183	0.254	0.324	0.408	
Species								
CO (mole%)	4.95	4.88	5.07	5.50	4.93	3.86	2.86	
CO_2 (mole%)	1.98	1.93	1.95	2.09	1.98	1.74	1.42	
O_2 (mole%)	2.15	2.15	1.94	1.44	0.80	0.50	0.90	
NO (ppm)	9.0	9.2	9.2	9.3	9.7	9.0	5.7	
NO_x (ppm)	-	-	-	-	-	-	-	
THC (mole%)	>10	>10	>10	>10	>10	>10	>10	

r/ro	0.453	0.491	0.536	0.578	0.619	0.707	0.802	0.940	
Species									
CO (mole%)	2.34	1.7	0.96	0.25	0.05	-	-	-	
CO_2 (mole%)	1.22	0.93	0.58	0.23	0.06	0.04	0.04	0.04	
O_2 (mole%)	1.87	4.06	9.3	16.7	20.5	21.1	21.2	21.2	
NO (ppm)	5.0	3.4	2.5	0.8	0.2	0.1	0.2	0.1	
NO_x (ppm)	-	-	-	3.4	1.45	0.85	0.59	0.43	
THC (mole%)	>10	>10	>10	>10	>10	>10	>10	>10	

x/ro = 5.17

r/ro	0 (℄)	0.145	0.266	0.412	0.532	0.632	0.731	0.869	0.940
Species									
CO (mole%)	11.7	11.1	9.18	5.83	3.12	1.59	0.593	0.15	0.08
CO_2 (mole%)	4.19	4.83	5.92	7.07	7.07	6.54	4.97	3.71	2.75
O_2 (mole%)	0.70	0.58	0.90	2.45	5.1	8.15	12.4	15.4	16.9
NO (ppm)	95	143	204	272	307	295	225	148	93
NO_x (ppm)	-	-	-	-	-	-	218	150	100
THC (mole%)	4.10	3.3	2.3	1.0	0.46	0.21	0.06	0.052	0.052

TABLE E-5 (CONT.)

x/ro = 5.17*

r/ro	0 (℄)	0.129	0.274	0.407	0.532	0.649	0.769	0.857	0.940
Species									
CO (mole%)	10.8	9.38	7.03	4.43	2.50	1.15	0.34	0.052	0.02
CO_2 (mole%)	5.33	5.82	6.93	7.38	7.24	6.53	5.03	3.77	3.32
O_2 (mole%)	0.15	0.40	1.18	3.20	5.60	8.55	12.4	14.6	15.7
NO (ppm)	220	263	350	390	375	345	235	140	92
NO_x (ppm)	-	-	-	-	-	-	230	148	120
THC (mole%)	1.35	1.07	0.65	0.33	0.17	0.0725	0.033	0.024	0.028

* Traverse made in combustor on opposite side of centerline from previous table

x/ro = 10.73

r/ro	0 (℄)	0.133	0.262	0.399	0.520	0.678	0.778	0.865	0.931
Species									
CO (mole%)	9.80	8.58	6.42	4/37	2/65	0.78	0.17	0.32	0.02
CO_2 (mole%)	6.05	6.60	7.20	7.43	7.30	6.30	5.27	4.40	4.19
O_2 (mole%)	0.23	0.60	1.30	2.90	5.05	9.20	11.9	13.7	13.9
NO (ppm)	300	370	406	450	445	345	255	177	155
NO_x (ppm)	-	-	-	-	-	-	243	180	170
THC (mole%)	0.78	0.53	0.35	0.205	0.12	0.045	0.019	0.015	0.017

x/ro = 13.50

r/ro	0 (℄)	0.200	0.395	0.607	0.765	0.936			
Species									
CO (mole%)	7.47	5.80	3.63	1.01	0.175	0.02			
CO_2 (mole%)	6.72	7.25	7.68	7.07	5.84	5.16			
O_2 (mole%)	0.5	1.19	2.85	7.15	10.6	11.9			
NO (ppm)	430	472	511	420	310	240			
NO_x (ppm)	-	-	-	-	-	240			
THC (mole%)	0.235	0.18	0.082	0.016	0.0025	0.001			

x/ro = 16.28

r/ro	0 (℄)	0.187	0.353	0.520	0.657	0.786	0.936		
Species									
CO (mole%)	7.24	5.68	3.81	1.54	0.042	0.1	0		
CO_2 (mole%)	7.15	7.63	8.07	8.08	7.20	6.48	6.14		
O_2 (mole%)	0.7	1.14	2.38	5.07	7.96	9.60	10.7		
NO (ppm)	508	577	603	650	460	370	344		
NO_x (ppm)	-	-	-	-	-	-	-		
THC (mole%)	0.13	0.087	0.048	0.017	0.0044	0.0008	0.00036		

TABLE E-6. SPECIES CONCENTRATION DISTRIBUTIONS FOR LIQUID PROPANE

Liquid-Propane Air
Overall Equivalence Ratio = 0.9
Pressure = 1 atm

Inlet **Air** Swirl **Number** = 0.3
Inlet Air Temperature = 741°K
$\dot{w}_{air}$ = 0.136 kg/sec

x/r_o = 5.17								
r/ro	0 (℄)	0.104	0.258	0.399	0.528	0.632	0.802	0.923
Species								
CO (mole %)	10.4	10.4	9.80	8.70	6.80	5.25	2.95	1.90
CO_2 (mole %)	6.65	6.80	7.05	7.35	7.70	7.50	6.35	5.25
O_2 (mole %)	0.60	0.57	0.80	1.40	2.25	3.75	8.0	11.6
NO (ppm)	128	128	130	128	125	81	57	47
NO_x (ppm)							97	79
THC (mole %)	5.40	4.40	3.60	2.55	1.65	1.3	1.3	1.0

x/r_o = 10.73								
r/ro	0 (℄)	0.125	0.233	0.391	0.516	0.636	0.778	0.923
Species								
CO (mole %)	12.3	13.6	12.9	8.70	6.65	4.70	2.57	1.28
CO_2 (mole %)	5.25	5.80	6.50	7.70	8.30	8.30	7.85	6.60
O_2 (mole %)	0.19	0.19	0.30	0.77	1.7	3.3	6.1	9.2
NO (ppm)	160	155	175	190	180	165	123	85
NO_x (ppm)	-	-	-	-	-	-	170	105
THC (mole %)	3.45	2.60	2.00	0.90	0.82	0.55	0.35	0.26

TABLE E - 6. (CONT.)

Conditions identical to previous page except:

Overall Equivalence Ratio = 1.04

$x/r_o = 5.17$								
r/ro	0 (℄)	0.129	0.245	0.383	0.520	0.640	0.802	0.923
Species								
CO (mole %)	9.75	9.70	9.35	8.60	7.15	5.50	3.35	2.10
CO_2 (mole %)	6.70	6.70	6.90	7.10	7.35	7.30	6.50	5.60
O_2 (mole %)	0.75	0.75	0.95	1.4	2.5	4.2	7.7	11.5
NO (ppm)	95	98	97	94	85	76	60	46
NO_x (ppm)	-	-	-	-	-	135	99	74
THC (mole %)	9.80	9.60	8.90	7.25	5.50	3.55	1.90	1.35

$x/r_o = 10.73$								
r/ro	0 (℄)	0.125	0.270	0.370	0.520	0.653	0.790	0.915
Species								
CO (mole %)	12.3	12.3	11.4	10.0	7.60	5.55	3.40	1.95
CO_2 (mole %)	6.35	6.40	6.70	7.40	8.00	8.30	8.15	7.40
O_2 (mole %)	0.17	0.17	0.30	0.55	1.3	2.6	5.3	8.0
NO (ppm)	145	147	165	182	188	165	125	90
NO_x (ppm)	-	-	-	-	-	200	162	105
THC (mole %)	4.45	4.25	3.25	2.20	1.25	0.88	0.62	0.45

TABLE E-7. BASELINE CASE VELOCITY PROFILES*

$x/r_o=0.32$		$x/r_o=5.17$		$x/r_o=5.17^+$		$x/r_o=7.95$		$x/r_o=10.73$		$x/r_o=13.50$		$x/r_o=16.28$	
r/r_o	V (m/sec)	r/r_o	V (m/sec)	r/r_o	V (m/sec)	r/r_o	V (m/sec)	r/r_o	V (m/sec)	r/r_o	V (m/sec)	r/r_o	V (m/sec)
0.76	92	0.76	86	0.76	82	0.76	74	0.76	76	0.76	67	0.76	80
0.59	93	0.64	76	0.64	85	0.63	87	0.63	81	0.63	77	0.65	73
0.54	91	0.51	75	0.51	...	0.51	80	0.49	75	0.52	83	0.52	79
0.52	87	0.37	75	0.38	82	0.36	77	0.39	89	0.38	84	0.38	80
0.51	82	0.25	84	0.24	83	0.22	81	0.24	...	0.27	75	0.23	82
0.46	45	0.06	74	0.06	80	0.11	84	0.13	82	0.12	90	0.11	86
0.33	11	0.03-℄	74	0.03-℄	80	0.01-℄	82	0.02-℄	80	0.01-℄	81	0.02-℄	84
0.23	22	0.17	79	0.17	80	0.18	71	0.17	88	0.09	90	0.09	83
0.12	24									0.17	88	0.16	90
0	26												

* Velocity profiles except for $x/r_o = 5.17^+$ taken on opposite side of ℄ from the majority of the concentration and temperature profiles.

TABLE E-8. BASELINE CASE TEMPERATURE PROFILES

$x/r_o=0.32$		$x/r_o=5.17$		$x/r_o=5.17$*		$x/r_o=7.95$		$x/r_o=10.73$		$x/r_o=13.50$		$x/r_o=16.28$	
r/r_o	T (°K)	r/r_o	T (°K)	r/r_o	T (°K)	r/r_o	T (°K)	r/r_o	T (°K)	r/r_o	T (°K)	r/r_o	T (°K)
0.0	840	0.0	1880	0.0	1900	0.0	1940	0.0	1960	0.0	1930	0.0	1890
0.12	820	0.12	1910	0.12	1880	0.14	1920	0.13	1940	0.12	1920	0.12	1890
0.25	850	0.25	1870	0.25	1870	0.25	1900	0.27	1920	0.24	1890	0.24	1830
0.37	790	0.39	1840	0.39	1840	0.41	1890	0.38	1880	0.38	1890	0.37	1830
0.51	760	0.51	1800	0.53	1850	0.54	1840	0.52	1880	0.51	1850	0.53	1800
0.59	760	0.71	1620	0.71	1800	0.65	1750	0.63	1830	0.64	1770	0.66	1730
0.64	750	0.84	1480	0.84	1740	0.78	1650	0.78	1630	0.78	1600	0.78	1590
		0.93	1420	0.93	1600	0.93	1440	0.93	1400	0.86	1480	0.86	1460
										0.94	1400	0.93	1370

* Temperature profile taken on opposite side of ℄ from majority of the temperature data.

TABLE E-9. VELOCITY PROFILES FOR LOW EQUIVALENCE RATIO CASE*

x/r_o=0.32		x/r_o=5.17		x/r_o=5.17+		x/r_o=7.95		x/r_o=10.73		x/r_o=13.50		x/r_o=16.28	
r/r_o	V (m/sec)	r/r_o	V (m/sec)	r/r_o	V (m/sec)	r/r_o	V (m/sec)	r/r_o	V (m/sec)	r/r_o	V (m/sec)	r/r_o	V (m/sec)
0.76	80	0.76	68	0.76	73	0.76	65	0.76	63	0.76	63	0.52	76
0.68	82	0.47	66	0.62	73	0.48	72	0.50	74	0.57	80	0.25	64
0.57	95	0.28	65	0.42	68	0.28	82	0.24	74	0.39	72	0.0(℄)	74
0.52	76	0.06	61	0.19	66	0.02	81	0.01	76	0.16	66	0.16	74
0.44	--			0.06	66	0.17-℄	72	0.17-℄	73	0.01-℄	70		
				0.08-℄	66					0.17	74		
					64								

TABLE E-10. TEMPERATURE PROFILES FOR LOW EQUIVALENCE RATIO CASE*

x/r_o=0.32		x/r_o=5.17		x/r_o=5.17+		x/r_o=7.95		x/r_o=10.73		x/r_o=13.50		x/r_o=16.28	
r/r_o	T (°K)	r/r_o	T (°K)	r/r_o	T (°K)	r/r_o	T (°K)	r/r_o	T (°K)	r/r_o	T (°K)	r/r_o	T (°K)
0.0	1050	0.0	1900	0.0	1840	0.0	1900	0.0	1890	0.0	1830	0.0	----
0.08	960	0.29	1830	0.14	1840	0.28	1860	0.26	1830	0.18	1840	0.24	1800
0.19	890	0.48	1720	0.34	1860	0.48	1760	0.52	1750	0.37	1800	0.46	1730
0.25	890	0.75	1510	0.72	1750	0.75	1550	0.78	1450	0.61	1680	0.76	1450
0.33	850			0.84	1670	0.94	1730	0.93	1180	0.78	1480	0.92	1220
0.41	800			0.93	1520					0.93	1240		
0.48	720												
0.57	710												
0.78	710												
0.93	730												

* ALL CONDITIONS SAME AS BASELINE EXCEPT $\Phi = 0.7$; Velocity profiles except for $x/r_o = 5.17+$ taken on opposite side of ℄ from the majority of the concentration and temperature profiles. Temperature data at $x/r_o = 5.17+$ also taken on opposite side of ℄ from most concentration data.

TABLE E-11. SYNTHESIZED GAS CASE VELOCITY PROFILES*

x/r_o=0.32		x/r_o=5.17		x/r_o=5.17 +		x/r_o=7.95		x/r_o=10.73		x/r_o=10.73 +		x/r_o=16.28	
r/r_o	V (m/sec)	r/r_o	V (m/sec)	r/r_o	V (m/sec)	r/r_o	V (m/sec)	r/r_o	V (m/sec)	r/r_o	V (m/sec)	r/r_o	V (m/sec)
0.76	71	0.76	30	0.77	119			0.76	74	0.76	79		
0.63	35	0.64	31	0.63	89			0.64	80	0.64	84		
0.50	37	0.52	22	0.49	99	NO DATA		0.52	82	0.39	86	NO DATA	
0.36	14			0.38	94			0.38	75	0.19	89		
				0.26	95			0.25	84	0.0(℄)	89		
				0.03	91			0.19	87	0.08	86		
				0.09 -℄	99			0.0(℄)	86	0.17	85		
				0.17	81			0.08	85				
								0.17	78				

TABLE E-12. SYNTHESIZED GAS CASE TEMPERATURE PROFILES*

x/r_o=0.32		x/r_o=5.17		x/r_o=5.17+		x/r_o=7.95		x/r_o=10.73		x/r_o=10.73+		x/r_o=16.28	
r/r_o	T (°K)	r/r_o	T (°K)	r/r_o	T (°K)	r/r_o	T (°K)	r/r_o	T (°K)	r/r_o	T (°K)	r/r_o	T (°K)
0.0	860	0.0	1970			0.0	1820	0.0	1850	0.58	1880	0.0	1750
0.13	800	0.13	1930			0.13	1860	0.13	1850	0.76	1760	0.13	1760
0.26	770	0.25	1920	NO DATA		0.26	1920	0.24	1820	0.85	1570	0.26	1750
0.42	680	0.40	1875			0.40	1800	0.38	1820	0.93	1330	0.38	1740
0.53	700	0.50	1800			0.52	1820	0.51	1780			0.50	1720
0.63	730	0.70	1670			0.63	1800	0.55	1800			0.63	1640
0.77	780	0.83	1580			0.77	1670	0.77	1590				
0.83	850	0.93	1440			0.84	1530	0.85	1470				
0.93	880					0.86	1450	0.93	1350				
						0.93	1370						

*Velocity profiles except for those at x/r_o=5.17 + and x/r_o=10.73 + taken on opposite side of ℄ for the majority of the concentration and temperature data. Temperature data at x/r_o=5.17 + and x/r_o=10.73 + also taken on opposite side of ℄ from most concentration data.

TABLE E-13. VELOCITY PROFILES FOR SWIRLING FLOW CASE*

x/r_o=0.32		x/r_o=5.17		x/r_o=5.17+		x/r_o=7.95		x/r_o=10.73		x/r_o=13.50		x/r_o=16.28	
r/r_o	V (m/sec)	r/r_o	V (m/sec)	r/r_o	V (m/sec)	r/r_o	V (m/sec)	r/r_o	V (m/sec)	r/r_o	V (m/sec)	r/r_o	V (m/sec)
0.76	56	0.76	120	0.76	110	0.76	124	0.76	113	0.76	111	0.76	111
0.65	67	0.64	108	0.64	116	0.64	112	0.63	105	0.62	114	0.64	114
0.58	77	0.50	107	0.50	97	0.50	103	0.51	103	0.50	108	0.51	100
0.56	58	0.38	80	0.38	70	0.38	81	0.38	97	0.38	101	0.39	98
0.54	48	0.25	70	0.25	60	0.25	61	0.24	91	0.25	85	0.25	93
0.50	35	0.13	49	0.13	44	0.13	49	0.12	82	0.11	91	0.13	89
0.44	...	0.0(℄)	33	0.0(℄)	36	0.0(℄)	45	0.0(℄)	74	0.01-℄	76	0.0(℄)	81
0.28	26	0.09	39	0.08	23	0.08	...	0.09	62	0.08	71	0.08	74
0.24	22	0.17	28	0.15	30	0.17	37	0.17	65	0.17	45	0.17	78
0.17	25												
0.07	26												
0.03-℄	16												
0.15	27												

* Velocity profiles except for x/r_o = 5.17'taken on opposite side of ℄ from the majority of the concentration and temperature profiles. All conditions the same as baseline case except S = 0.3.

TABLE E-14. FLOW DIRECTION DATA FOR SWIRLING FLOW CASE*

x/r_o = 0.32				x/r_o = 5.17				x/r_o = 5.17+				x/r_o = 10.73				x/r_o = 13.50			
r/r_o	α (deg)	β (deg)	θ (deg)	r/ro	α (deg)	β (deg)	θ (deg)	r/ro	α (deg)	β (deg)	θ (deg)	r/ro	α (deg)	β (deg)	θ (deg)	r/ro	α (deg)	β (deg)	θ (deg)
0.58	-14	29	32	0.76	-10	30	32	0.76	-9	35	36	0.76	-10	27	29	0.76	-12	25	28
0.56	-5	38	38	0.64	-15	39	41	0.63	-10	29	30	0.63	-5	31	31	0.62	-10	23	26
0.54	8	--	--	0.50	-15	32	35	0.51	7	47	47	0.51	-10	31	32	0.50	-6	24	25
0.50	9	10	13	0.38	---	--	--	0.38	10	--	--	0.38	-5	31	31	0.38	4	26	26
0.40	11	2	11	0.25	-7	--	--	0.25	--	--	--	0.24	8	27	28	0.25	-6	25	26
				0.13	6	--	--	0.13	--	--	--	0.12	7	27	28	0.01	13	14	19
				0.0	-6	15	16	0.0	7	25	26	0.0	8	9	12	0.08	11	9	14
																0.17	17	5	18

* Profiles except for x/r_o = 5.17'taken on opposite sides of ℄ from the majority of the concentration and temperature profiles.

TABLE E-15. TEMPERATURE PROFILES FOR SWIRLING FLOW CASE

r/r_o	TEMPERATURE (°K)	
	$x/r_o = 5.17$	$x/r_o = 10.73$
0.90	...	1879
0.88	1923	...
0.80	...	2003
0.78	2062	...
0.68	2146	2090
0.59	2215	2144
0.49	2230	2184
0.39	2230	2224
0.28	...	2224
0.26	2212	...
0.18	2192	2243
0.10	2111	...
0.06 -℄	...	2199
*0.03	2022	2134
*0.12	2005	...
*0.14	...	2176
*0.23	...	2128
*0.25	2073	...
*0.32	...	2137
*0.34	2150	...
*0.43	2208	2170
*0.53	2324	...
*0.59	...	2193
*0.63	2310	2183
*0.75	2334	2144
*0.84	2246	...
*0.87	...	2056

* Most local concentration data taken on this side of combustor ℄

TABLE E-16. TEMPERATURE PROFILES FOR HIGH PRESSURE CASE*

x/r_o=0.32		x/r_o=5.17		x/r_o=7.95		x/r_o=10.73		x/r_o=13.50		x/r_o=16.28	
r/r_o	T (°K)	r/r_o	T (°K)	r/r_o	T (°K)	r/r_o	T (°K)	r/r_o	T (°K)	r/r_o	T (°K)
0.0	900	0.0	1980	0.0	2020	0.0	1940	0.0	2130	0.0	2150
0.07	1080	0.13	1980	0.12	2070	0.26	2020	0.20	2080	0.19	2190
0.18	1190	0.27	1980	0.27	2130	0.40	2070	0.39	2110	0.35	2130
0.26	980	0.41	1980	0.40	2100	0.51	2020	0.60	2100	0.51	2110
0.33	920	0.53	1920	0.53	2040	0.68	1910	0.76	1800	0.65	2010
0.40	820	0.63	1820	0.65	1970	0.76	1700	0.93	1600	0.78	1880
0.45	770	0.76	1720	0.76	1730	0.86	1550			0.93	1580
0.49	780	0.85	1580	0.85	1540	0.92	1490				
0.53	760	0.93	1430	0.93	1410						
0.58	800										
0.62	830										
0.70	850										
0.80	830										
0.93	770										

* Conditions same as baseline case except P = 3.6 atm.

TABLE E-17. TEMPERATURE PROFILES FOR LIQUID PROPANE COMBUSTION

r/ro	TEMPERATURE (°K)			
	Φ = 0.92 ± 0.01		Φ = 1.04 ± 0.01	
	x/ro = 5.17	x/r_o = 10.73	x/r_o = 5.17	x/r_o = 10.73
0.90	1631	1617	1611	1816
0.80	1795	-	-	-
0.78	-	1881	1859	2012
0.68	1984	2052	1952	2106
0.58	-	2134	2041	2183
0.56	2091	-	-	-
0.49	2112	-	2059	2215
0.47	-	2201	-	-
0.38	2121	2211	-	2206
0.36	-	-	2041	-
0.29	2063	-	2004	-
0.27	-	2148	-	2151
0.18	-	2038	-	-
0.17	1975	-	-	-
0.16	-	-	1913	2058
0.09	1871	1921	1823	1982
℄ 0.03	1791	1881	-	1911
0.05	-	-	1745	-
0.13	1789	-	-	1863
0.14	-	1883	-	-
0.15	-	-	1736	-
0.24	1817	1898	1780	-
0.25	-	-	-	1893
0.35	1905	2027	1876	1987
0.44	2003	2142	1946	2089
0.55	-	-	[illegible]	2150
0.57	2075	2187	-	-
0.66	2099	2173	2061	2163
0.75	2076	2104	2035	-
0.77	-	-	-	-
0.87	1882	-	-	-
0.88	-	7864	1852	1917

APPENDIX F

FUEL COMPOSITION

Natural Gas

TABLE F-1. NATURAL GAS COMPOSITION

Species	Mole Percent			
	Trailer No. 1	No. 2	No. 3	Average
CH_4	96.26	96.71	96.11	96.21
C_2H_6	1.89	1.87	2.17	1.98
CO_2	0.70	0.55	0.59	0.61
C_3H_6,C_3H_8	0.24	0.19	0.28	0.24
O_2+A_r	0.10	0.04	0.08	0.07
N_2	0.73	0.55	0.66	0.65
i-C_4H_{10}	0.04	0.05	0.06	0.05
n-C_4H_{10}	0.04	0.04	0.05	0.04

Synthesized Fuel ($CH_4/H_2/CO$)

TABLE F-2. SYNTHESIZED FUEL COMPOSITION*

Species	Mole Percent
H_2	27.18
CH_4	69.83
C_2H_6	1.04
C_3H_8	0.85
N_2	0.83
CO_2	0.27

*CO was mixed with fuel mixture prior to injection into burner. The nominal $CH_4/H_2/CO$ ratio was 1/0.39/0.34.

APPENDIX F (CONT.)

Propane (Natural Grade)

TABLE F-3. PROPANE FUEL COMPOSITION

Species	Mole Percent
C_3H_8	96
C_4H_{10} and lighter fractions	4

NOMENCLATURE

A	Defined by Eq. (B-3a)
A*	Orifice Throat Diameter, cm^2
B	Defined by Eq. (B-3b)
C_D	Nozzle flow coefficient
d	Outer diameter of air annulus, cm
d_e	Effective diameter for swirl number ≡ $d(1-Z^2)^{0.5}$, cm
d_f	Fuel delivery duct inner diameter, cm
d_h	Inner diameter of air annulus, cm
d_o	Combustor duct diameter, cm
f	Frequency, Hz
F	Function of ratio of specific heats and molecular weight
ℓ	Annular air gap height, cm
m	Air-fuel velocity ratio
P	Combustor pressure level, atm
P_1, P_3	Pitch plane static pressure, in H_2O
P_2, P_4	Yaw plane static pressures, in H_2O
P_{T_1}	Impact pressure, torr
P_{T_2}	Downstream orifice total pressure, torr
ΔP	Geometric average pressure, Eq. (B-5), torr
Q	Volumetric flow rate, cm^3/sec
q	Dynamic pressure, torr
r	Radial dimension, cm

NOMENCLATURE (CONT.)

r_o	Combustor radius, cm
S	Swirl number, Eq. (A-1)
t	Temperature, °R
T	Temperature, °K
T_A	Uncorrected free stream temperature, °K
T_C	Conduction correction, °K
T_R	Radiation correction, °K
T_T, T_{T_1}	Free stream stagnation temperature, °K
T_{T_2}	Downstream orifice temperature, °K
V	Axial velocity, m/sec
$\dot{w}$	Mass flow, kg/sec
x	Axial (longitudinal) dimension, cm
y_E	Average exhaust concentration
Z	Ratio of inner and outer diameters of the air annulus
α	Pitch angle, deg.
β	Yaw angle, deg.
η	Swirl vane angle, deg.
θ	Total flow angle, deg.
ψ	Jet thrust, kg-m/sec^2
ρ	Density, kg/m^3
τ	Nozzle torque, kg-m^2/sec^2
Φ	Overall fuel/air equivalence ratio $= (\dot{w}_f/\dot{w}_{air})/(\dot{w}_f/\dot{w}_{air})_{stoichiometric}$

NOMENCLATURE (CONT.)

Subscripts

a	Air stream
f	Fuel stream
w	Wall
1	Orifice no. 1 (upstream orifice) of DSO probe
2	Orifice no. 2 (downstream orifice) of DSO probe

REFERENCES

1. a) M. P. Heap, T. M. Lowes and R. Walmsley: The Effect of Burner Parameters on Nitric Oxide Formation in Natural Gas and Pulverized Fuel Flames, Paper presented at First American Flame Days Meeting, Chicago, Illinois, September 1972.

b) M. P. Heap, T. M. Lowes and R. Walmsley: Emission of Nitric Oxide From Large Turbulent Diffusion Flames, *Fourteenth Symposium (International) on Combustion* (The Combustion Institute, Pittsburgh, 1973), p. 883.

2. D. R. Shoffstall and D. H. Larson: Aerodynamic Control of Nitrogen Oxides and Other Pollutants from Fossil Fuel Combustion, EPA Report 650/2-73-033a, October 1973.

3. a) A. M. Mellor, R. D. Anderson, R. A. Altenkirch and J. H. Tuttle: Emissions from and within an Allison J-33 Combustor, Combust. Sci, and Tech. 6, 169 (1972).

b) J. H. Tuttle, R. A. Altenkirch and A. M. Mellor: Emissions from and within an Allison J-33 Combustor II: The Effect of Inlet Air Temperature, Combust. Sci. and Tech. 7, 125 (1973).

4. R. E. Jones and J. Grobman: Design and Evaluation of Combustors for Reducing Aircraft Engine Pollution, AGARD Document CP-125, April 1973.

5 F. C. Gouldin: Role of Turbulent Fluctuations in NO Formations, Combust. Sci. and Tech. 9, 17 (1974).

6. R. F. Anasoulis and H. McDonald: A Study of Combustor Flow Computations and Comparison with Experiment, EPA Report 650/2-73-045, December 1973.

7. L. S. Caretto: Modeling Pollutant Formation in Combustion Processes, *Fourteenth Symposium (International) on Combustion* (The Combustion Institute, Pittsburgh, 1973), p. 803.

8. D. B. Spalding: Mathematical Models of Continuous Combustion, *Proceedings of the Symposium on Emissions from Continuous Combustion Systems* (Plenum Press, New York, 1972), p. 3.

9. J. M. Beér and N. A. Chigier: *Combustion Aerodynamics* (Halsted Press Division, John Wiley & Sons, Inc., New York,1972).

REFERENCES (CONT.)

10. C. T. Bowman, L. S. Cohen and M. N. Director: Nitric Oxide Formation in Combustion Processes with Strong Recirculation, EPA Report EPA-R2-73-291, July 1973.

11. T. Rozenman and H. Weinstein: Recirculation Patterns in the Initial Region of Coaxial Jets, NASA CR-1595, May 1970.

12. A. J. Giramonti: Advanced COGAS Power Systems for Low Pollution Emissions, Paper presented at the ACS Symposium on Novel Combined Power Cycles, April 1973.

13. J. B. Kennedy and J. B. McVey: An Experimental Study of Fuel Spray Vaporization Rates, United Aircraft Research Laboratories Report UAR-N139, September 1974.

14. F. K. Owen: Laser Velocimeter Measurements in Free and Confined Coaxial Jets with Recirculation, AIAA Paper 75-120, presented at 13th AIAA Aerospace Sciences Meeting, January 1975,

15. J. H. Tuttle, R. A. Shisler and A. M. Mellor: Nitrogen Dioxide Formation in Gas Turbine Engines - Measurements and Measurement Methods, Report PURDU-CL-73-06, December 1973.

16. N. P. Cernansky: Formation of NO and NO_2 in a Turbulent Propane/Air Diffusion Flame, Ph.D. Thesis, University of California, Berkeley, California, 1974.

17. R. W. Schefer, R. D. Matthews, N. P. Cernansky and R. F. Sawyer: Measurement of NO and NO_2 in Combustion Systems, Paper 73-31, Fall Meeting, Western Section/The Combustion Institute, 1973.

18. N. Syred and J. M. Beér: Combustion in Swirling Flows: A Review, Combust. and Flame 23, 143 (1974).

19. R. W. Bilger: Turbulent Diffusion Flame Structure and Implications for Suppression of Pollutant Formation, Paper presented at the Spring Meeting, Western and Central Sections/The Combustion Institute, 1975.

20. L. S. Cohen and R. N. Guile: Measurements in FreeJet Mixing/Combustion Flows. AIAA J. 8, 1053 (1970).

REFERENCES (CONT.)

21. N. M. Kerr and D. Fraser: Swirl. Part I: Effect on Axisymmetrical Turbulent Jets, J. Inst. Fuel 38, 519 (1965).

22. A. H. Shapiro: The Dynamics and Thermodynamics of Compressible Fluid Flow, Vol. I. (Ronald Press, New York, 1953).

23. R. J. Flaherty: Arbitrary Pressure Gradient Integral Technique for Predicting Boundary Layer and Thermal Parameters. J. Aircraft 11, 293 (1974).

24. Methods of Air Sampling and Analysis (American Public Health Association, Washington, D. C., 1972), p. 199.

25. E. L. Merryman and A. Levy: Nitrogen Oxide Formation in Flames: The Roles of NO_2 and Fuel Nitrogen, Fifteenth Symposium (International) on Combustion (to be published).

26. J. D. Allen: Probe Sampling of Oxides of Nitrogen from Flames, Combust. and Flame 24, 133 (1975).

27. H. Amin: Analytical Study of Probe Effects on Sampling of Nitrogen Oxides from Flames (to be published).